

ผลของสารตั้งต้นของโคบอลต์ต่อคุณลักษณะและสมบัติในการเร่งปฏิกิริยาของตัวเร่ง
ปฏิกิริยาโคบอลต์บนตัวรองรับ MCM-41 สำหรับปฏิกิริยาไฮโดรจิเนชันของ
คาร์บอนมอนอกไซด์

นางสาว สุจารี แก้วกัน

วิทยานิพนธ์นี้เป็นส่วนหนึ่งของการศึกษาตามหลักสูตรปริญญาวิทยาศาสตรมหาบัณฑิต

สาขาวิชาวิศวกรรมเคมี ภาควิชาวิศวกรรมเคมี

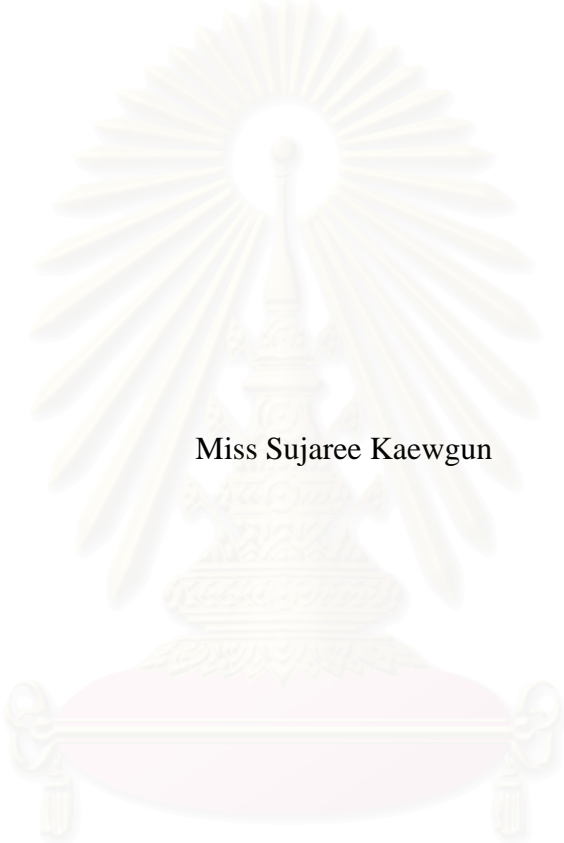
คณะวิศวกรรมศาสตร์ จุฬาลงกรณ์มหาวิทยาลัย

ปีการศึกษา 2546

ISBN: 974-17-4424-2

ลิขสิทธิ์ของจุฬาลงกรณ์มหาวิทยาลัย

INFLUENCE OF COBALT PRECURSORS ON THE
CHARACTERISTICS AND CATALYTIC PROPERTIES OF MCM-41
SUPPORTED COBALT CATALYSTS FOR CARBON MONOXIDE
HYDROGENATION



Miss Sujaree Kaewgun

A Thesis Submitted in Partial Fulfillment of the Requirements
for the Degree of Master of Engineering in Chemical Engineering

Department of Chemical Engineering

Faculty of Engineering

Chulalongkorn University

Academic Year 2003

ISBN: 974-17-4424-2

Thesis Title INFLUENCE OF COBALT PRECURSORS ON THE
CHARACTERISTICS AND CATALYTIC PROPERTIES OF
MCM-41 SUPPORTED COBALT CATALYSTS FOR
CARBON MONOXIDE HYDROGENATION

By Miss Sujaree Kaewgun
Field of Study Chemical Engineering
Thesis Advisor Joongjai Panpranot, Ph.D.
Thesis Co-advisor Professor Piyasan Praserthdam, Dr.Ing.

Accepted by the Faculty of Engineering, Chulalongkorn University in Partial
Fulfillment of the Requirements for the Master's Degree

..... Dean of Faculty of Engineering
(Professor Direk Lavansiri, Ph.D.)

THESIS COMMITTEE

..... Chairman
(Associate Professor Suttichai Assabumrungrat, Ph.D.)

..... Thesis Advisor
(Joongjai Panpranot, Ph.D.)

..... Thesis Co-advisor
(Professor Piyasan Praserthdam, Dr.Ing.)

..... Member
(Muenduen Phisalaphong, Ph.D.)

..... Member
(Bunjerd Jungsomjit, Ph.D.)

สุจาวี แก้วกัน: ผลของสารตั้งต้นของโคบอลต์ต่อคุณลักษณะและสมบัติในการเร่งปฏิกิริยาของตัวเร่งปฏิกิริยาโคบอลต์บนตัวรองรับ MCM-41 สำหรับปฏิกิริยาไฮโดรจิเนชันของคาร์บอนมอนอกไซด์ (INFLUENCE OF COBALT PRECURSORS ON THE CHARACTERISTICS AND CATALYTIC PROPERTIES OF MCM-41 SUPPORTED COBALT CATALYSTS FOR CARBON MONOXIDE HYDROGENATION). อ. ที่ปรึกษา: ดร. จุงใจ ปั้นประณต, อ. ที่ปรึกษาร่วม: ศ. ดร. ปิยะสาร ประเสริฐธรรม, 152 หน้า. ISBN: 974-17-4424-2

วิทยานิพนธ์นี้ศึกษาผลของสารตั้งต้นของโคบอลต์ต่อคุณลักษณะและสมบัติในการเร่งปฏิกิริยาของตัวเร่งปฏิกิริยาโคบอลต์บนตัวรองรับ MCM-41 สำหรับปฏิกิริยาไฮโดรจิเนชันของคาร์บอนมอนอกไซด์ โดยทำการเตรียมตัวเร่งปฏิกิริยาโคบอลต์บนตัวรองรับ MCM-41 ด้วยสารตั้งต้นของโคบอลต์ที่แตกต่างกันดังต่อไปนี้ โคบอลต์ไนเตรด โคบอลต์คลอไรด์ โคบอลต์อะซิเตรด และโคบอลต์อะซิโตนอะซิโตนเรด พบว่าการใช้สารตั้งต้นอินทรีย์เช่น โคบอลต์อะซิเตรด และโคบอลต์อะซิโตนอะซิโตนเรด จะได้ขนาดของผลึกโคบอลต์ออกไซด์ที่เล็กมากซึ่งไม่สามารถตรวจสอบได้ด้วยเทคนิคการกระเจิงรังสีเอ็กซ์ ถึงแม้ว่าตัวเร่งปฏิกิริยาจะมีปริมาณโคบอลต์ประมาณ 8 เปอร์เซ็นต์โดยน้ำหนักก็ตาม อนุภาคของโคบอลต์นี้มีขนาดเล็กพอที่จะเข้าไปในรูพรุนของตัวรองรับ MCM-41 ได้ และพบว่าตัวเร่งปฏิกิริยาดังกล่าวมีปริมาณการดูดซับด้วยไฮโดรเจนน้อยมากและมีความว่องไวสำหรับปฏิกิริยาไฮโดรจิเนชันของคาร์บอนมอนอกไซด์ต่ำมาก เนื่องจากอาจจะมีสารประกอบโคบอลต์ซิลิเกตเกิดขึ้น การใช้โคบอลต์คลอไรด์เป็นสารตั้งต้นพบว่าได้ผลึกโคบอลต์ออกไซด์ขนาดใหญ่และเหลือคลอไรด์ตกค้าง ซึ่งคลอไรด์ตกค้างนี้ไปขัดขวางตำแหน่งที่ว่องไวของตัวเร่งปฏิกิริยาเป็นผลให้มีพื้นที่ผิวที่ว่องไวต่อการเกิดปฏิกิริยาต่ำ ส่วนเมื่อใช้โคบอลต์ไนเตรดเป็นสารตั้งต้นให้ผลดังนี้ มีอนุภาคโคบอลต์บางส่วนเป็นขนาดเล็กสามารถกระจายตัวผ่านเข้าไปในรูพรุนของตัวรองรับ MCM-41 ได้และมีอีกส่วนที่มีอนุภาคขนาดใหญ่กว่าเกาะอยู่ภายนอกพื้นผิวของตัวรองรับ MCM-41 พบว่าโคบอลต์ไนเตรดเป็นสารตั้งต้นโคบอลต์ที่ดีที่สุดในการเตรียมตัวเร่งปฏิกิริยาโคบอลต์บนตัวรองรับ MCM-41 ซึ่งมีความว่องไวของตัวเร่งปฏิกิริยาสำหรับปฏิกิริยาไฮโดรจิเนชันของคาร์บอนมอนอกไซด์สูงที่สุด นอกจากนี้แรงกระทำระหว่างโลหะโคบอลต์และตัวรองรับยังขึ้นอยู่กับขนาดของอนุภาคโลหะและขนาดรูพรุนของตัวรองรับ จึงเปรียบเทียบคุณสมบัติของตัวเร่งปฏิกิริยา Co/MCM-41 และตัวเร่งปฏิกิริยาโคบอลต์บนตัวรองรับซิลิกาซึ่งมีพื้นที่ผิวสูงและขนาดรูพรุนของตัวรองรับใกล้เคียงกับตัวรองรับ MCM-41 จากผลการทดลอง TPR พบว่าแรงกระทำระหว่างโลหะโคบอลต์และตัวรองรับของตัวรองรับทั้งสองมีลักษณะเหมือนกัน ถึงอย่างไรก็ตาม Co/MCM-41 มีความว่องไวสำหรับปฏิกิริยาไฮโดรจิเนชันของคาร์บอนมอนอกไซด์มากกว่า Co/SiO₂ เนื่องจากมีการกระจายตัวของโลหะโคบอลต์บนตัวรองรับ MCM-41 สูงกว่าบนตัวรองรับซิลิกา การใช้สารตั้งต้นอินทรีย์เช่น โคบอลต์อะซิเตรด และโคบอลต์อะซิโตนอะซิโตนเรด และตัวรองรับที่มีรูพรุนแคบจะส่งผลให้แรงกระทำระหว่างโลหะโคบอลต์และตัวรองรับสูงมาก สรุปว่าตัวเร่งปฏิกิริยาโคบอลต์ที่มีความว่องไวสูงต้องมีความสมดุลระหว่างขนาดของโลหะโคบอลต์ที่เหมาะสม แรงกระทำระหว่างโลหะโคบอลต์และตัวรองรับและไม่ทำให้เกิดสารประกอบโคบอลต์ซิลิเกต

ภาควิชา.....วิศวกรรมเคมี.....

ลายมือชื่อนิสิต.....

สาขาวิชา.....วิศวกรรมเคมี.....

ลายมือชื่ออาจารย์ที่ปรึกษา.....

ปีการศึกษา.....2546.....

ลายมือชื่ออาจารย์ที่ปรึกษาร่วม.....

4570599721 : MAJOR CHEMICAL ENGINEERING

KEY WORDS : COBALT CATALYST PREPARATION/ COBALT PRECURSORS/ MCM-41/
CO HYDROGENATION

SUJAREE KAEWGUN: INFLUENCE OF COBALT PRECURSORS ON THE
CHARACTERISTICS AND CATALYTIC PROPERTIES OF MCM-41 SUPPORTED
COBALT CATALYSTS FOR CARBON MONOXIDE HYDROGENATION. THESIS
ADVISOR: JOONGJAI PANPRANOT, Ph.D., THESIS COADVISOR: PROFESSOR
PIYASAN PRASERTHDAM, Dr.Ing., 152 pp. ISBN: 974-17-4424-2

Co/MCM-41 catalysts were prepared using the incipient wetness impregnation technique with aqueous solutions of different cobalt compounds such as cobalt nitrate, cobalt chloride, cobalt acetate, and cobalt acetylacetonate. MCM-41 is known to have a restricted pore structure; however, using organic precursors such as cobalt acetate and cobalt acetylacetonate resulted in very small cobalt oxide particles that could not be detected by XRD even for a Co loading as high as 8 wt%. These Co particles were small enough to fit into the pores of MCM-41. However, they were found to chemisorb H₂ and CO in only relatively small amounts and to have low activities for CO hydrogenation – probably due to the formation of cobalt silicates. Use of cobalt chloride resulted in very large cobalt particles/clusters and/or residual Cl⁻ blocking active sites, consequently very small active surface area was measurable. Use of cobalt nitrate resulted in a number of small cobalt particles dispersed throughout MCM-41 and some larger particles located on the external surface of MCM-41. Cobalt nitrate appeared to be the best precursor for preparing high activity MCM-41-supported Co FTS catalysts. Furthermore, the metal-support interaction in supported Co Fischer-Tropsch catalysts depends strongly on the metal particle size and pore size of the supports. The properties of Co/MCM-41 catalysts prepared from different Co precursors were then compared to high surface area amorphous Co/SiO₂ catalysts with similar support pore size. High surface area SiO₂ showed similar metal-support interaction to MCM-41-supported catalysts as shown by similar TPR profiles. High activities for Co/MCM-41 catalysts were due primarily to higher Co dispersion in mesoporous structure of MCM-41 than in amorphous SiO₂. Using organic cobalt precursors such as cobalt acetate and cobalt acetylacetonate and narrow pore supports resulted in very small cobalt particles deposited in the pores, leading to stronger metal-support interaction. The results suggest that there is a need for a balance between dispersion-enhancing, metal-support interaction and loss of metallic Co due to metal-support compound formation in order to obtain high activity supported Co catalysts.

Department	Chemical Engineering	Student's signature
Field of Study	Chemical Engineering	Advisor's signature
Academic year	2003	Co-advisor's signature

ACKNOWLEDGEMENTS

The author would like to express her sincere gratitude and appreciation to her advisor, Dr. Joongjai Panpranot, for her invaluable suggestions, stimulating, useful discussions throughout this research and devotion to revise this thesis otherwise it can not be completed in a short time. Without the comments from her co-advisor, Professor Piyan Praserthdam, this work would never have been achieved. The author would like to thank Professor James Goodwin, Jr. from Clemson University, SC, USA for many discussions of this work. The author also would like to thank Professor Abdel Sayari, University of Ottawa, Canada, and Dr. Aticha Chisuwan, Chulalongkorn University, Thailand for the assistance with MCM-41 preparation. In addition, the author would also be grateful to Associate Professor Suttichai Assabumrungrat, as the chairman, and Dr. Muenduen Phisalaphong and Dr. Bunjerd Jungsomjit, as the members of the thesis committee. The supports from TRF and TJTTP-JBIC are also gratefully acknowledged.

Most of all, the author would like to express her highest gratitude to her parents who always pay attention to her all the times for suggestions and have provided her support and encouragement. The most success of graduation is devoted to her parents.

Finally, the author wishes to thank the members of the Center of Excellence on Catalysis and Catalytic Reaction Engineering, Department of Chemical Engineering, Faculty of Engineering, Chulalongkorn University for their assistance especially Dr. Choowong Chaisuk, Dr. Okorn Mekasuwandumrong, Dr. Bongkot Ngamsom, and Miss Kanda Pattamakomsan.

TABLE OF CONTENTS

	Page
ABSTRACT (IN THAI)	iv
ABSTRACT (IN ENGLISH)	v
ACKNOWLEDGEMENTS	vi
TABLE OF CONTENTS	vii
LIST OF TABLES	xi
LIST OF FIGURES	xii
CHAPTERS	
I INTRODUCTION	1
II THEORY	4
2.1 Fischer-Tropsch Synthesis (FTS).....	4
2.2 Co-based catalysts	6
2.3 Ordered Mesoporous Materials	6
III LITERATURE REVIEWS	9
3.1 Synthesis of MCM-41.....	9
3.2 Mesoporous Silica Supported Cobalt Catalysts	10
3.3 Effect of Cobalt Precursors on Supported Cobalt Catalysts	15
IV EXPERIMENTAL	17
4.1 Catalyst Preparation	17
4.1.1 Preparation of Catalyst Support	17
4.1.2 Cobalt Loading.....	18
4.1.3 Catalyst Nomenclature.....	18
4.2 Catalyst Characterization	19
4.2.1 Atomic Adsorption Spectroscopy (AAS).....	19
4.2.2 N ₂ Physisorption	19
4.2.3 X-Ray Diffraction (XRD).....	19
4.2.4 Thermalgravimetric Analysis (TGA).....	19
4.2.5 Temperature Programmed Reduction (TPR).....	20

TABLE OF CONTENTS (Cont.)

	Page
4.2.6 CO-Pulse Chemisorption	20
4.2.7 Hydrogen Chemisorption	20
4.2.8 Scanning Electron Microscopy (SEM), Elemental Mapping, and Energy Dispersive X-Ray Spectroscopy (EDX)	21
4.2.9 Transmission Electron Microscopy (TEM).....	21
4.2.10 Raman spectroscopy.....	21
4.2.11 Acid Leaching	22
4.3 Reaction Study in CO Hydrogenation	23
4.3.1 Materials	23
4.3.2 Equipment.....	23
4.3.2.1 Reactor.....	23
4.3.2.2 Automation Temperature Controller	23
4.3.2.3 Electrical Furnace	24
4.3.2.4 Gas Controlling System.....	24
4.3.2.5 Gas Chromatograph	24
4.3.3 CO hydrogenation procedure.....	24
V RESULTS AND DISCUSSION	27
5.1 Effect of Cobalt Precursors on the Dispersion of Cobalt on MCM-41.....	27
5.1.1 Atomic Adsorption Spectroscopy (AAS).....	27
5.1.2 N ₂ Physisorption	28
5.1.3 X-Ray Diffraction (XRD).....	30
5.1.4 Scanning Electron Microscopy (SEM), Elemental Mapping, and Energy Dispersive X-Ray Spectroscopy (EDX)	35
5.1.5 Transmission Electron Microscopy (TEM).....	45
5.1.6 CO-Pulse Chemisorption	48
5.1.7 Hydrogen Chemisorption	49
5.1.8 Thermalgravimetric Analysis (TGA).....	51

TABLE OF CONTENTS (Cont.)

	Page
5.1.9 Raman Spectroscopy	63
5.1.10 Strong-Metal Support Interaction Effect.....	65
5.2 CO Hydrogenation Activity over Co/MCM-41.....	67
5.2.1 Temperature Programmed Reduction (TPR).....	67
5.2.2 CO Hydrogenation	71
5.2.3 Catalysts Characterization after CO Hydrogenation	73
5.2.3.1 X-Ray Diffraction (XRD).....	73
5.2.3.2 Hydrogen Chemisorption	78
5.2.3.3 Transmission Electron Microscopy (TEM).....	79
5.3 A Comparative Study of Co/MCM-41 and Co/SiO ₂ Catalysts in CO Hydrogenation	84
5.3.1 Characterization of Co/SiO ₂ Catalysts.....	84
5.3.1.1 N ₂ Physisorption	84
5.3.1.2 Atomic Adsorption Spectroscopy (AAS).....	85
5.3.1.3 X-Ray Diffraction (XRD).....	87
5.3.1.4 Scanning Electron Microscopy (SEM) and Elemental Mapping.....	89
5.3.1.5 Transmission Electron Microscopy (TEM).....	97
5.3.1.6 Hydrogen Chemisorption	100
5.3.2 CO Hydrogenation Results over Co/SiO ₂	101
5.3.2.1 CO Hydrogenation	101
5.3.2.2 Temperature Programmed Reduction (TPR).....	104
VI CONCLUSIONS AND RECOMMENDATIONS	109
6.1 Conclusions	109
6.2 Recommendations	111
REFERENCES	112
APPENDICES	
APPENDIX A. CALCULATION FOR CATALYST PREPARATION	118

TABLE OF CONTENTS (Cont.)

	Page
APPENDIX B. CALCULATION OF THE CRYSTALLITE	
SIZE	120
APPENDIX C. CALCULATION FOR METAL ACTIVE	
SITES AND DISPERSION.....	123
APPENDIX D. CALCULATION FOR TOTAL H₂	
CHEMISORPTION AND DISPERSION.....	124
APPENDIX E. CALCULATION FOR REDUCIBILITY.....	125
APPENDIX F. CALIBRATION CURVES.....	127
APPENDIX G. CALCULATION OF CO CONVERSION,	
REACTION RATE AND SELECTIVITY.....	135
APPENDIX D. LIST OF PUBLICATION	137
VITA	152


 สถาบันวิทยบริการ
 จุฬาลงกรณ์มหาวิทยาลัย

LIST OF TABLES

TABLE		Page
4.1	Chemicals used in the synthesis of MCM-41.....	18
4.2	Chemical used in cobalt loading.....	18
4.3	Operating conditions of TCD for TPR and CO-pulse chemisorption....	20
4.4	Operating condition for gas chromatograph.....	25
5.1	Atomic Adsorption Results.....	28
5.2	N ₂ Physisorption Results.....	30
5.3	Elemental analysis using SEM-EDX on different locations of the cross-sectioned catalysts.....	45
5.4	Characterization results of Co/MCM-41 catalysts.....	48
5.5	Results from CO-Pulse Chemisorption.....	49
5.6	Results from H ₂ chemisorption.....	51
5.7	Results from TGA.....	52
5.8	Evidence for “non”-SMSI (strong-metal support interaction).....	65
5.9	Results from TPR.....	69
5.10	Results CO Hydrogenation Reaction at methanation conditions.....	72
5.11	Results from H ₂ chemisorption of the spent catalysts with and re-calcination treatment.....	78
5.12	Co ₃ O ₄ average particle size of Co/MCM-41 catalyst after reduction and reaction with and re-calcination treatment.....	79
5.13	N ₂ physisorption results of Co/SiO ₂ catalysts.....	85
5.14	Atomic adsorption results of Co/SiO ₂ catalysts.....	85
5.15	Comparison of Co ₃ O ₄ Average Particle Size between Co/SiO ₂ and Co/MCM-41.....	87
5.16	Results from H ₂ chemisorption.....	100
5.17	Results CO Hydrogenation Reaction at methanation conditions.....	102
5.18	A comparison of %reducibility of Co/SiO ₂ and Co/MCM-41 from TPR experiments.....	105

LIST OF FIGURES

FIGURE		Page
2.1	Possible mechanistic pathways for the formation of MCM-41.....	8
2.2	Structure model of M41S family.....	8
4.1	Flow diagram of CO hydrogenation system.....	26
5.1	Pore size distribution of MCM-41 and MCM-41-supported Co catalysts.....	28
5.2	Effect of cobalt precursors on the XRD patterns of Co/MCM-41 catalysts (low 2θ).....	32
5.3	Effect of cobalt precursors on the XRD patterns of Co/MCM-41 catalysts (high 2θ).....	33
5.4	XRD pattern of residual Cl ⁻ after calcination at 500°C for 2 h.....	34
5.5	SEM micrographs of catalyst granules for Co/MCM-41.....	36
5.6	Catalyst granule size distribution of MCM-41 supported cobalt catalysts.....	38
5.7	SEM micrographs of Co/MCM-41.....	39
5.8	SEM elemental mapping of Co/MCM-41.....	41
5.9	SEM-EDX of the cross-sectioned Co/MCM-41.....	43
5.10	TEM micrographs of Co/MCM-41.....	46
5.11	Generalized mechanism of chemisorption on Co active sites.....	50
5.12	Thermogravimetric analysis (TGA) experiments for Co precursors (bulk).....	53
5.13	Thermogravimetric analysis (TGA) experiments of Co/MCM-41 in high temperature H ₂ treatment.....	57
5.14	Thermogravimetric analysis (TGA) experiments for MCM-41 in air.....	61
5.15	Thermogravimetric analysis (TGA) experiments for MCM-41 in high temperature H ₂ treatment.....	62
5.16	Raman spectra of different Co precursors of MCM-41-supported Co catalysts.....	64

LIST OF FIGURES (Cont.)

FIGURE	Page
5.17	TPR profiles of the Co/MCM-41 catalysts with different Co precursors.....70
5.18	XRD results for acid-leached MCM-41-supported Co catalysts.....75
5.19	XRD results for the spent MCM-41 supported Co catalysts after reduction and reaction without re-calcination treatment.....76
5.20	XRD results for spent Co/MCM-41 catalysts after reduction and reaction with re-calcination treatment at 500°C 2 hrs.....77
5.21	TEM micrographs of calcined spent Co/MCM-41.....80
5.22	Raman spectra of Co/M-Ac after reduce in flow H ₂ at 500°C 10h.....83
5.23	Pore size distribution of MCM-41 and SiO ₂ support.....86
5.24	Effect of cobalt precursors on the XRD patterns of Co/SiO ₂ catalysts (high degree 2θ).....88
5.25	SEM micrographs of catalyst granules for Co/SiO ₂90
5.26	Catalyst granule size distribution of SiO ₂ supported cobalt catalysts.....92
5.27	SEM micrographs of Co/SiO ₂93
5.28	SEM elemental mappings of cobalt on the exteriors of Co/SiO ₂95
5.29	TEM micrographs of Co/SiO ₂98
5.30	CO hydrogenation activities at 220°C, 1 atm, H ₂ /CO = 10.....103
5.31	TPR profiles of the Co/SiO ₂ catalysts with different Co precursors.....106
5.32	Temperature program reduction (TPR) profiles of Co/MCM-41 and Co/SiO ₂ catalysts prepared with different cobalt precursors107

CHAPTER I

INTRODUCTION

Production of hydrocarbons from synthetic gas (CO+H₂) through Fischer-Tropsch synthesis (FTS) has received much attention in both catalysis and chemical engineering fields due to the potential of the technology providing an optional route for liquid fuel production (Schulz, 1999). The high quality FTS product as transportation fuel has been proven to be environmentally friendly compared with those from conventional crude oil route, for example, Shell's SMDS (Shell Middle Distillate Synthesis) technology in Malaysia has been able to produce high quality diesel fuel (Sie *et al.*, 1991). Another factor that make FTS an important technique is the fact that there are abundant of coal and natural gas reserves in many remote locations around the world that are being under-utilized to supply as the feed of FTS (Jess *et al.*, 1999).

Cobalt-based catalysts are widely used in Fischer-Tropsch synthesis based on natural gas-derived synthetic gas because of their high activity and selectivity for making long chain paraffins, low water-gas shift activity, and relatively low price compared to noble metal such as Ru (Reuel and Bartholomew, 1984; Backman *et al.*, 1998; Haddad *et al.*, 1995). As is generally true in hydrogenation reactions, the active phase of cobalt for FTS is metallic cobalt. Having the cobalt well-dispersed and reduced is required for a catalyst to have high activity. The metal surface areas can be increased by dispersing the cobalt precursor on high surface area supports such as silica and alumina. Several methods can be used to deposit the metal on the surface of the support. These include precipitation, ion exchange, and impregnation. Due to its simplicity, the most frequently used method in laboratories is incipient wetness impregnation, in which a metal salt dissolved in a solvent, usually water, is added to the support in an amount equal to the pore volume of the support. Subsequently, the solvent is removed and the precursor is reduced to obtain the active metal catalyst. A calcination step may be introduced after drying the precursor material. The activity of supported Co catalysts is proportional to the number of exposed cobalt atoms. A requirement for highly active Co catalyst is therefore a high dispersion of cobalt metal.

Support effects in Fischer-Tropsch synthesis (FTS) catalysts have been investigated. The non-uniform pore size distribution of supports, such as Al_2O_3 , SiO_2 , TiO_2 , and ZrO_2 , etc., usually leads to a wide distribution of hydrocarbon products. Zeolite-supported catalysts were found to produce lighter and more highly branched products due to the secondary acid-catalyzed reactions of the primary F-T products in the zeolite pores (Bessell, 1993). Support physical structure also can have an effect on the reaction products diffusion and subsequent readsorption by modifying the residence times of hydrocarbons in the catalyst, resulting in longer chain hydrocarbons (C_{5+}) (Brady and Petit, 1981; Iglesia *et al.*, 1992; Iglesia *et al.*, 1993; Koh *et al.*, 1995).

A new class of mesoporous molecular sieve materials designated as MCM-41 was first reported in 1992 by the researchers of the Mobil Oil Corporation, USA (Kresge *et al.*, 1992). The structure of MCM-41 consists of uniform cylindrical pores arranged in a hexagonal array. The pore dimensions can be tailored in the range of 1.5-10 nm depending on synthesis chemicals and conditions. The BET surface area is usually greater than $1000 \text{ m}^2/\text{g}$ with high sorption capacities of 0.7 ml/g. It can also be synthesized in a large range of framework Si/Al ratio, therefore, can develop acid sites of different strengths. MCM-41 has been studied as a catalyst, a catalyst support, and a sorbent (Zhao *et al.*, 1996).

Recently, the use of high surface area ordered mesoporous materials such as MCM-41 and SBA-15 for preparing Co-based Fischer-Tropsch catalysts has been explored (Yin *et al.*, 2001; Panpranot *et al.*, 2002; Wang *et al.*, 2001; Khodakov *et al.*, 2002; Martinez *et al.*, 2003). Compared to amorphous silica-supported catalysts with similar Co loading, Co supported on these mesoporous materials have shown higher FTS activity due to a better dispersion of cobalt in mesoporous structure. However, stronger interaction of cobalt species and the support in these catalysts were often found, resulted in catalysts with lower reducibilities. Such catalysts showed higher activity compared to conventional catalysts (Song and Reddy, 1999). In a previous study, Panpranot *et al.*, 2002 reported that CoRu/MCM-41 prepared from Co and Ru nitrate resulted in a higher FTS activity compared to CoRu/ SiO_2 catalysts prepared with the same precursors. However, cobalt was found to concentrate more toward the external surface area than in the interior of MCM-41. It is know that metal dispersion and catalytic activity of

supported metal catalysts also depend on the type of metal precursors. For example, titania-supported Co catalysts prepared from Co oxalate, Co acetate, and Co acetyl acetonate resulted in a higher FTS activity than the ones prepared from cobalt nitrate due to higher cobalt dispersion (Kraum and Baerns, 1999). However, less is known about the influence of cobalt precursors on the dispersion of cobalt when restricted pore structure supports such as MCM-41 are used.

This study is aimed to investigate the impact of different organic and inorganic cobalt precursors on the characteristic and the catalytic properties of MCM-41-supported cobalt catalysts. Selection of a proper Co precursor will produce a catalyst with higher Co dispersion and consequently a better performance. In addition, the effects of pore structure, pore size as well as the cobalt precursors on the metal-support interaction in supported Co F-T catalysts were extensively investigated.



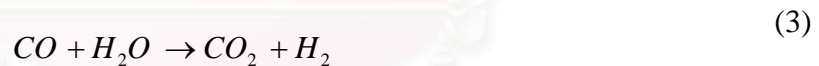
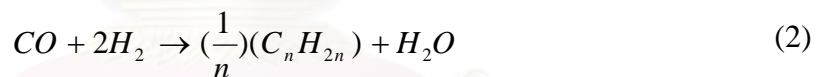
สถาบันวิทยบริการ
จุฬาลงกรณ์มหาวิทยาลัย

CHAPTER II

THEORY

2.1 CO Hydrogenation Reaction or Fischer-Tropsch synthesis (FTS)

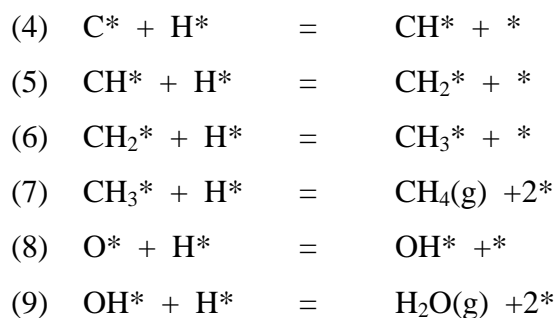
CO Hydrogenation Reaction or Fischer-Tropsch synthesis (FTS), the production of liquid hydrocarbons from synthesis gas (CO and H₂) is a promising, developing route for environmentally sound production of chemicals and fuels from coal and natural gas. During the past decades, FTS has been developed continuously by many researchers, although the rise and fall in research intensity on this process has been highly related to the demands for liquid fuels and relative economics. This synthesis is basically the reductive polymerization (oligomerization) of carbon monoxide by hydrogen to form organic products containing mainly hydrocarbons and some oxygenated products in lesser amounts. The main reactions of FTS are:



Equations (1) is the formation of methane, the equation (2) is the synthesis of hydrocarbons higher than methane, the equation (3) is the water-gas shift reaction, and the equation (4) is the Boudouard reaction resulting in which results in deposition of carbon.

The reaction mechanism of methanation can be described by the following set of mechanism:





Normally, catalysts used for FTS are group VIII metals. By nature, the hydrogenation activity increases in order of $\text{Fe} < \text{Co} < \text{Ni} < \text{Ru}$. Ru is the most active. Ni forms predominantly methane, while Co yields much higher ratios of paraffins to olefins and much less oxygenated products such as alcohols and aldehydes than Fe does.

Commercially, Entrained bed reactors or slurry bubble column reactors are used in FTS since they can remove heat from this exothermic synthesis, allowing better temperature control.

The current main goal in FTS is to obtain high molecular weight, straight chain hydrocarbons. However, methane and other light hydrocarbons are always present as less desirable products from the synthesis. According to the Anderson-Schulz-Flory (ASF) product distribution, typically 10 to 20% of products from the synthesis are usually light hydrocarbon ($\text{C}_1\text{-C}_4$). These light alkanes have low boiling points and exist in the gas phase at room temperature, which is inconvenient for transportation. Many attempts have been made to minimize these by-products and increase the yield of long chain liquid hydrocarbons by improving chain growth probability. It would be more efficient to be able to convert these less desirable products into more useful forms, rather than re-reforming them into syngas and recycling them (Farrauto and Bartholomew, 1997). Depending upon the type of catalyst used, promoters, reaction conditions (pressure, temperature and H_2/CO ratios), and type of reactors, the distribution of the molecular weight of the hydrocarbon products can be noticeably varied.

2.2 Co-based FTS catalysts

Supported cobalt (Co) catalysts are the preferred catalysts for the synthesis of heavy hydrocarbons from natural gas based syngas (CO and H₂) because of their high Fischer-Tropsch (FT) activity, high selectivity for linear hydrocarbons, and low activity for the water gas shift reaction. It is known that reduced cobalt metal, rather than its oxides or carbides, is the most active phase for CO hydrogenation. Investigations have been done to determine the nature of cobalt species on various supports such as alumina, silica, titania, magnesia, carbon, and zeolites. The influence of various types of cobalt precursors used was also investigated. It was found that the used of organic precursors such as Co (III) acetyl acetate resulting in an increase of CO conversion compared to that of cobalt nitrate (Kraum and Baerns, 1999).

2.3 Ordered Mesoporous Materials

According to the definition of IUPAC, mesoporous materials are those that have pore diameters between 20 and 500 Å. Examples of mesoporous solids include silica gel and modified layered materials, but the pores in these materials are irregularly spaced and usually have a wide distribution of pore sizes. A considerable synthetic effort has been devoted to developing highly uniform frameworks with pore diameters within the mesoporous range. The structure of this mesoporous silicate and aluminosilicate family that has received the most attention is referred to as MCM-41, which consists of uniform cylindrical pores arranged in a hexagonal array. The pore dimensions can be tailored in the range of 1.5-10 nm depending on synthesis chemicals and conditions. The BET surface area is usually greater than 1000 m² /g with high sorption capacities of 0.7 ml/g.

The MCM-41 mesoporous structure is based upon biomineralization and biomimetic chemistry in which organic and inorganic species interact and self-assemble into nanosize structures. A typical synthesis starts with preparation of an aqueous surfactant solution. A silica source, combined with an acid or base liquid catalyst to aid in the polymerization of the silica, is then added to the aqueous

surfactant solution. The slurry is stirred vigorously at room temperature. During the mixing, the hydrophilic heads of the surfactant will interact with the silica in the solution by electrostatically attracting silica molecules to the micelle surface. The solution is then heated under autogeneous pressure at temperatures of 100-200 °C for 24 to 48 hours. At these elevated temperatures, the silica extensively polymerizes and condensed around the micelles. The interaction of the inorganic and organic phases is believed to align the micelles via a self-assembly mechanism to form the as-synthesized mesostructured composite. Subsequent removal of the organic surfactant by calcination in air or by solvent extraction creates the highly ordered mesoporous structure. Beck et al.(1992) proposed two possible mechanistic pathways: (1) a liquid crystal templating mechanism, where the MCM-41 structure is formed around micelles existing as single cylindrical aggregates; (2) a mechanism where the addition of the silicate results in the ordering of the subsequent silicate-encaged surfactant micelles. A schematic of this formation mechanism is shown in Figure 2.1.

The synthesis of these mesoporous materials has been found to be a strong function of several variables in the system (Corma, 1997; Kruk *et al.*, 1999; Carrott *et al.*, 1999; Chen *et al.*, 1997; Liepold *et al.*, 1996; Kruk *et al.*, 2000). The surfactant-to-silica ratio in the synthesis mixture has been identified as capable of determining the type of mesoporous structure formed. Typically, this molar ratio is less than or equal to 0.5 for MCM-41 formation. At values greater than 0.5, other mesostructures i.e., cubic symmetry MCM-48 and Lamellar symmetry MCM-50, have been reported and shown in Figure 2.2. The basicity, temperature, and time also determine the rate of polymerization of the silica precursor.

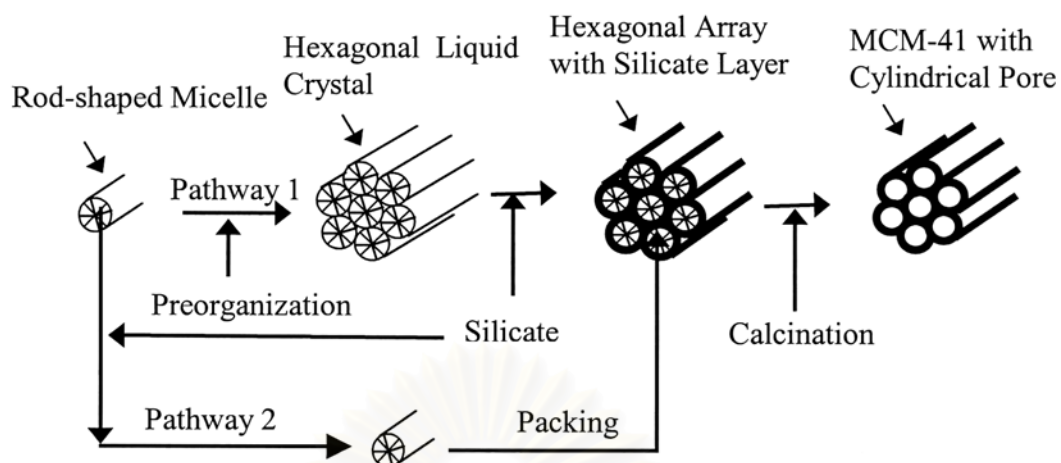


Figure 2.1 Possible mechanistic pathways for the formation of MCM-41: (1) liquid crystal initiate and (2) silicate anion initiate

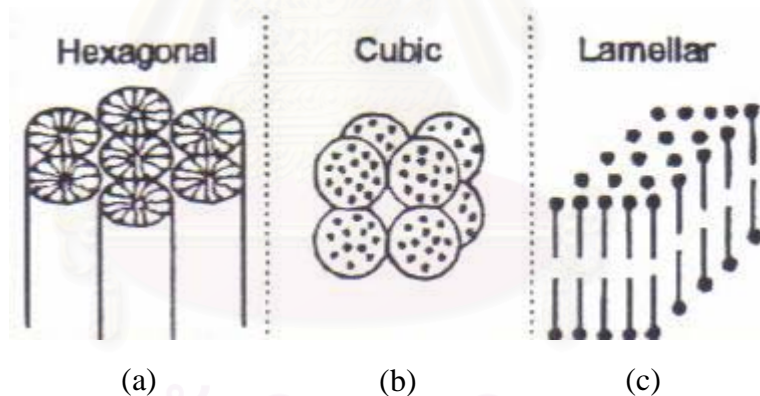


Figure 2.2 Structure model of M41S family (a) MCM-41, (b) MCM-48, and (c) MCM-50.

CHAPTER III

LITERATURE REVIEWS

This chapter reviews the works about several synthesis methods of MCM-41. Mesoporous silica supported cobalt catalysts have been applied in many reactions such as FTS, methanation, sulfidation, reaction of NO_x with propane, Pauson-Khand reaction, liquid phase oxidation with H₂O₂ and hydrodesulfurization. The last section of this review shows a few research investigations about the effect of cobalt precursors on supported cobalt catalysts.

3.1 Synthesis of MCM-41

Mesoporous silica can be prepared by a variety of procedures and over a wide range of compositions using various different surfactant templates. These syntheses are covered in this review.

C. T. Kresge et al. (1992) studied a new synthetic composition of ultra-large pore crystalline material and use thereof as sorbent and in catalytic conversion of organic and inorganic compounds. The new crystalline material exhibits unusually large sorption capacity demonstrated by its benzene adsorption capacity of greater than about 15 grams benzene/100 grams at 50 torr and 25°C, a hexagonal electron diffraction pattern that can be indexed with a *d*₁₀₀ value greater than about 18 Å and a hexagonal arrangement of uniformly sized pores with a maximum perpendicular cross section of at least about 13 Å.

J. S. Beck et al. (1992) synthesized a new synthetic composition of ultra-large pore crystalline material. This material is called M41S family. Different mesostructures have been named as MCM-41 (hexagonal), MCM-48 (cubic), and MCM-50 (lamellar).

X. S. Zhao *et al.* (1996) studied the characteristic of mesoporous molecular sieves, MCM-41, which possesses a regular hexagonal array of uniform pore openings. They

presented a comprehensive overview of recent advances in the field of MCM-41 and showed formation mechanisms.

A. Corma (1997) prepared new materials containing stronger Bronsted sites in the pillars. They not only combine three well-defined porosities in the range of 3.0-6.0 nm (mesopores formed by the ordering of layers), 1.2 nm (corresponding to the galleries between pillars), and 0.4-0.7 nm (pores in the potential microporous layer), but also improve the stability of the resultant materials. The introduction of M41S type materials has opened a very complete new field for preparing mesoporous materials. Besides an even better knowledge of the mechanism of formation, it would be highly desirable to produce highly thermally and hydrothermally stable materials. Possible research directions include achieving a better polymerization in the walls with fewer connectivity defects and increasing the size of the walls.

3.2 Mesoporous Silica Supported Cobalt Catalysts

Many studies have been done on noble metals, i.e., Pt, Pd, and Rh supported on MCM-41. However, only a few reports have appeared on the use of mesoporous MCM-41 as a support for non-noble metals, especially cobalt.

A. Jentys *et al.* (1996) reported the synthesis and characterization of mesoporous materials containing highly dispersed cobalt that were prepared by direct addition of CoCl_2 to the synthesis gel. The pore volume and the surface area of this material were slightly smaller compared to MCM-41 indicating that indeed Co is placed inside the pores. During reduction in H_2 at 673 K and sulfidation in $\text{H}_2\text{S}/\text{H}_2$ at 673 K the initial particle size of about 5 to 6 Co atoms did not increase. This indicates that the Co clusters retain their size for longer period of time on stream within the MCM-41 channels. The reason for this high stability of Co clusters in MCM-41 lies in the strong interaction of Co with the lattice.

W. Schieber *et al.* (1998) reported a comparison of Pt, Rh, and Co supported on siliceous MCM-41 for the catalytic reduction of NO_x with propene. Co/MCM-41 was found to have a low level of activity for such reaction.

A. Jentys *et al.* (1998) investigated the structure properties of Co/MCM-41 with pore diameters between 2.9 and 3.6 nm prepared by direct synthesis and impregnation. For both preparation methods, the size of the metal particles decreased with the pore diameter. For Co/MCM-41 with the same pore diameter they observed that the direct synthesis method led to significantly smaller metal clusters compared to the impregnation method.

T. Iwasaki *et al.* (1998) reported the use of silicate crystallite mesoporous materials (SCMM) as the support of 5 wt% Co catalysts. The conversion of CO was higher on SCMM than that of silica gel. When the reactions were carried out at high pressure (2.1 MPa), the pore size and surface negative charge characteristics in SCMM also affected the selectivity of hydrocarbons. The product distribution obtained using Co/SCMM was found to deviate from the classic ASF straight line. The heavier hydrocarbons ($>C_{10}$) were inhibited from being formed. However, they did not address the issue of pore condensation, which probably could occur and would result in only an apparent chain limitation in the hydrocarbon chain growth.

C. Song and K. M. Reddy (1999) studied MCM-41 supported Co-Mo catalysts for hydrodesulfurization of petroleum residuals. High metal loaded Co-Mo/MCM-41 catalysts prepared by impregnation showed higher hydrogenation and hydrocracking activities than conventional Co-Mo/Al₂O₃ catalysts.

S. W. Kim *et al.* (2000) reported metallic cobalt supported on mesoporous silica MCM-41 for the Pauson-Khand reaction (cycloaddition of alkynes with alkenes and carbon monoxide to cyclopentanones).

S. Suvanto and T.A. Pakkanen (2000) studied SiO₂ and MCM-41 supported cobalt catalysts prepared by gas phase deposition of Co₂(CO)₈. The effects of direct and pulsing gas phase deposition methods on reactivity of the Co/MCM-41 and Co/SiO₂ samples toward oxygen and hydrogen treatments were investigated. It was found that the reducibility of the samples decreased in the order: MCM-41 + pulsing method > SiO₂ + pulsing method > SiO₂ + direct method > MCM-41 + direct method. Oxygen/hydrogen consumptions of the samples decreased in the decarbonylation atmosphere inert >

oxidizing > reducing. Co/SiO₂ and Co/MCM-41 samples prepared via pulsing method indicated a good stability during oxidation/reduction treatments.

S. Suvanto *et al.* (2000) reported the preparation of Co/MCM-41 samples by deposited Co₂(CO)₈ from the gas phase onto the MCM-41 surface in a fluidized bed reactor. Two different kinds of preparation methods were used, direct deposition in order to achieve the monolayer coverage of Co₂(CO)₈ with one deposition treatment and the pulse deposition method to further increase the metal loading on the support. The results of IR spectroscopy indicated that all silanols are accessible to the cobalt carbonyl. According to the N₂ adsorption/desorption studies, the surface area and pore size distribution were almost unaffected even in the case of high cobalt loadings.

D. Yin *et al.* (2001) have synthesized hexagonal mesoporous silica (HMS) and used it as a support of 15% Co catalysts. HMS is different from MCM-41 in part by its thicker framework wall and smaller domain size with shorter channels. High CO conversion and high yield of hydrocarbons were obtained at high pressure (2 MPa). They have concluded that HMS materials facilitate the reactants to access the active sites, permit better transport of higher hydrocarbon products, and diminish secondary reactions, such as cracking and isomerization of long chain hydrocarbons, from occurring in channel.

A. Y. Khodakov *et al.* (2001) studied the effect of porosity in a wide range of mesopore diameters ($d_p = 20\text{-}330 \text{ \AA}$) on the dispersion and reducibility of cobalt species in mesoporous silicas. It is shown that modification of mesoporous silicas by cobalt via aqueous impregnation results in small Co₃O₄ crystallites located in the pores of silicas. An increase in the pore sizes of the supports leads to both an increase in Co₃O₄ particle sizes and the reducibility of intermediary CoO particles. The extent of Co reduction rises sharply as the pore sizes in mesoporous silicas become large than 50 Å.

V. Parvulescu and B.-L. Su (2001) studied the effect of incorporated metal, Fe-MCM-41, Co-MCM-41, and Ni-MCM-41 catalysts, on the MCM-41 surface hydroxyl groups. The catalyst activity and selectivity of these catalysts in liquid phase oxidation of 1-hexene, styrene and benzene with hydrogen peroxide were studied. The structure and morphology of the catalysts before and after reaction were also compared. The results

showed a high activity and selectivity of catalysts having higher Co content to benzaldehyde from styrene or phenol from benzene, and a low activity of all the catalysts in the oxidation of the 1-hexene. The activity and efficiency of H_2O_2 increases with the metal content and depend on the reaction parameters.

A. Y. Khodakov *et al.* (2002) reported pore size effect on Fisher Tropsch reaction rate and selectivities over cobalt catalysts using periodic (SBA-15 and MCM-41) and commercial mesoporous silica as catalyst supports. Catalytic experiments showed that Co species located in the narrow pore silicas were much less active in Fischer Tropsch synthesis and produce methane with selectivities higher than larger cobalt particle in the wide pore supports. Lower FT activities and higher methane selectivities observed on the narrow pore cobalt catalysts are principally attributed to lower reducibility of small cobalt particles.

J. Panpranot *et al.* (2002) reported that CoRu/MCM-41 prepared from Co and Ru nitrate resulted in a higher FTS activity compared to CoRu/SiO₂ catalysts prepared with the same precursors. However, cobalt was found to concentrate more toward the external surface area than in the interior of MCM-41.

J. Panpranot *et al.* (2002) studied CO hydrogenation on MCM-41 and SiO₂-supported Ru-promoted Co catalysts. The activity was found to vary in the order 14CoRu/M1 (small pore) \approx 14CoRu/M2 (large pore) > 14CoRu/S for FTS conditions, and 14CoRu/M1 > 14CoRu/M2 > 14CoRu/S for methanation conditions.

J. Panpranot *et al.* (2003) studied the effect of H₂ partial pressure on surface reaction parameters during CO hydrogenation on Ru-promoted silica-supported Co catalysts. They found that the increase in rate with increasing hydrogen partial pressure resulted due to the increase in methane surface intermediates and, more importantly, the increase in hydrogen surface concentration.

U. T. Turaga and C. Song (2003) investigated the activity of a mesoporous molecular sieve MCM-41-supported Co-Mo catalyst in comparison to a commercial γ -alumina (Al₂O₃)-supported Co-Mo catalyst for the desulfurization of a light cycle oil

(LCO) with a sulfur content of 2.19 wt.%. The MCM-41-supported catalyst demonstrates consistently higher activity for the deep hydrodesulfurization (HDS) of the refractory dibenzothiophenic sulfur compounds.

V. Parvolescu *et al.* (2003) proposed a comparative study of a series of Nb- and NbCo-containing mesoporous catalysts with variable Nb/Si molar ratios and two different preparing methods of MCM-41 with hydrothermal treatment. A highly ordered hexagonal arrangement of the pores has been hydrothermally synthesized from sodium silicate or tetraethylortosilicate (TEOS). XRD and TEM confirm the ordered mesoporous structure of all the Nb-MCM-41 and NbCo-MCM-41 samples prepared (except NbCoS sample prepared with sodium silicate) with TEOS and sodium silicate as silica source. The incorporation of metal ions is favored with sodium silicate as silica source while a less well ordered structure is obtained. All the materials synthesized show a high activity in oxidation of styrene and a low and very low activity in oxidation of benzene and toluene, respectively, with H₂O₂. It is surprising that the amorphous catalyst with NbCo gives the highest activity.

A. Y. Khodakov *et al.* (2003) studied the effect of support mesoporous structure and cobalt dispersion and reducibility using two series of Fischer-Tropsch (FT) silica supported cobalt catalysts. The first series of catalysts was SBA-15 periodic mesoporous silica with narrow pore size distribution, the second series was supported by a commercial mesoporous silica with broader pore size distribution. Co dispersion was higher in Co catalysts supported by the SBA-15 silica with a pore diameter of 9.1 nm than in the commercial mesoporous silica with average pore diameter of 33 nm. In the range of cobalt surface densities from 5 to 15 Co/nm², higher Fischer-Tropsch reaction rates were observed over cobalt catalysts supported by the SBA-15 periodic mesoporous silica. This effect was attributed to higher cobalt dispersion on these catalysts.

P. Karandikar *et al.* (2004) synthesized copper and cobalt (salen) complexes immobilized on the walls of MCM-41 modified with aminopropyl groups. FT-IR and UV-Vis spectra show evidence of adduct formation of the amino group through the axial coordination with the metal which enhances the catalytic activity. The molecular dispersion of the complex with sufficient void space and the hydrophobic surface are

appropriate for activation of hydrocarbons as evidenced by higher TON on immobilization.

3.3 Effect of Cobalt Precursors on Supported Cobalt Catalysts

M. P. Rosynek and C. A. Polansky (1991) studied the effect of cobalt source on the reduction properties of silica-supported cobalt catalysts. TPR, XPRD, and XPS were used to characterize the reduction, calcination, and catalytic behaviors of a series of 6 wt% Co/SiO₂ catalysts prepared from nitrate, chloride, and acetate precursors. The bulk reduction properties of the silica-supported, uncalcined nitrate and acetate precursors are similar; both involve multiple steps and are much more resistant to complete reduction by H₂ to metallic than are the corresponding unsupported salts. By contrast, reduction of CoCl₂/SiO₂ occurs in a single step that is virtually unaffected by the presence of the silica support.

M.K. Niemela *et al.* (1996) reported the effect of the precursor on the characteristics of the Co/SiO₂ catalysts prepared from Co(NO₃)₂, Co₂(CO)₈ and Co₄(CO)₁₂. The hydrogen chemisorption, CO desorption, XRD and XPS measurements indicated that the dispersion of the metallic species decreased in the precursor order Co₂(CO)₈ > Co₄(CO)₁₂ >> Co(NO₃)₂.

E.V.Steen *et al.* (1996) investigated the influence of different steps in the preparation of impregnated Co/SiO₂ catalysts by incipient wetness on the reducibility of the catalyst precursor and on the formation of cobalt silicates. The TPR spectra of cobalt catalysts starting from chloride or sulphate are essentially the same as for the unsupported metal salt showing negligible interaction between the support and the salt. In the case of the nitrate or acetate precursor, however, a number of peaks can be seen in the TPR-spectra indicating the formation of different cobalt species during the preparation steps. The TPR-spectra of the nitrate and the acetate precursors are very similar, with only the intensities of the peaks differing markedly.

M. Kraum and M. Baerns (1999) studied the influence of various cobalt compounds applied in the preparation of titania-supported cobalt catalysts on their

performance. The use of oxalate, acetate and acetylacetonate as cobalt precursors resulted in a higher activity compared with reference catalyst prepared from nitrate.

C. J. Huang *et al.* (2000) reported the cobalt precursor affects the catalytic performance of Co/SiO₂ catalyst remarkably for CO₂ reforming of CH₄. This paper compared the activity between cobalt nitrate/SiO₂ and cobalt acetate/SiO₂ catalysts at different cobalt contents and reaction temperature. It was found that the activity of Co(A)/SiO₂ is higher than Co(N) /SiO₂, especially at high cobalt content and low temperature.

A. Martinez *et al.* (2003) reported that Co/SBA-15 catalysts at similar cobalt loading (20 wt%), a much better dispersion and a stronger cobalt-support interaction leading to the formation of low reducible cobalt silicates was observed for oxidized samples prepared from acetate and acetylacetonate precursors as compared to that derived from cobalt nitrate, as evidenced by TEM, XPS, and TPR.

CHAPTER IV

EXPERIMENTAL

This chapter describes the experimental systems and procedures used in this study. The chapter is divided into three parts; (1) catalyst preparation (2) catalyst characterization and (3) reaction study. The first part (section 4.1) presents catalyst preparation including preparation of MCM-41 support, cobalt loading and catalyst nomenclature. The second part (section 4.2) shows the details of characterization techniques such as AAS, BET, XRD, TGA, TPR, CO-pulse chemisorption, SEM, and TEM. And the last part (section 4.3) illustrates the reaction study in CO hydrogenation.

4.1 Catalyst Preparation

4.1.1 Preparation of Catalyst Support

Pure silica MCM-41 with 3 nm pore diameter was prepared in the same manner as that of Cho et al. (Cho *et al.*, 2000) using the gel composition of CTABr: 0.3 NH₃: 4 SiO₂: Na₂O: 200 H₂O, where CTABr denotes cetyltrimethyl ammonium bromide. Briefly, 20.03 g of colloidal silica Ludox AS 40% (Aldrich) was mixed with 22.67 g of 11.78% sodium hydroxide solution. Another mixture comprised of 12.15 g of CTABr (Aldrich) in 36.45 g of deionized water, and 0.4 g of an aqueous solution of 25% NH₃. Both of these mixtures were transferred into a Teflon lined autoclave, stirred for 30 min, then heated statically at 100°C for 5 days. The pH of the gel was adjusted to 10.2 using 30% acetic acid every 24 h. The obtained solid material was filtered, washed with water until no base was detected and then dried at 100°C. The sample was then calcined in flowing nitrogen up to 550°C (1-2 °C/min), then in air at the same temperature for 5 hours. The chemicals used in the synthesis of MCM-41 are shown in Table 4.1. For comparison purposes, amorphous silica small pore (Davison Chemical) was also used as a catalyst support.

4.1.2 Cobalt Loading

Series of Co/MCM-41 and Co/SiO₂ catalysts were prepared by the incipient wetness impregnation of the supports with aqueous solution of different cobalt precursors such as Co(NO₃)₂· 6H₂O, CoCl₂· 6H₂O, Co(CH₃COCH=COCH₃)₂ and Co(CH₃COO)₂· 4H₂O. Cobalt loading was approximately 8% by weight of catalyst. The samples were dried at 110°C for 1 day and then were calcined in air at 500°C for 4 h. Finally, the catalysts were cooled down and stored in desiccators. The chemicals used in cobalt loading are shown in Table 4.2.

Table 4.1 Chemicals used in the synthesis of MCM-41

Chemical	Supplier
cetyltrimethyl ammonium bromide	Aldrich
colloidal silica Ludox AS 40%	Aldrich
aqueous solution of 25% NH ₃	BDH
30% acetic acid	Carlo Erba

Table 4.2 Chemical used in cobalt loading

Chemical	Supplier
cobalt (II) nitrate hexahydrate	Aldrich
cobalt (II) chloride hexahydrate	Fluka
cobalt (II) acetyl acetonate	Aldrich
cobalt (II) acetate. tetrahydrate	APS

4.1.3 Catalyst Nomenclature

The catalysts with different cobalt precursors are respectively designated as Co/M-NO, Co/M-Cl, Co/M-AA and Co/M-Ac in which Co/M refers to cobalt supported on MCM-41 and the last two letters reflect the type of the cobalt precursor

used: NO for cobalt nitrate, Cl for cobalt chloride, AA for cobalt acetyl acetonate and Ac for cobalt acetate. Co catalysts supported on silica small pore (SiO_2) catalysts are referred to Co/S-NO, Co/S-Cl, Co/S-AA and Co/S-Ac.

4.2 Catalyst Characterization

4.2.1 Atomic Adsorption Spectroscopy (AAS)

AAS was performed to determine the composition of elements in the bulk of catalysts. The composition content of catalysts was collected using Varian, Spectra A800 at the Department of Science Service Ministry of Science Technology and Environment.

4.2.2 N_2 Physisorption

The BET surface area, pore volume, average pore diameter, and pore size distribution of the catalysts were determined by N_2 physisorption using a Micromeritics ASAP 2000 automated system. Each sample was degassed in the Micromeritics ASAP 2000 at 150°C for 4 hours prior to N_2 physisorption.

4.2.3 X-Ray Diffraction (XRD)

The XRD spectrum of the catalysts were collected using an X-ray diffractometer, SIEMENS D5000, using $\text{Cu K}\alpha$ radiation with Ni filter, accurately measured in the $2-8^\circ$ or $10-80^\circ$, 2θ angular region.

4.2.4 Thermalgravimetric Analysis (TGA)

TGA was used to determine the weight loss pattern and the reducibility of catalysts by Shimadzu TGA model 50. The catalyst sample of ca. 10-20 mg and temperature ramping from 35°C to 700°C at $10^\circ\text{C}/\text{min}$ were used in the operation. The carrier gas was H_2 UHP.

4.2.5 Temperature Programmed Reduction (TPR)

TPR was used to determine the reducibility of catalysts. The catalyst sample of ca. 100 mg and temperature ramping from 35°C to 800°C at 10°C/min were used in the operation. The carrier gas was 5 %H₂ in Ar. During reduction, a cold trap was placed to before the detector to remove water produced. A thermal conductivity detector (TCD) was used to measure the amount of hydrogen consumption. The operating condition of the TCD is shown in Table 4.3. The amount of hydrogen consumption was calibrated using bulk cobalt oxide (Co₃O₄) at the same conditions.

4.2.6 CO-Pulse Chemisorption

Cobalt dispersion was determined by pulsing carbon monoxide over the reduced catalyst. Approximately 0.2 g of catalyst was filled in a quartz tube, incorporated in a temperature-controlled oven and connected to a thermal conductivity detector (TCD). The carrier gas was helium. Prior to chemisorption, the catalyst was reduced in a flow of hydrogen (50 cc/min) at 350°C for 2 h. Afterward, the sample was purged with helium at 350°C for 1 h and finally cooled down to room temperature. Carbon monoxide was pulsed at 25°C over the reduced catalyst until the TCD signal was constant. The operating condition of the TCD is also shown in Table 4.3.

Table 4.3 Operating conditions of TCD for TPR and CO-pulse chemisorption

Detector	TCD
Carrier gas flow	30 ml/min
Detector temperature	80°C
Detector current	80 mA

4.2.7 Hydrogen Chemisorption

Static H₂ chemisorption at 100 °C on the reduced catalysts (re-reduced at 350°C for 10h) was used to determine the number of reduce surface cobalt metal atoms and overall cobalt dispersion. The total hydrogen chemisorption was calculated from the number of injection of a known volume. H₂ chemisorption was carried out following the procedure described by Reuel and Bartholomew (1984) using a Micromeritics Pulse Chemisorb 2700 instrument at the Analysis Center of Department of Chemical Engineering, Faculty of Engineering, Chulalongkorn University. Prior to chemisorption, the catalysts were reduced at 350°C for 10 hours after ramping up at a rate of 1°C/min. Details of calculation of the total hydrogen chemisorption and % Co dispersion are given in Appendix D.

4.2.8 Scanning Electron Microscopy (SEM), Elemental Mapping, and Energy Dispersive X-Ray Spectroscopy (EDX)

Catalyst granule morphology and elemental distribution were obtained using a JEOL JSM-35CF scanning electron microscope at the Scientific and Technological Research Equipment Centre, Chulalongkorn University (STREC), Bangkok, Thailand. The SEM was operated using the back scattering electron (BSE) mode at 20 kV. After a SEM micrograph was taken, EDX was performed to determine the elemental concentration distribution on the catalyst granules using Link Isis 300 software

4.2.9 Transmission Electron Microscopy (TEM)

The cobalt oxide particle size and particle size distribution on MCM-41 were observed using JEOL-JEM 200CX transmission electron microscope operated at 100 kv at the Scientific and Technological Research Equipment Centre, Chulalongkorn University (STREC), Bangkok, Thailand.

4.2.10 Raman spectroscopy

Raman spectroscopy was used to determine the surface compositions of catalyst samples. The Raman spectra of the samples were collected by projecting a

continuous wave laser of argon ion (Ar^+), 514.5 nm through the samples. A scanning range between 200 and 1000 cm^{-1} was applied. The data were analyzed using Raman microscope (Renishaw Raman Microscope System 2000) with CCD chip detector at National Metal and Materials Technology Center (MTEC), Klong Luang, Pathumthani.

4.2.11 Acid Leaching

Acid leaching was performed in order to remove the metals. A 30% hydrochloric acid solution ($\text{pH} = 1$) was used to treat the catalysts for 48 h. After cobalt was dissolved, the residues were filtered and rinsed with deionized water for several times to remove all dissolved components. Then, the residue was dried under vacuum at room temperature over night in order to avoid any further reaction caused by heating. The acid leached catalysts were then collected and characterized.

4.3 Reaction Study in CO Hydrogenation

4.3.1 Materials

The reactant gas mixture used for the reaction study was composed of 9.73 vol% carbon monoxide in hydrogen and supplied by Thai Industrial Gas Limited (TIG). The total flow rate was 30 ml/min. Ultra high purity hydrogen and high purity argon manufactured by Thai Industrial Gas Limited (TIG) were used for reduction and balanced flowrate.

4.3.2 Equipment

The CO hydrogenation system is schematically shown in Figure 4.1. The system is consisted of a reactor, an automatic temperature controller, an electrical furnace and a gas controlling system.

4.3.2.1 Reactor

The reactor was made from a stainless steel tube (O.D. 3/8"). Two sampling points were provided above and below the catalyst bed. Catalyst was placed in the middle of the reactor and held by two quartz wool layers.

4.3.2.2 Automation Temperature Controller

This unit is consisted of a magnetic switch connected to a variable voltage transformer and a solid state relay temperature controller model no. SS2425DZ connected to a thermocouple. Reactor temperature was measured at the bottom of the catalyst bed in the reactor. The temperature control set point is adjustable within the range of 0-800°C at the maximum voltage output of 220 volt.

4.3.2.3 Electrical Furnace

The electrical furnace was used to supply heat to the reactor for CO hydrogenation. The reactor could be operated from room temperature up to 800°C at the maximum voltage of 220 volt.

4.3.2.4 Gas Controlling System

The flowrate of each gas used in this study was controlled by a gas controlling system which consisted of a pressure regulator, an on-off valve and the gas flow rates were adjusted by using metering valves.

4.3.2.5 Gas Chromatograph

The composition of hydrocarbons in the product stream was analyzed by a Shimadzu GC14B gas chromatograph equipped with a flame ionization detector. A Shimadzu GC8A (molecular sieve 5A) gas chromatograph equipped with a thermal conductivity detector was used to analyze CO and H₂ in the feed and product streams. The operating conditions for each instrument are shown in the Table 4.4.

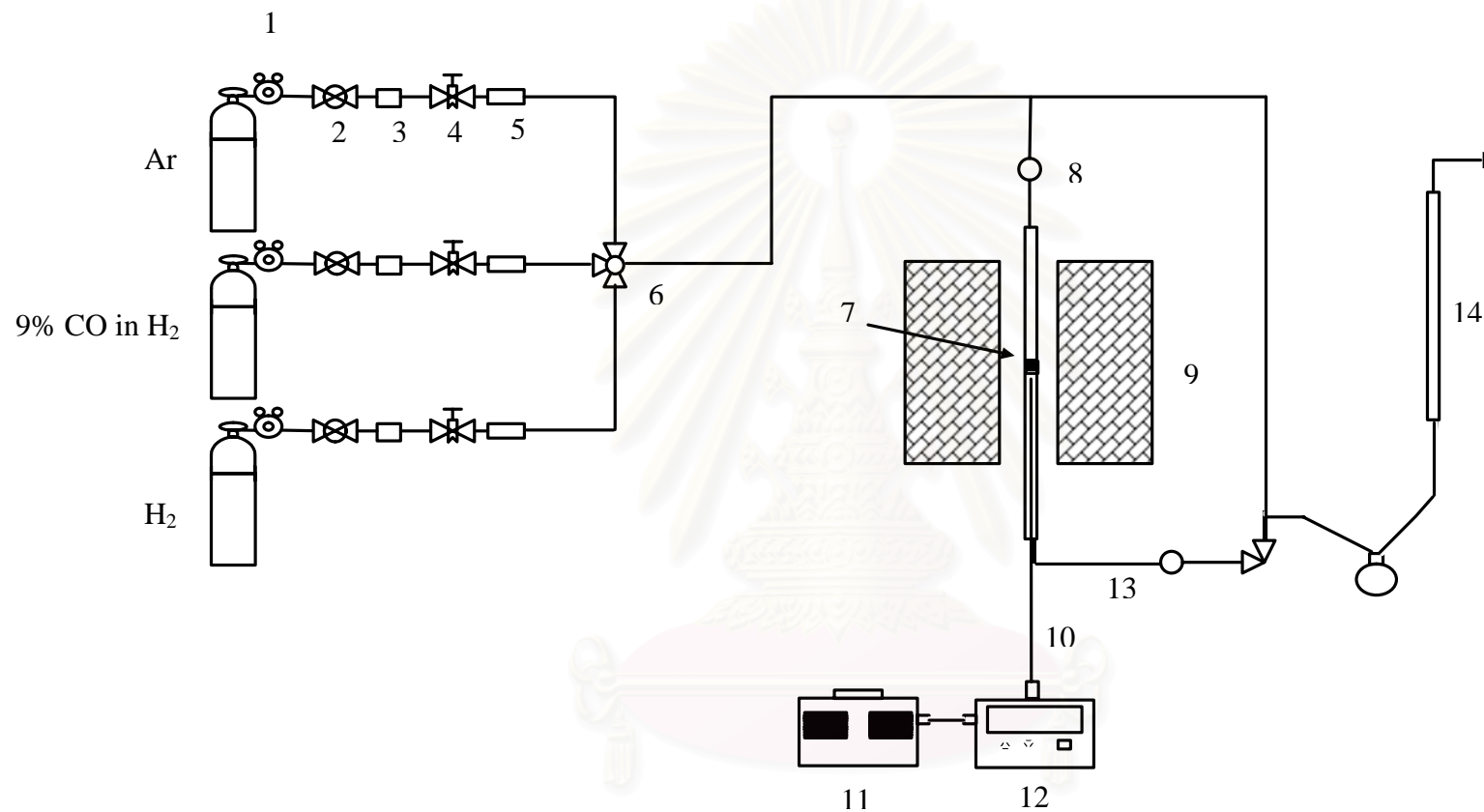
4.3.3 CO hydrogenation procedure

CO hydrogenation was performed using 0.1 g of catalyst packed in the middle of the stainless steel microreactor, which locate in the electrical furnace. The total flow rate was 30 ml/min with the H₂/CO ratio of 10/1. The catalyst sample was reduced *in situ* in flowing H₂ at 350°C for 10 h prior to CO hydrogenation. CO hydrogenation was carried out at 220°C and 1 atm total pressure. The product streams were analyzed by gas chromatography technique.

Table 4.4 Operating condition for gas chromatograph

Gas chromatograph	Shimadzu GC8A	Shimadzu GC14B
Detector	TCD	FID
Column	Molecular Sieve 5A	VZ10
Carrier gas	He (99.999%)	N ₂ (99.999%)
Carrier gas flow	30 ml./min.	30 ml./min.
Column temperature		
- Initial	60°C	70°C
- Final	60°C	70°C
Detector temperature	100°C	100°C
Injector temperature	100°C	150°C
Analyzed gas	N ₂ , CO, O ₂	Hydrocarbon C ₁ -C ₄

สถาบันวิทยบริการ
จุฬาลงกรณ์มหาวิทยาลัย



- | | | | |
|-----------------------|-----------------------|----------------------------------|----------------------------|
| 1. Pressure Regulator | 2. On-Off Valve | 3. Gas Filter | 4. Metering Valve |
| 5. Back Pressure | 6. 3-way Valve | 7. Catalyst Bed | 8. Sampling point |
| 9. Furnace | 10. Thermocouple | 11. Variable Voltage Transformer | 12. Temperature Controller |
| 13. Heating Line | 14. Bubble Flow Meter | | |

Figure 4.1 Flow diagram of CO hydrogenation system

CHAPTER V

RESULTS AND DISCUSSION

5.1 Effect of Cobalt Precursors on the Dispersion of Cobalt on MCM-41

In this section, the effect of cobalt precursors on the dispersion of cobalt on MCM-41 was investigated. Supported metal catalysts are usually prepared by impregnation of a support with an aqueous solution containing the desired amount of metal. It is known that different cobalt precursors can produce different final cobalt particle size and different cobalt dispersion. Typically, high surface area support yield higher metal dispersion than low surface area support. MCM-41 possesses a unique hexagonal pore structure with relatively high surface area ($>1000 \text{ m}^2/\text{g}$). Therefore, metal dispersion on MCM-41 can be different from other commercial oxide supports, such as Al_2O_3 , SiO_2 , TiO_2 , and ZrO_2 , etc. The cobalt dispersion on MCM-41 was characterized by various analysis techniques such as AAS, N_2 physisorption, XRD, SEM, TEM, CO and H_2 chemisorption, TGA, and Raman spectroscopy.

5.1.1 Atomic Absorption Spectroscopy (AAS)

The actual amounts of cobalt loading for the catalyst samples were determined by atomic absorption spectroscopy by measuring photon absorption of a vaporized aqueous solution prepared from the starting material (catalyst). AAS results are given in Table 5.1. In this study, cobalt loading on the catalyst samples was approximately 7-8 wt%. It is intended to have a relatively high Co loading in order to make it close to that required for a commercial catalyst.

Table 5.1 Atomic Adsorption Results

Catalyst	Co (wt%)
Co/M-Ac	8.3
Co/M-AA	7.8
Co/M-Cl	7.1
Co/M-NO	8.1

5.1.2 N₂ Physisorption

BET surface areas, pore volumes, and average pore diameters of MCM-41 supported cobalt catalysts were determined by the adsorption and condensation of N₂ at liquid N₂ temperature using static vacuum procedure. This technique is so-called “BET method” according to the inventors’ name (Brunauer, Emmett, and Teller). The results are given in Table 5.2. The pure silica MCM-41 support before cobalt impregnation had a BET surface area of 1,234 m²/g and a pore volume of 0.77 cm³/g. The BET surface areas of the cobalt catalysts prepared with different cobalt precursors were found to be in the range of 646-756 m²/g and in the order of Co/M-Ac > Co/M-NO > Co/M-AA > Co/M-Cl. The pore size distributions of MCM-41 and MCM-41 supported Co catalysts are shown in Figure 5.1. The average pore diameters for MCM-41 were determined to be approximately 2.5 nm. The significant decrease in surface area of the original support material suggests that cobalt was deposited significantly in the pores of MCM-41. The Co precursor did not have a significant impact on the average pore diameter of MCM-41 after cobalt loading since all the catalyst samples retained a narrow pore size distribution as the original MCM-41.

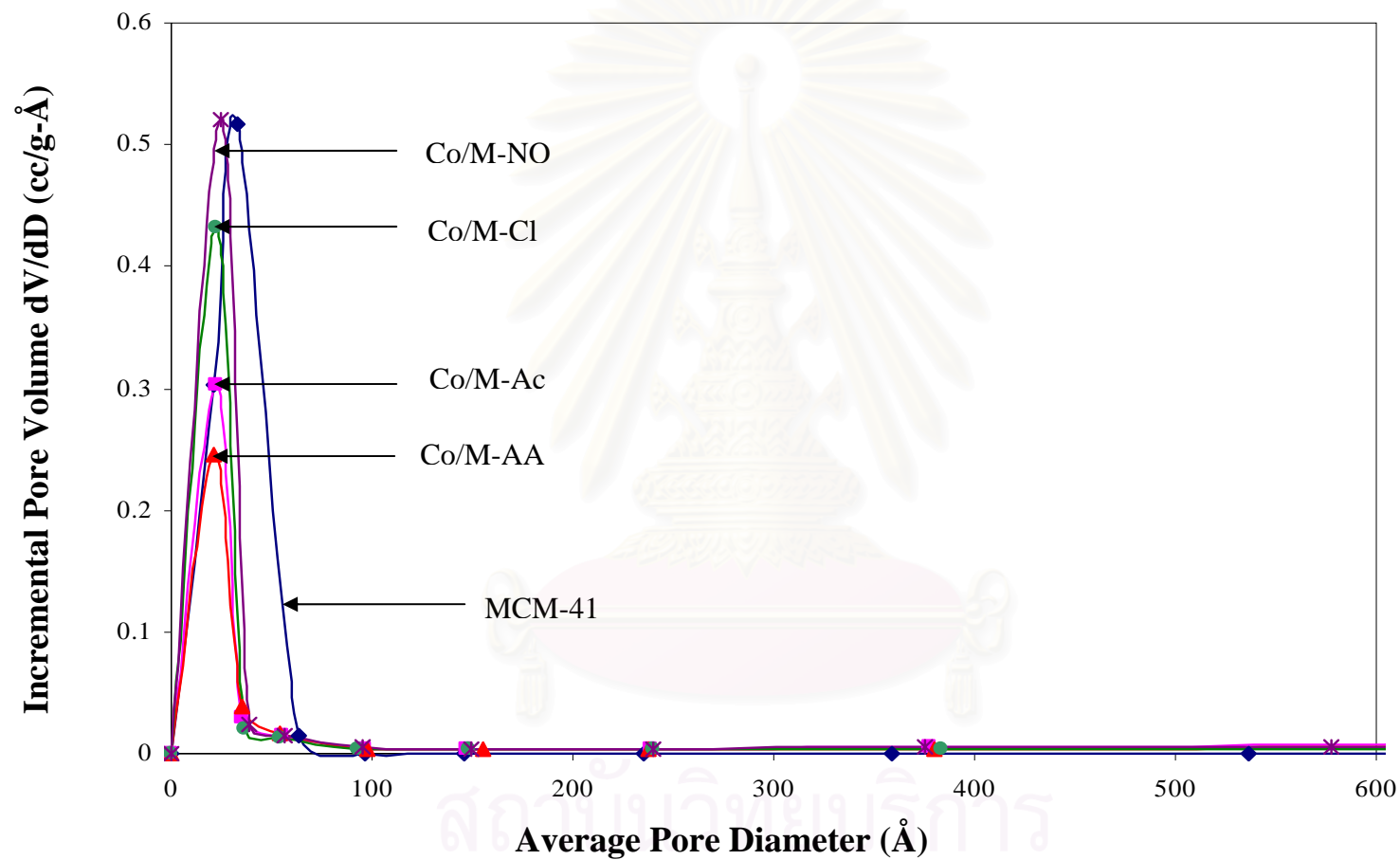


Figure 5.1 Pore size distribution of MCM-41 and MCM-41-supported Co catalysts.

Table 5.2 N₂ Physisorption Results

Catalysts	BET S.A.* (m ² /g)	Pore Volume (cm ³ /g)	Avg. Pore Diameter (nm)
MCM-41	1234	0.77	2.50
Co/M-Ac	756	0.42	2.20
Co/M-AA	675	0.37	2.22
Co/M-Cl	646	0.40	2.48
Co/M-NO	747	0.45	2.41

* Using N₂ Physisorption at 77 K. Error of measurement = +/- 10%.

5.1.3 X-ray diffraction (XRD)

The X-ray diffraction patterns of the MCM-41-supported cobalt catalysts are shown in Figure 5.2. For the unsupported MCM-41, the ordered structure of MCM-41 gave an XRD peak at low^o 2θ around 2.58 degrees. After impregnation of cobalt the intensity of the XRD peaks for MCM-41 was decreased for all the catalyst samples and the peaks became broader due to the structure of MCM-41 becoming less ordered by impregnation of cobalt or due to secondary scattering of the X-ray. The structure of MCM-41 was not destroyed but the long-range order of MCM-41 may have shrunk (Pasqua *et al.*, 2001).

The XRD patterns at higher diffraction angles of the MCM-41-supported cobalt catalysts prepared with different cobalt precursors in the calcined state are shown in Figures 5.3. Co/M-NO and Co/M-Cl exhibited diffraction peaks at 2θ of ca. 31.3°, 36.8°, 45.1°, 59.4°, and 65.4° indicate that after calcinations at 500°C, cobalt was primarily in the form of Co₃O₄ spinel in the catalyst particles. Surprisingly, Co/M-Ac and Co/M-AA did not exhibit any distinct XRD patterns. This suggests that the crystallite size of cobalt oxide prepared from cobalt acetate and cobalt acetylacetonate on MCM-41 was below the lower limit for XRD detectability (5 nm) even though Co loading was as high as 8 wt%. It is also possible that on Co/M-Ac

and Co/M-AA, Co did not form Co_3O_4 crystallites but an amorphous cobalt oxide may have formed similar to what has been suggested for Co/TiO₂ prepared from cobalt EDTA (Kraum and Baerns, 1999). The average cobalt oxide crystallite sizes were calculated using the Scherrer's equation and are given in Table 5.4 (Klug and Alexander, 1974). For Co/M-NO and Co/M-Cl, they were found to be 13.3 nm and 46.1 nm, respectively. These cobalt particles were much larger than the average pore diameter of MCM-41 (3 nm), suggesting that using cobalt nitrate and cobalt chloride precursors to prepare MCM-41-supported Co catalysts by incipient wetness impregnation resulted in some large cobalt oxide particles deposited on the external surface of MCM-41.

It is known that when Cl-containing compounds are used as the catalyst precursor, residual Cl⁻ has often been found after calcination (Mahata and Vishwanathan, 2000; Zhou *et al.*, 1994; Johnston and Joyner, 1993). For our Co/M-Cl catalyst, after calcination at 500°C for 4 hours, residual Cl⁻ was not detected by XRD (Figure 5.4). Residual Cl⁻, however, was observed for bulk CoCl₂ after calcination at 500°C. Thus, residual Cl⁻ may also be present in our Co/M-Cl catalyst but it was probably highly dispersed or present in very small amounts so that it could not be detected by XRD. One should note that residual Cl⁻ has been shown to be significantly decreased in metal catalysts when water vapor is present, such as during reduction and CO hydrogenation.

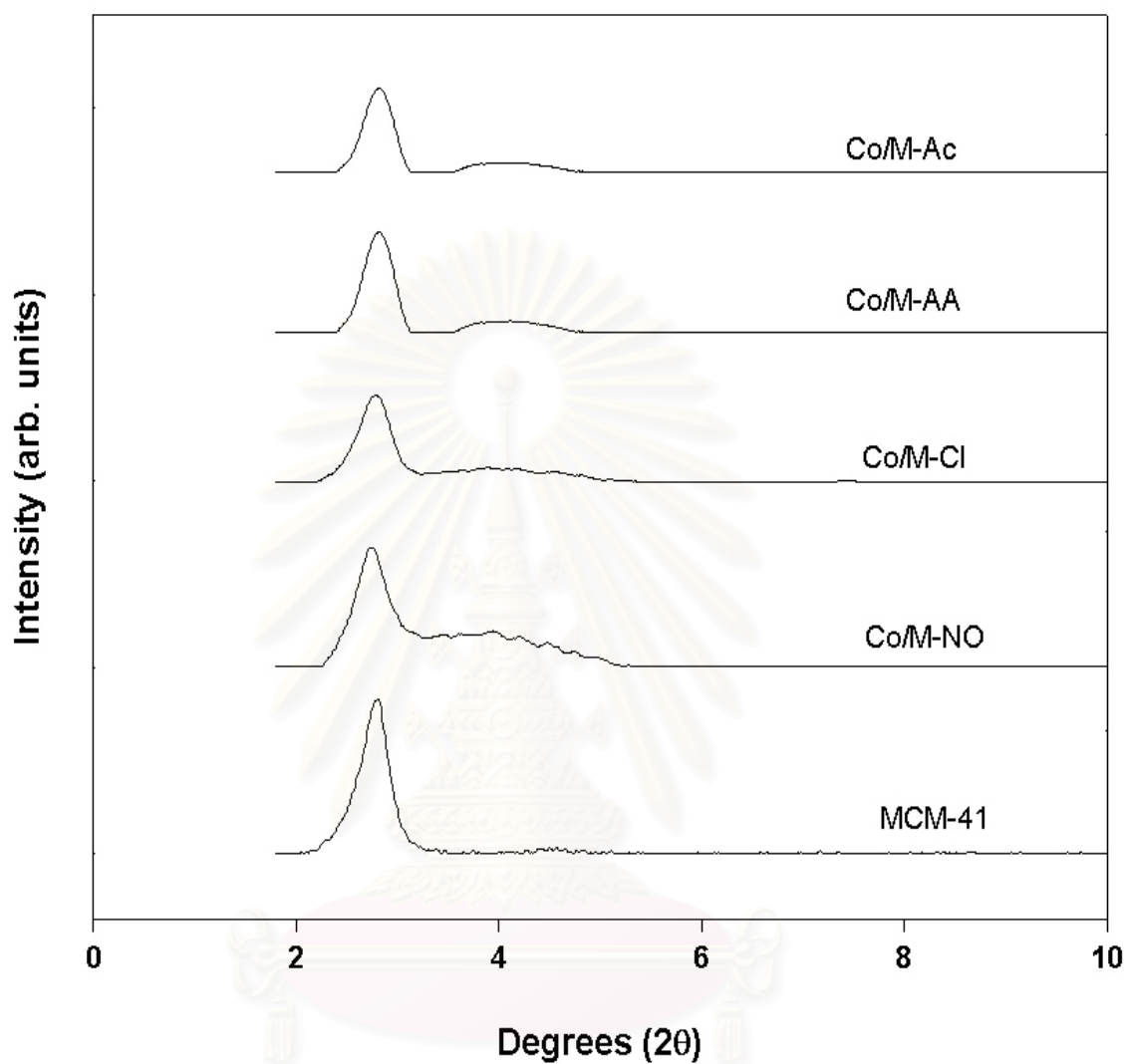


Figure 5.2 Effect of cobalt precursors on the XRD patterns of Co/MCM-41 catalysts (low 2θ)

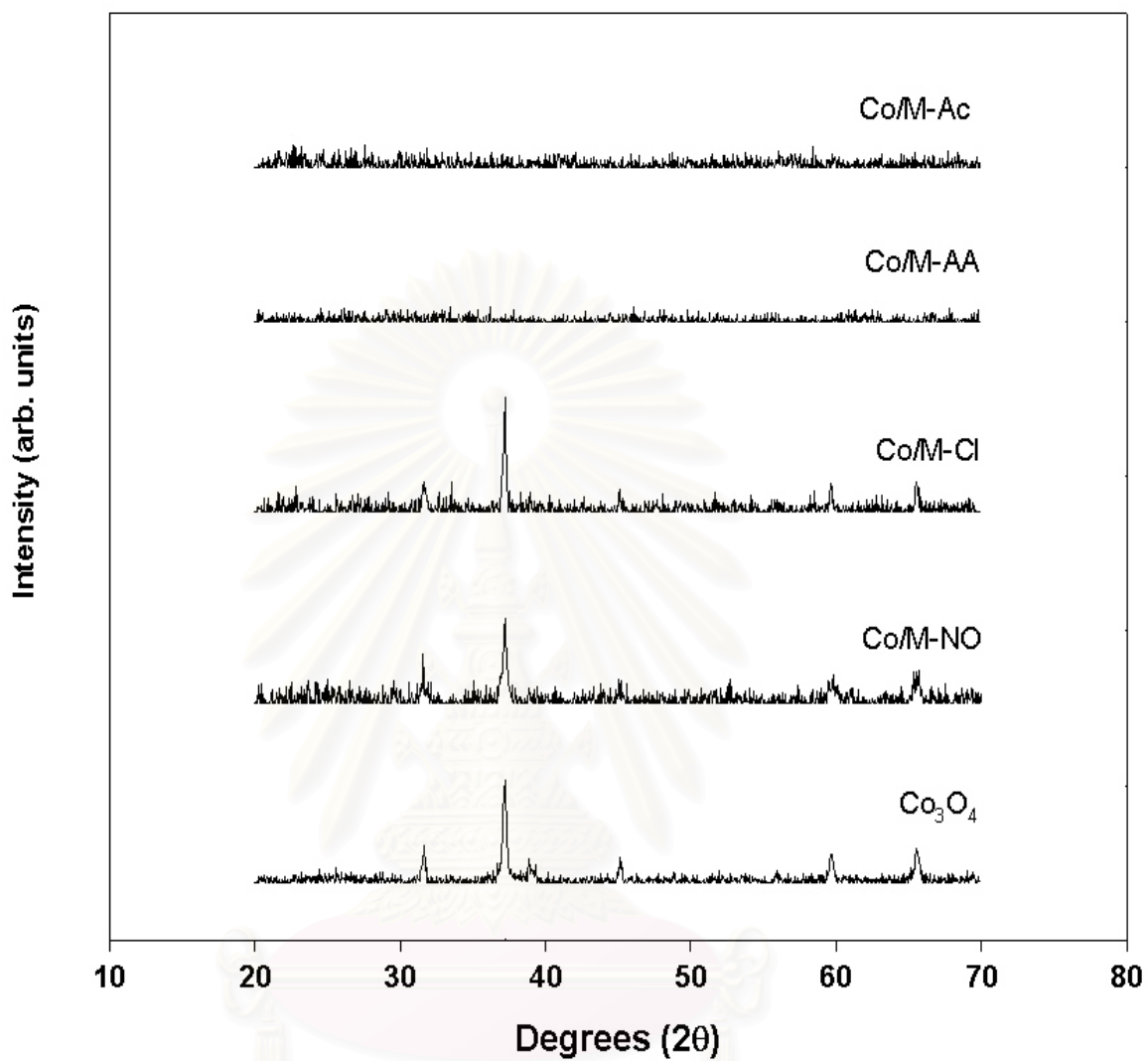


Figure 5.3 Effect of cobalt precursors on the XRD patterns of Co/MCM-41 catalysts (high 2θ)

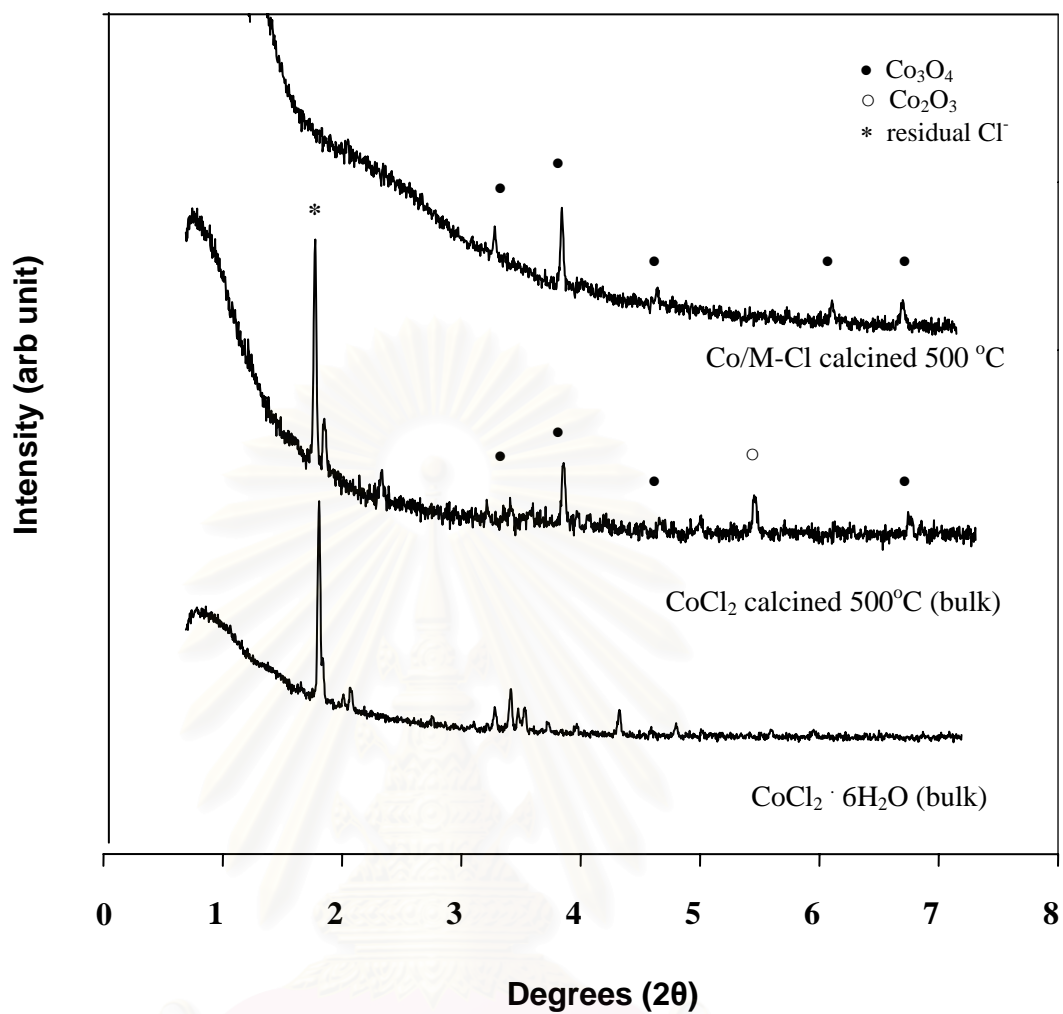


Figure 5.4 XRD pattern of residual Cl⁻ after calcination at 500°C for 2 h.

สถาบันวิทยบริการ
จุฬาลงกรณ์มหาวิทยาลัย

5.1.4 Scanning Electron Microscopy (SEM), Elemental Mapping, and Energy Dispersive X-ray Spectroscopy (EDX)

SEM, elemental mapping, and EDX were carried out for all the catalyst samples. SEM micrographs of catalyst granules for MCM-41 are shown in Figure 5.5. Figure 5.6 demonstrates the catalyst granule size distribution of MCM-41 supported cobalt catalysts that were counted from SEM micrographs of the primary one hundred catalyst granules. Typical SEM micrographs at higher magnification of catalyst granules of MCM-41-supported cobalt catalysts prepared with different cobalt precursors are shown in Figure 5.7. The term “granule” here refers to a catalyst particle composed of cobalt and silica. In all the SEM figures, the white or light spots on the catalyst granules represent a high concentration of cobalt and its compounds while the darker areas of the granules indicate the support with minimal/no cobalt present. The dark background is due to the carbon tape used for holding the catalyst samples. The SEM micrographs of catalyst granules for Co/MCM-41 prepared with different cobalt precursors show similar catalyst granule sizes of 30-50 microns. The elemental mappings of cobalt for Co/MCM-41 are shown in Figure 5.8. The presence of very large cobalt clusters non-uniformly distributed on the granule exteriors was observed for Co/M-Cl. Dispersion of the cobalt was better for the other catalysts.

SEM-EDX was performed on cross-sectioned catalyst granules in order to determine the cobalt concentration at different locations on the cross-sectioned catalyst granules (in the pores versus on the external surface). The SEM micrographs of cross-sectioned catalyst granules with locations of EDX analysis for Co/MCM-41 are shown in Figure 5.9. The corresponding elemental distributions are reported in Table 5.3. Again we observed a very high concentration of cobalt on the external surface of Co/M-Cl; whereas distribution of cobalt for the other catalysts was not significantly different across the cross-sectioned granules. SEM-EDX results thus confirm that, except for Co/M-Cl, the cobalt catalysts had their Co primarily located in the pores of MCM-41.

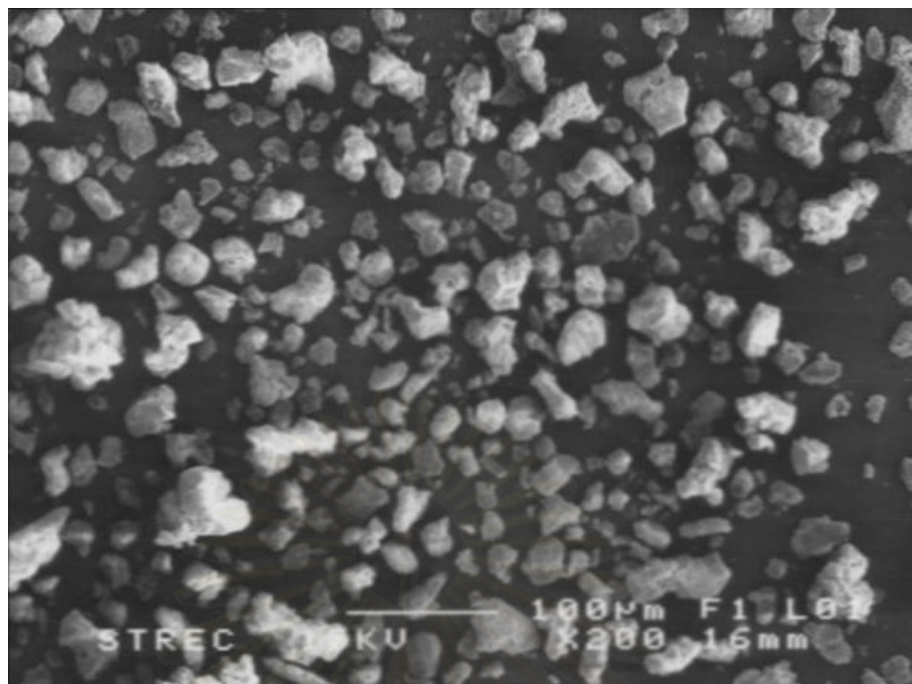


Figure 5.5 (a) SEM micrograph of catalyst granules for Co/M-Ac

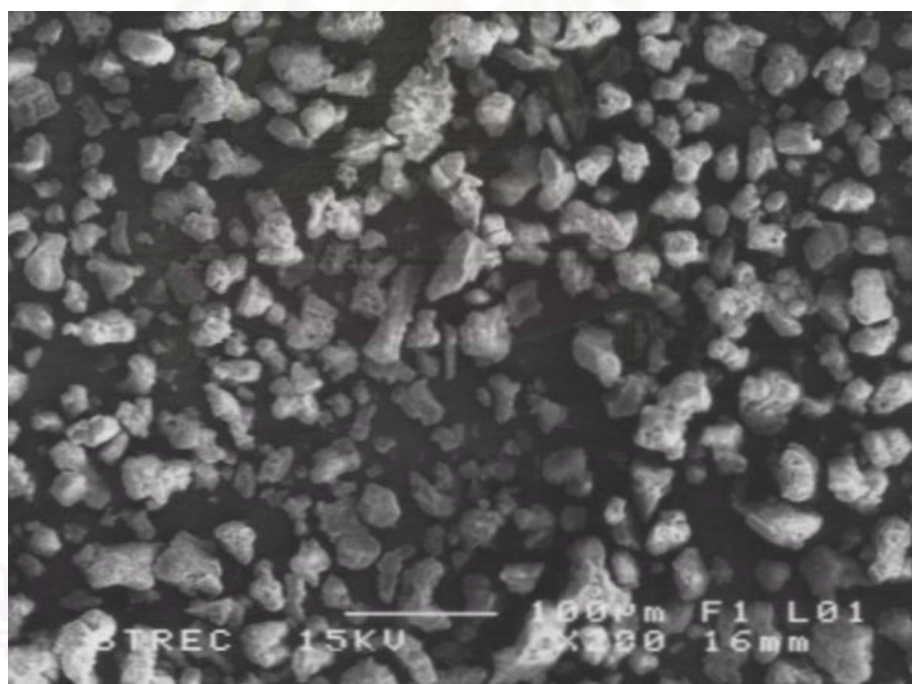


Figure 5.5 (b) SEM micrograph of catalyst granules for Co/M-AA

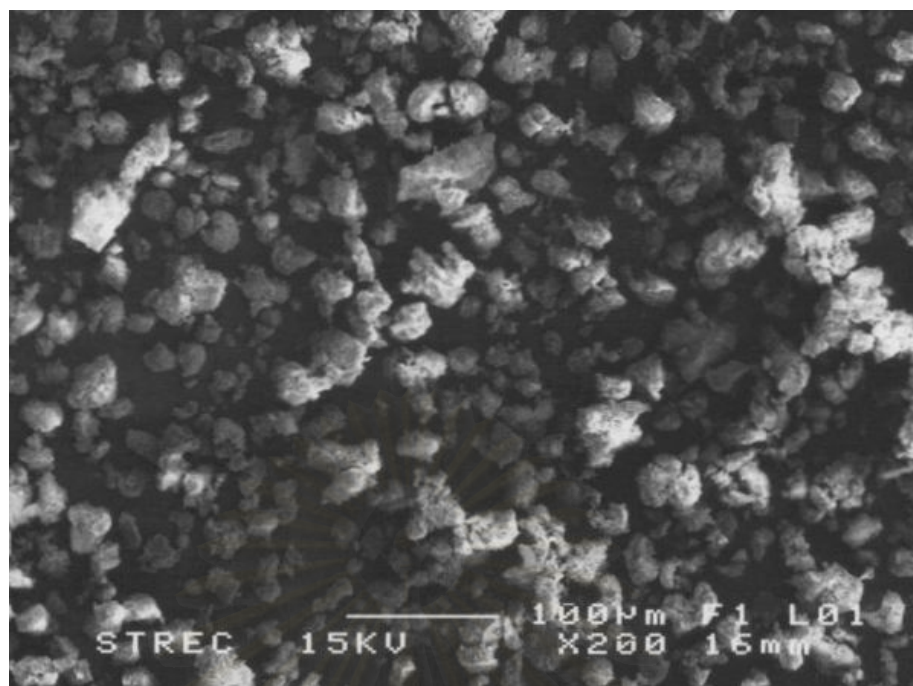


Figure 5.5 (c) SEM micrograph of catalyst granules for Co/M-Cl

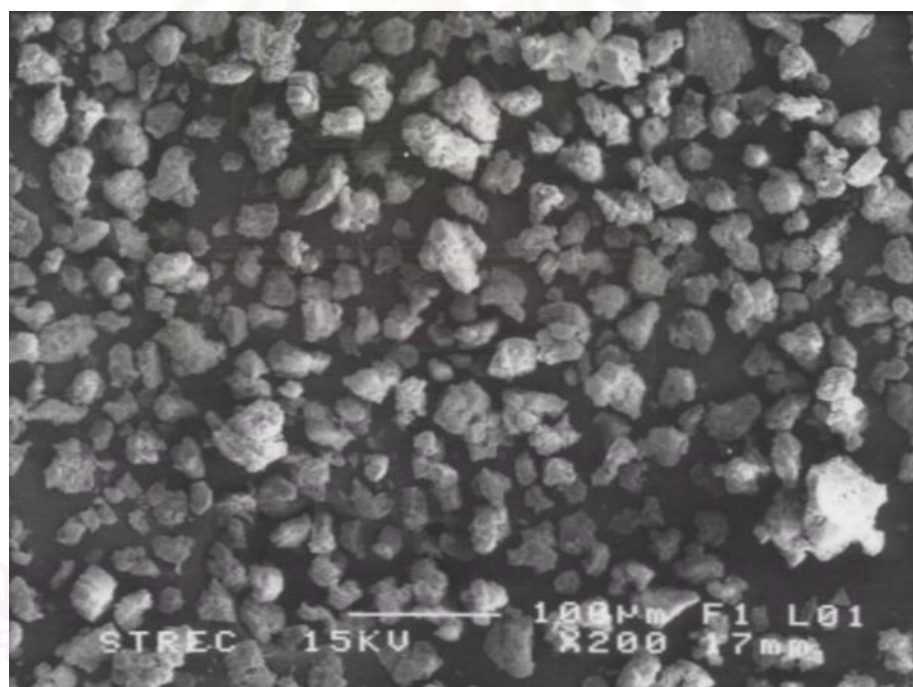


Figure 5.5 (d) SEM micrograph of catalyst granules for Co/M-NO

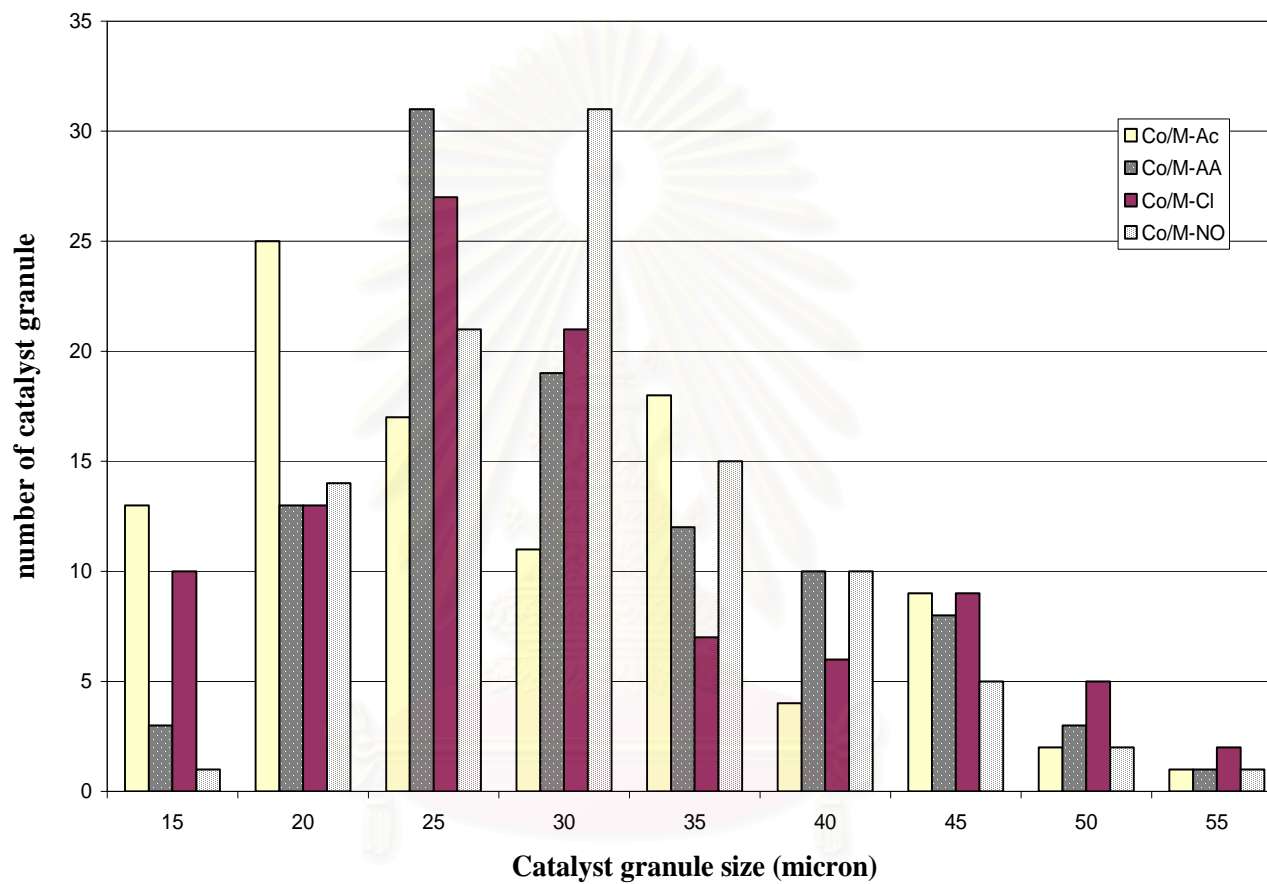


Figure 5.6 Catalyst granule size distribution of MCM-41 supported cobalt catalysts.

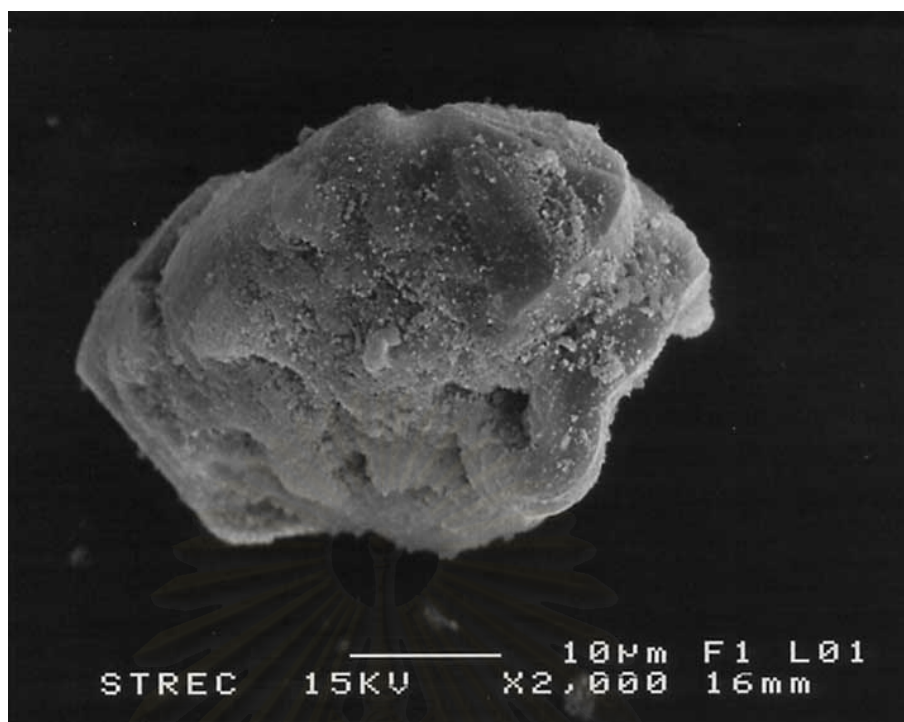


Figure 5.7 (a) SEM micrograph of Co/M-Ac

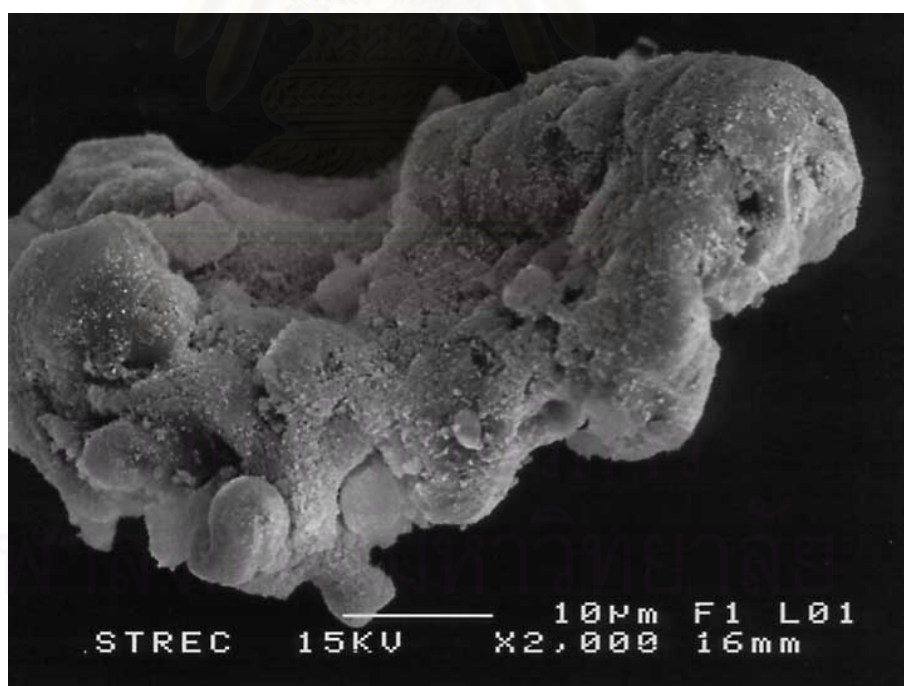


Figure 5.7 (b) SEM micrograph of Co/M-AA

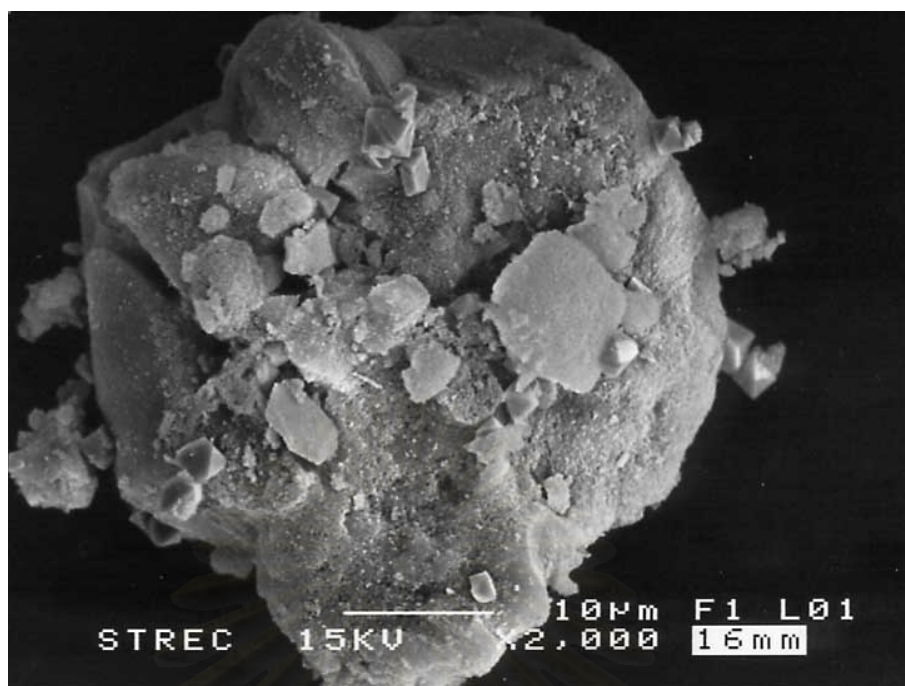


Figure 5.7 (c) SEM micrograph of Co/M-Cl

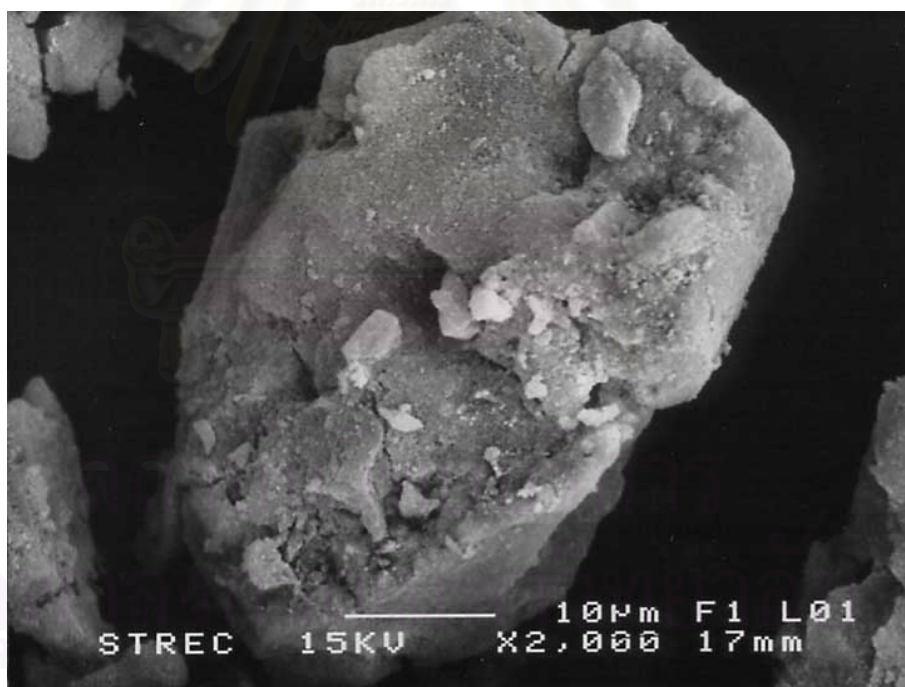


Figure 5.7 (d) SEM micrograph of Co/M-NO

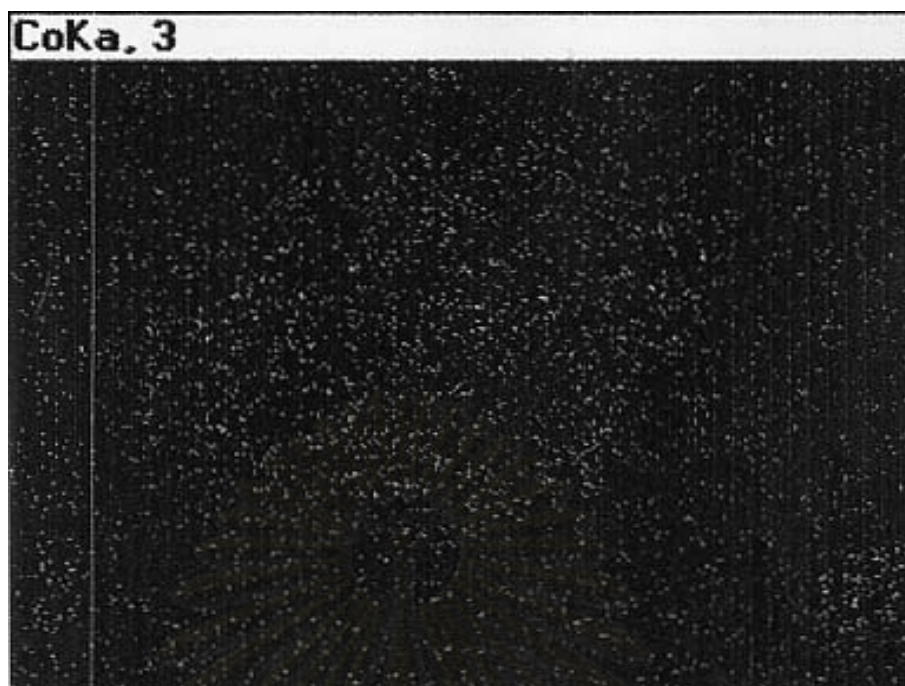


Figure 5.8 (a) SEM elemental mapping of Co/M-Ac

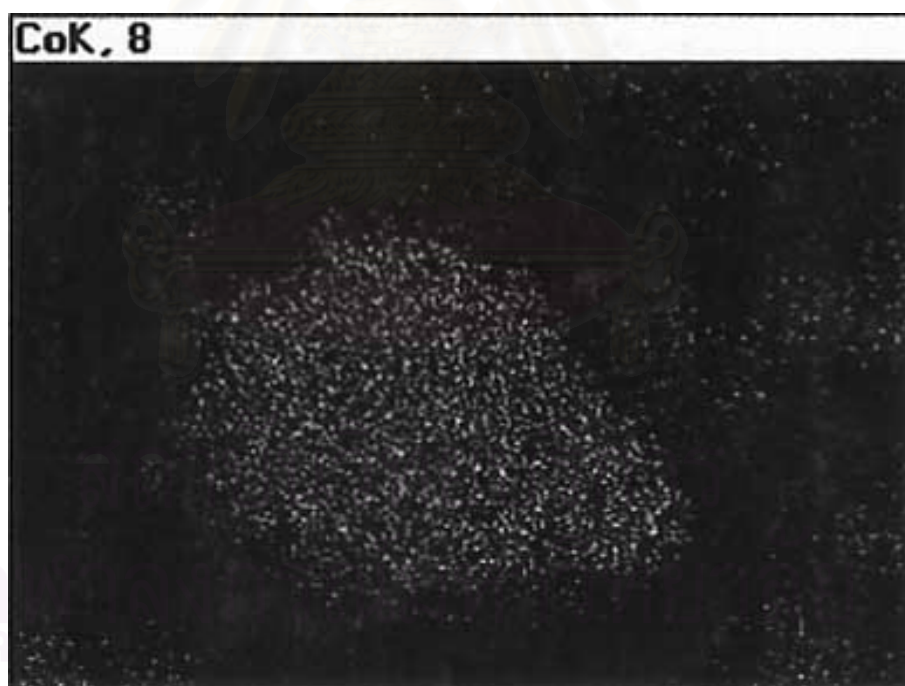


Figure 5.8 (b) SEM elemental mapping of Co/M-AA

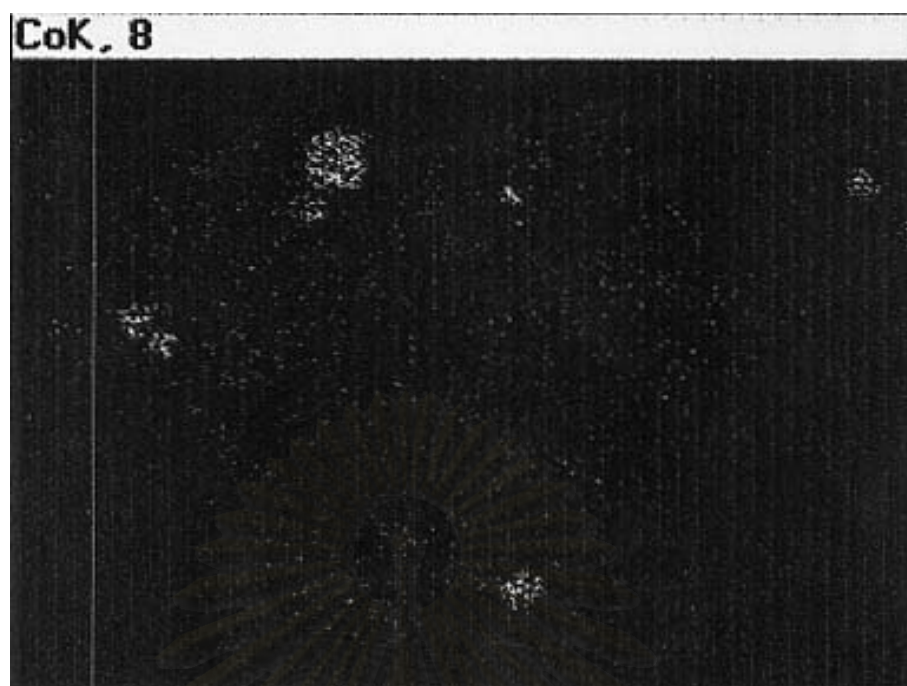


Figure 5.8 (c) SEM elemental mapping of Co/M-Cl

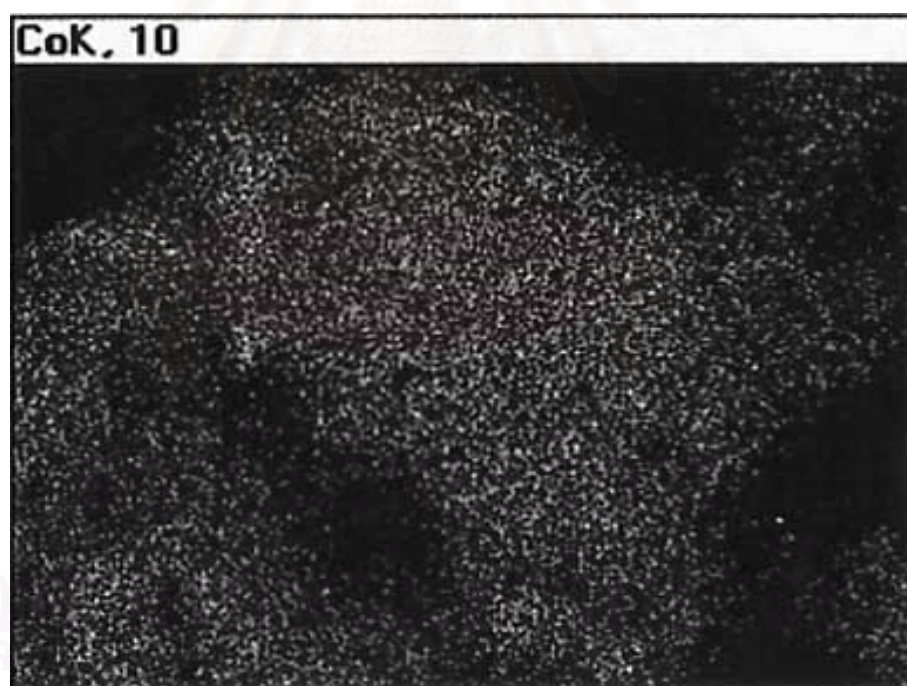


Figure 5.8 (d) SEM elemental mapping of Co/M-NO

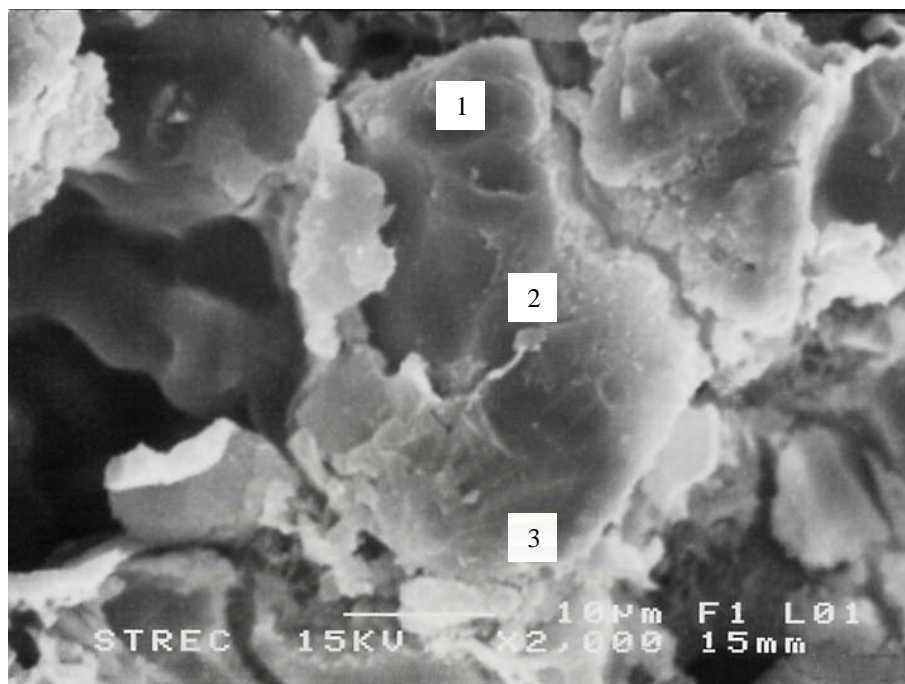


Figure 5.9 (a) SEM-EDX of the cross-sectioned Co/M-Ac

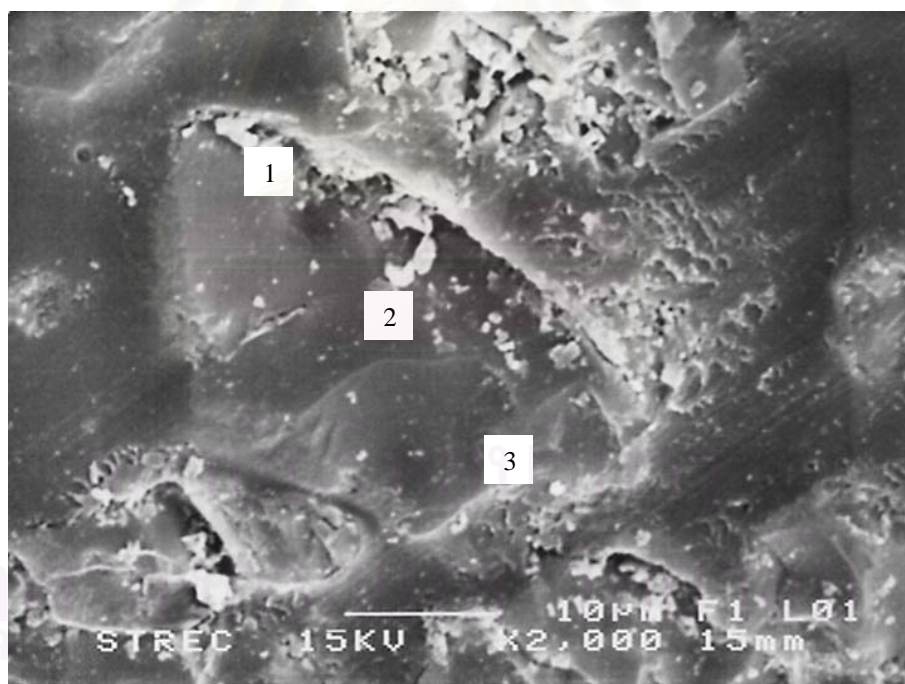


Figure 5.9 (b) SEM-EDX of the cross-sectioned Co/M-AA

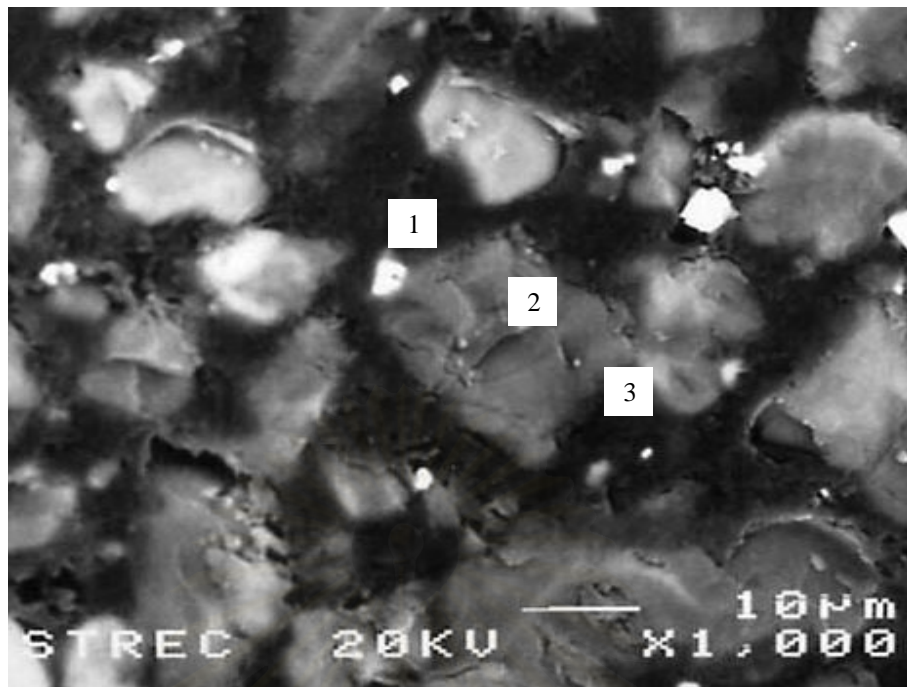


Figure 5.9 (c) SEM-EDX of the cross-sectioned Co/M-Cl

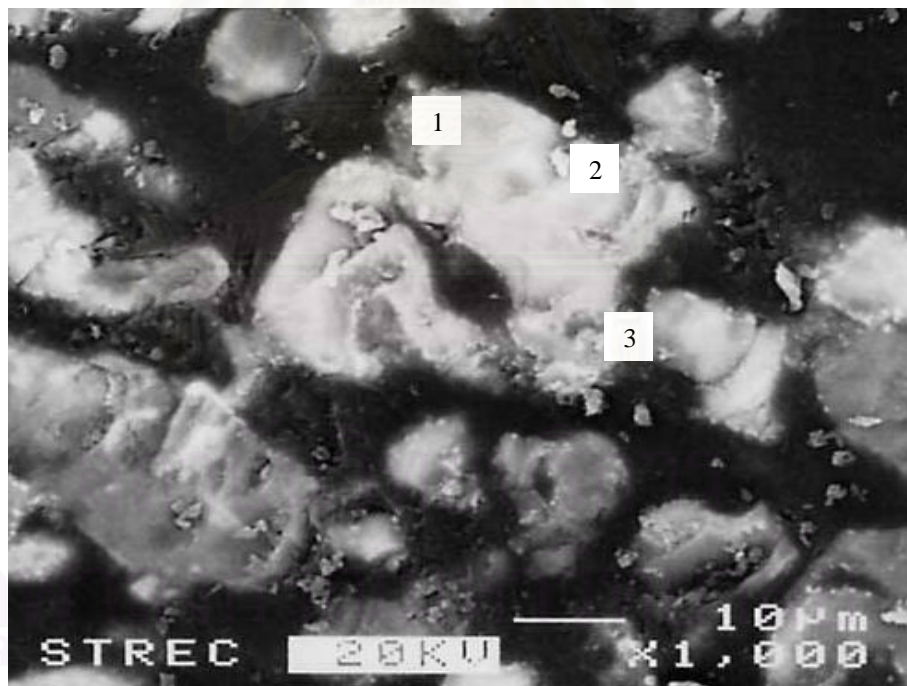


Figure 5.9 (d) SEM-EDX of the cross-sectioned Co/M-NO

Table 5.3 Elemental analysis using SEM-EDX on different locations of the cross-sectioned catalysts.

Catalyst	Co (wt.%) ^a		
	location 1	location 2	location 3
Co/M-Ac	7.5	10.6	7.8
Co/M-AA	11.4	12.4	6.5
Co/M-Cl	18.6	4.9	6.9
Co/M-NO	7.9	6.0	7.7

^a Error of measurement +/- 10%.

5.1.5 Transmission Electron Microscopy (TEM)

TEM micrographs were taken for all the catalysts in order to physically measure the size of cobalt oxide particles and/or cobalt clusters. The TEM micrographs for MCM-41-supported Co catalysts are shown in Figure 5.10. TEM images were found to be in accordance with the results from XRD and EDX that very large cobalt clusters (1-2 μm) were present on Co/M-Cl while dispersion of the cobalt was better for the other catalysts. Although TEM measurements were only done for a very small portion of each catalyst, the results are able to provide further evidence about Co dispersion. The average cobalt oxide crystallite sizes calculated from TEM are given in Table 5.4.

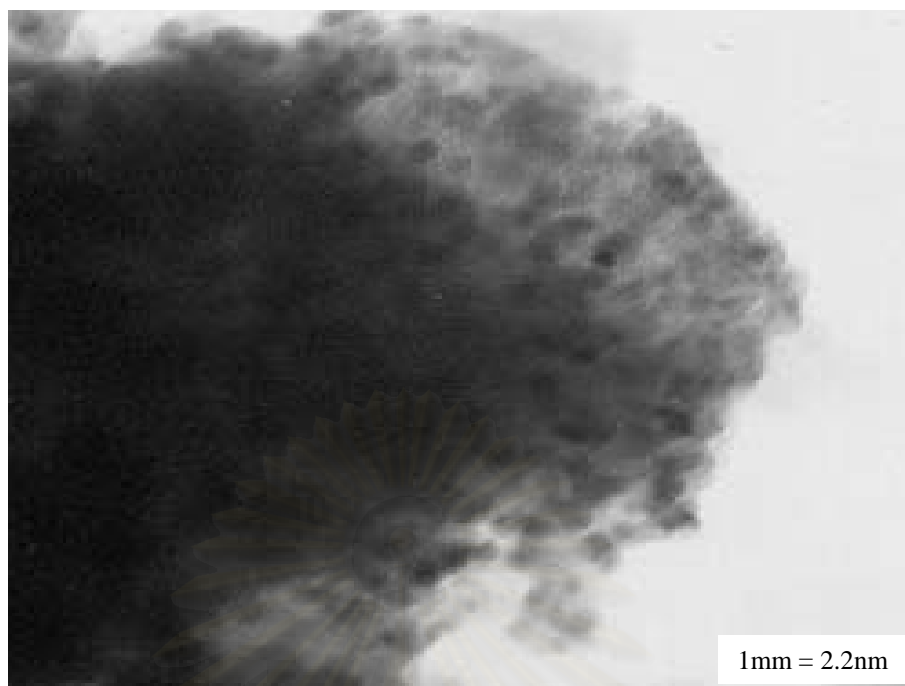


Figure 5.10 (a) TEM micrographs of Co/M-Ac.



Figure 5.10 (b) TEM micrographs of Co/M-AA.

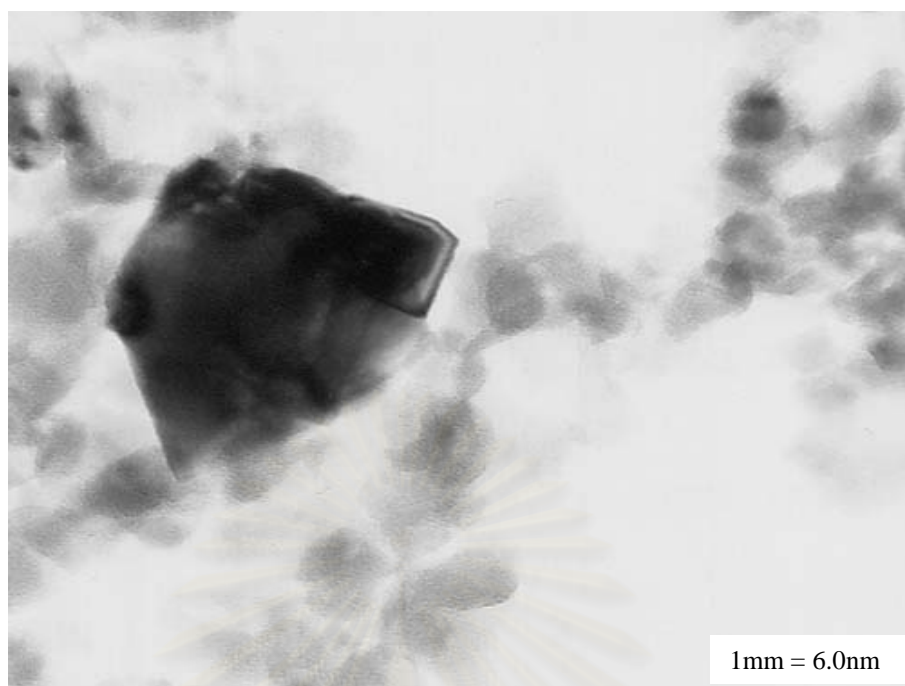


Figure 5.10 (c) TEM micrographs of Co/M-Cl.

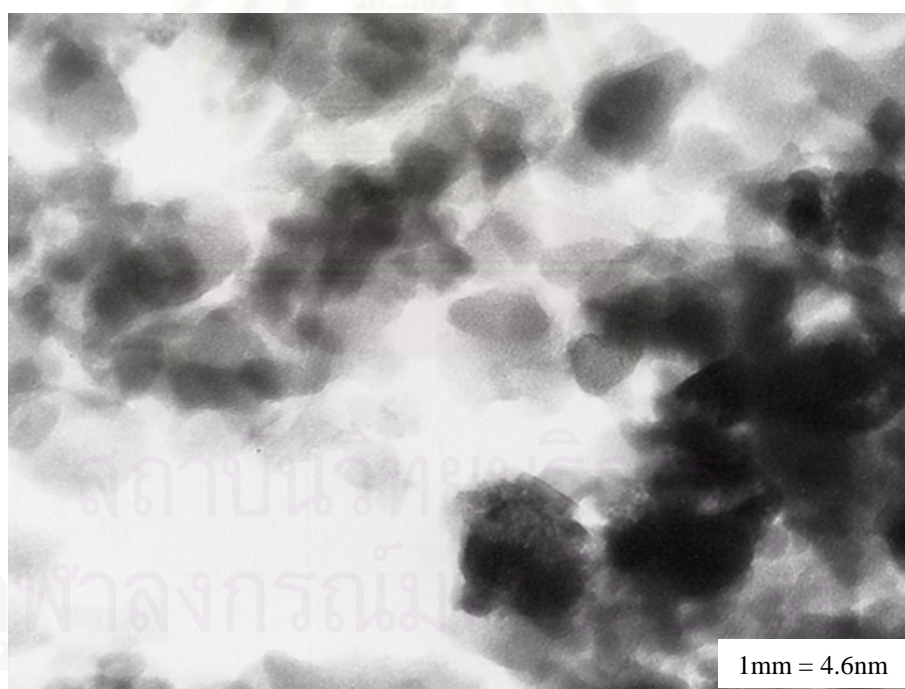


Figure 5.10 (d) TEM micrographs of Co/M-NO.

Table 5.4 Characterization results of Co/MCM-41 catalysts.

Catalyst	Co ₃ O ₄ Average Particle Size (nm)		SEM
	TEM	XRD	avg. catalyst granule size (μm)
Co/M-Ac	6.7	<5	28
Co/M-AA	12.5	<5	30
Co/M-Cl	60.0	46.1	30
Co/M-NO	18.4	13.3	31

5.1.6 CO-Pulse Chemisorption

The relative ranking of Co dispersion was calculated from CO-pulse chemisorption experiments that shown in Table 5.5. Since for CO-chemisorption on cobalt, bridge bonding may occur, there is no precise ratio of CO molecules to cobalt metal surface atoms able to be used. However, for strictly identical measurement conditions, CO-chemisorption can yield a relative ranking of Co dispersion. The mechanism of CO adsorption on Co active sites is illustrated in Figure 5.11. It was found that CO chemisorption was only measurable for Co/M-AA and Co/M-NO, with Co/M-AA exhibiting higher amount of CO chemisorption than Co/M-NO. Co/M-Cl exhibited negligible CO chemisorption probably due to its low dispersion of cobalt and/or due to residual Cl blocking the Co sites. Co/M-Ac had well-dispersed Co as determined by XRD and TEM; therefore it is surprising that no CO adsorption was able to be measured at the conditions used.

The percentage metal dispersion is defined as:

$$\% \text{ dispersion} = \frac{N_s (\text{atoms of gas adsorbed})}{N_T (\text{total number of metal atoms present})} \times 100$$

Table 5.5 Results from CO-Pulse Chemisorption

Catalyst	Co active sites ($\times 10^{17}$ CO molecule /g of cat.)	Total Co atoms present ($\times 10^{19}$ molecule /g of cat.)	Relative Co dispersion (CO/Co) ^a $\times 100$
Co/M-Ac	nil	-	nil
Co/M-AA	8.44	1.11	7.6
Co/M-Cl	nil	-	nil
Co/M-NO	9.34	3.60	2.6

^a The relative %Co dispersion from pulse CO chemisorption experiments.

5.1.7 H₂ Chemisorption

H₂ chemisorption technique also provides the information on the number of Co active site and % dispersion. However, for H₂ chemisorption, H/Co stoichiometry is normally equal to 1 whereas for CO-chemisorption, CO/Co maybe 1, 1/2 or 1/3 stoichiometry depending on the bonding of CO molecule to Co metal surface. The mechanism of CO and H₂ adsorption on Co active sites is illustrated in Figure 5.11. The total hydrogen uptakes and the percentages of cobalt dispersion are reported in Table 5.6. It was found that H₂ chemisorption was only measurable for Co/M-NO. For Co/M-Ac and Co/M-Cl, these catalysts did not chemisorb any H₂, similar to CO chemisorption results. On the other hand, Co/M-AA showed CO chemisorption but did not adsorb any H₂.

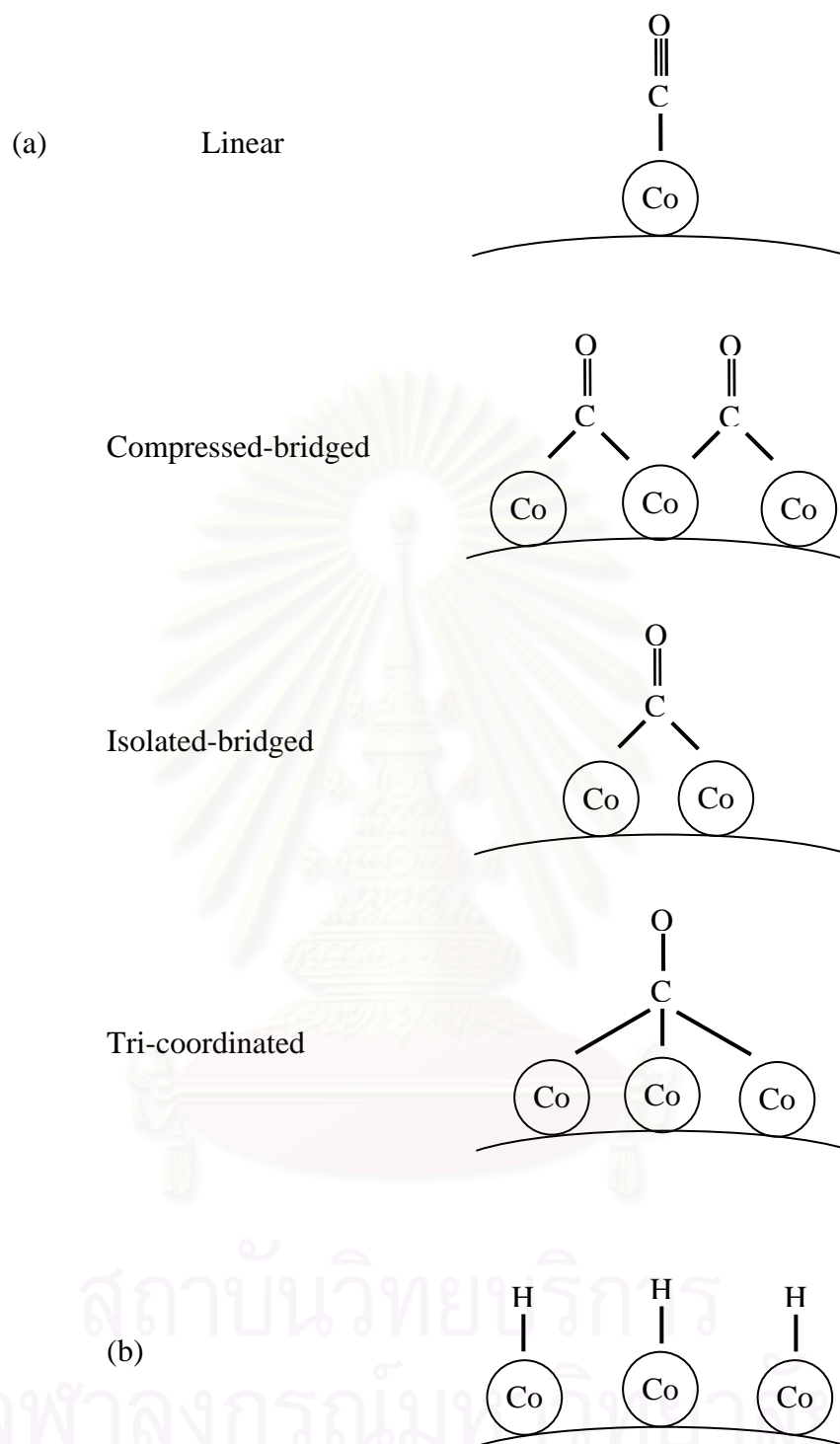


Figure 5.11 Generalized mechanism of (a) CO chemisorption and (b) H₂ chemisorption on Co active sites

Table 5.6 Results from H₂ chemisorption

Catalyst	H ₂ chemisorption ^a	
	Total (μmol H ₂ /gcat.)	% Co Dispersion
Co/M-Ac	nil	nil
Co/M-AA	nil	nil
Co/M-Cl	nil	nil
Co/M-NO	8.73	1.27

5.1.8 Thermogravimetric analysis (TGA)

To determine a suitable temperature for calcination of the cobalt precursors, Thermogravimetric analysis (TGA) experiments were performed with bulk cobalt nitrate, cobalt acetate, cobalt acetylacetonate, and cobalt chloride (Figure 5.12). All cobalt precursors appeared to be fully decomposed for calcination temperatures above 400°C. Thus, a calcination procedure using 500°C for 4 hours was used to produce the cobalt oxide phase in all the various catalysts prepared.

The degrees of reduction of the catalysts calculated from TGA experiment under H₂ flow 100 cc/min from 30-800°C (Figure 5.13) are reported in Table 5.7. The degrees of reduction of the catalysts from 30-800°C were not significantly different, ranging from 53-64%, with Co/M-NO showing the highest degree of reduction. Any Co not reducible during the H₂ reduction up to 800°C is identified as “non-reducible” Co silicate (Backman *et al.*, 1998; Kogelbauer *et al.*, 1995).

In order to examine the decomposition of MCM-41 during calcination and reduction, TGA experiment was also performed on unsupported MCM-41. TGA profiles of the unsupported MCM-41 during calcination and reduction that are presented in Figure 5.14 and 5.15, respectively. No MCM-41 weight loss was observed when it was heated in atmospheric air to 550°C and treated in H₂ flow up to 900°C. Thus, it is confirmed that the weight loss observed during TGA experiments

of all the catalysts during H₂ treatment were due to the reduction of cobalt oxide to cobalt metal.

Table 5.7 Results from TGA

Catalyst	Reducibility^a (30-800°C)
Co/M-Ac	59
Co/M-AA	53
Co/M-Cl	58
Co/M-NO	64

^a From thermogravimetric experiments.

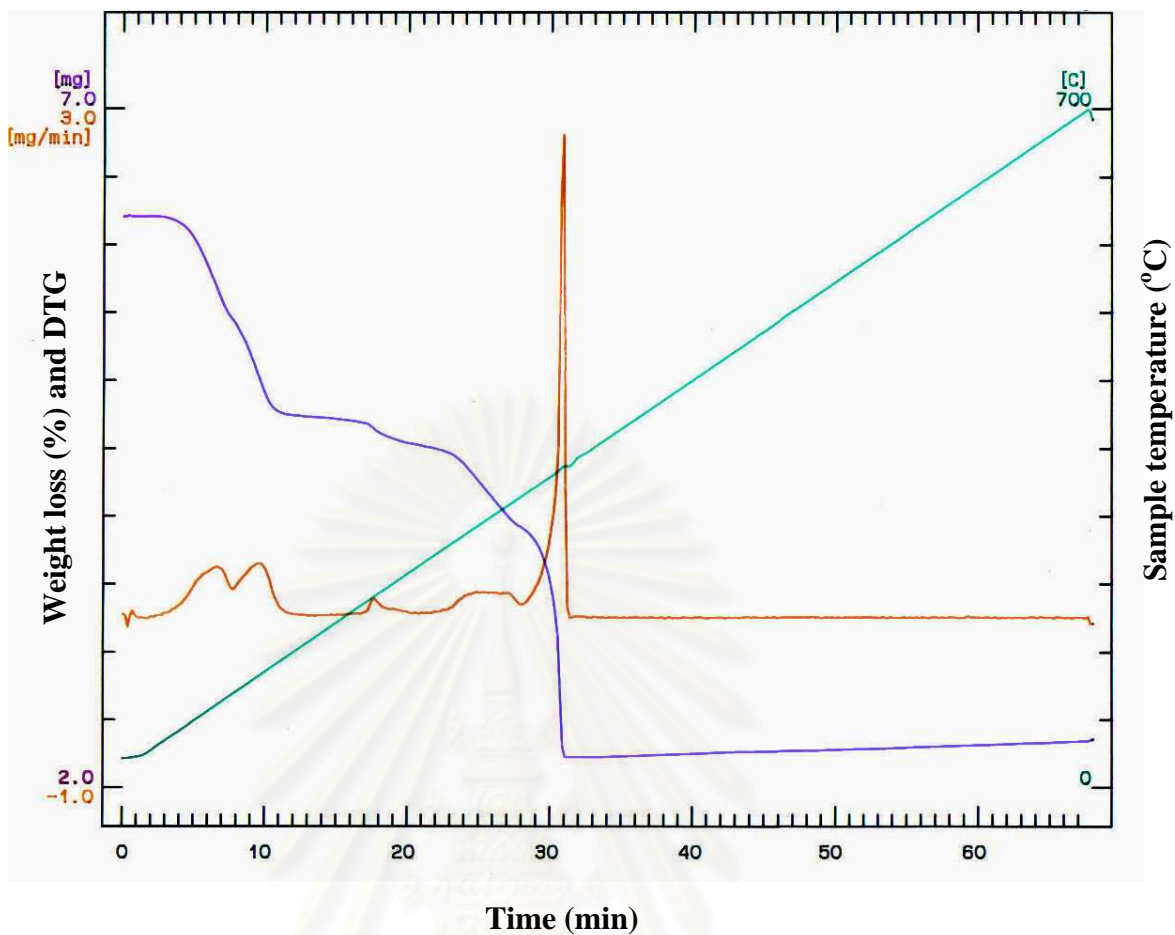


Figure 5.12 (a) Thermogravimetric analysis (TGA) experiments for Co-Acetate (bulk).

สถาบันวิทยบริการ
จุฬาลงกรณ์มหาวิทยาลัย

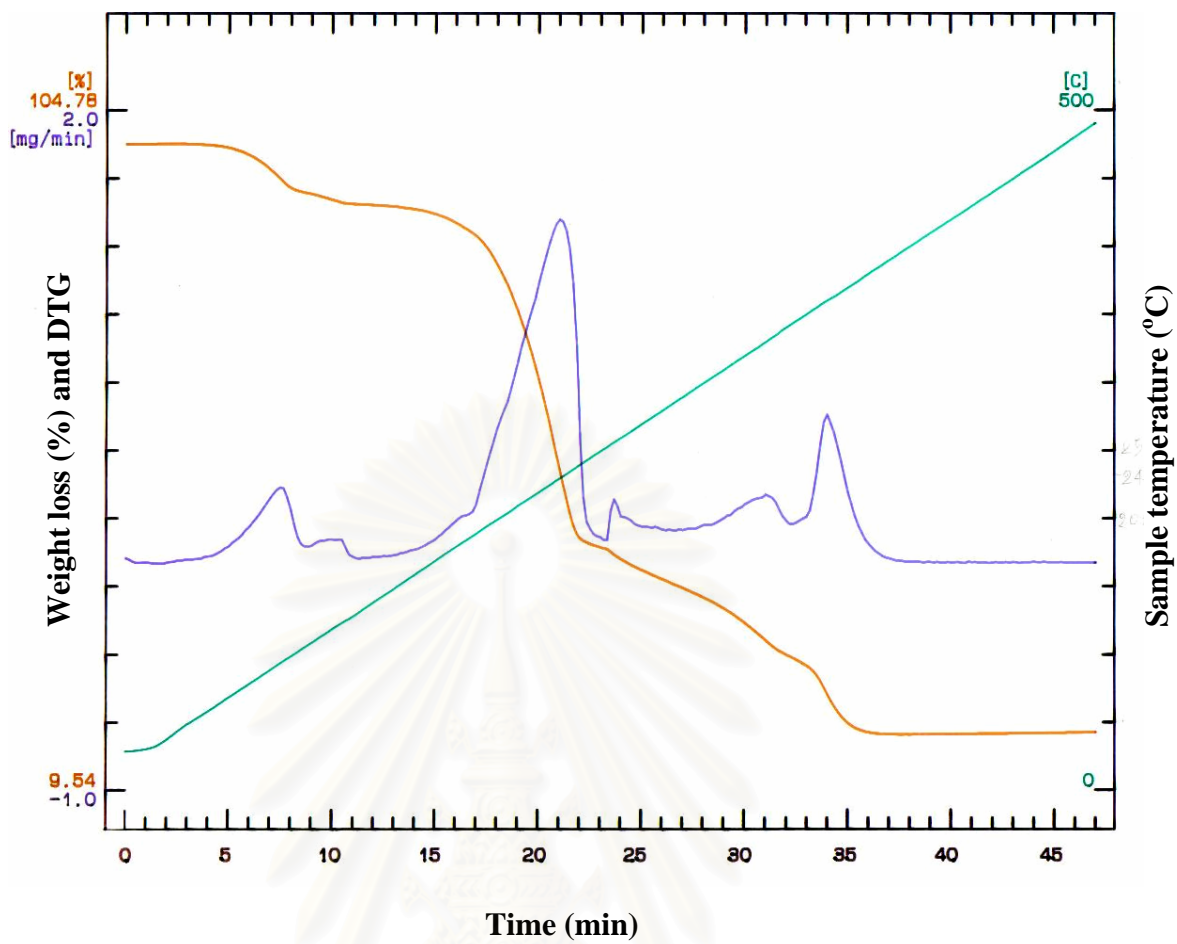


Figure 5.12 (b) Thermogravimetric analysis (TGA) experiments for Co-Acetyl acetate (bulk).

สถาบันวิทยบริการ
จุฬาลงกรณ์มหาวิทยาลัย

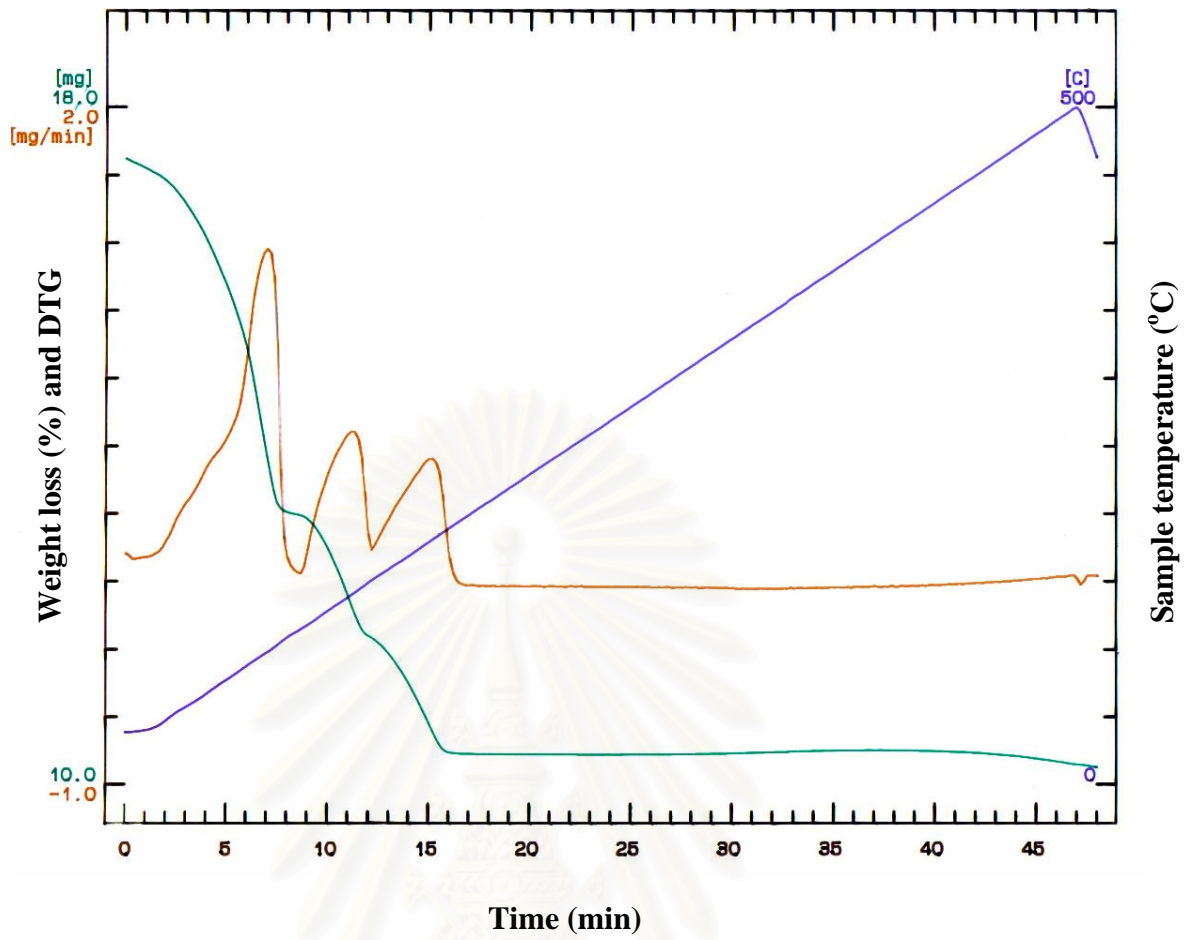


Figure 5.12 (c) Thermogravimetric analysis (TGA) experiments for Co-Chloride (bulk).

สถาบันวิทยบริการ
จุฬาลงกรณ์มหาวิทยาลัย

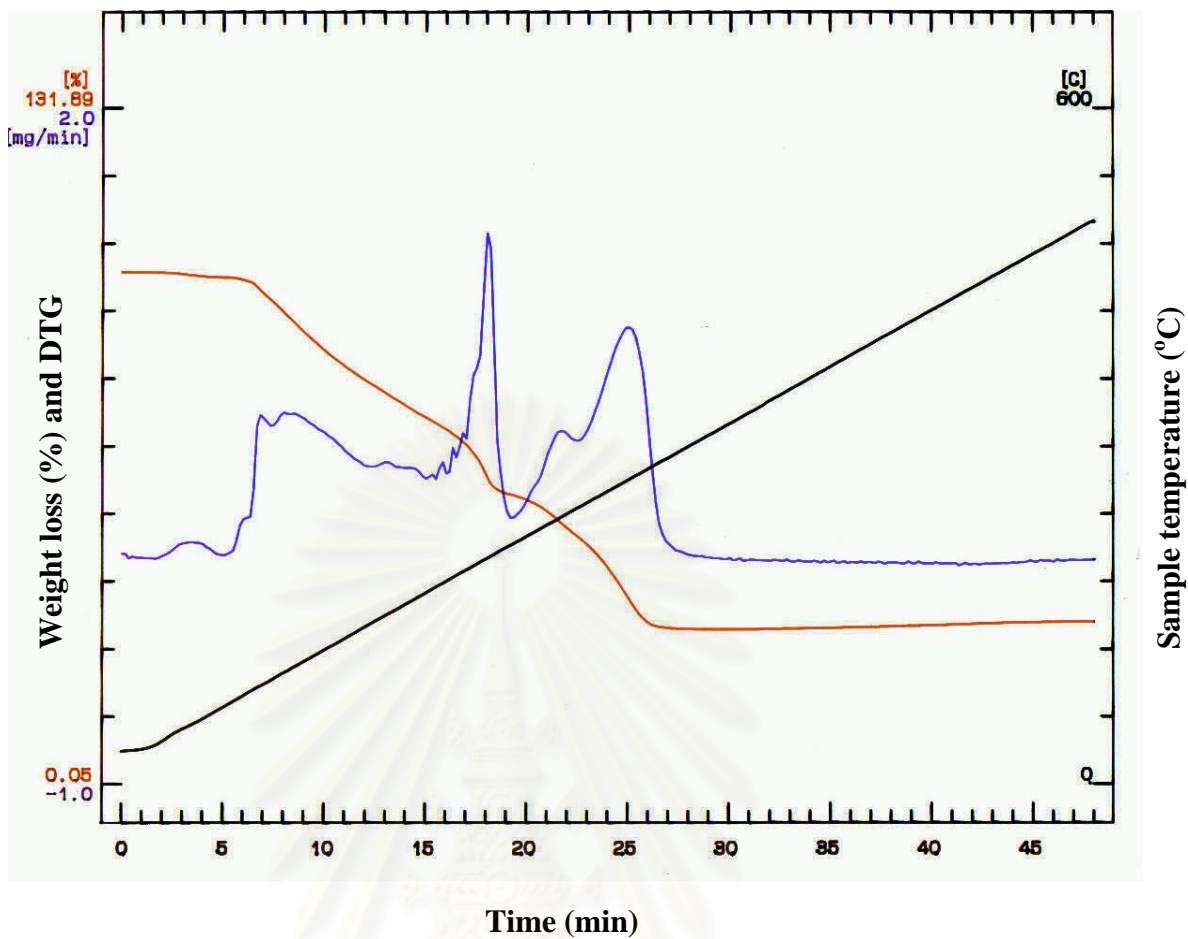


Figure 5.12 (d) Thermogravimetric analysis (TGA) experiments for Co-Nitrate (bulk).

สถาบันวิทยบริการ
จุฬาลงกรณ์มหาวิทยาลัย

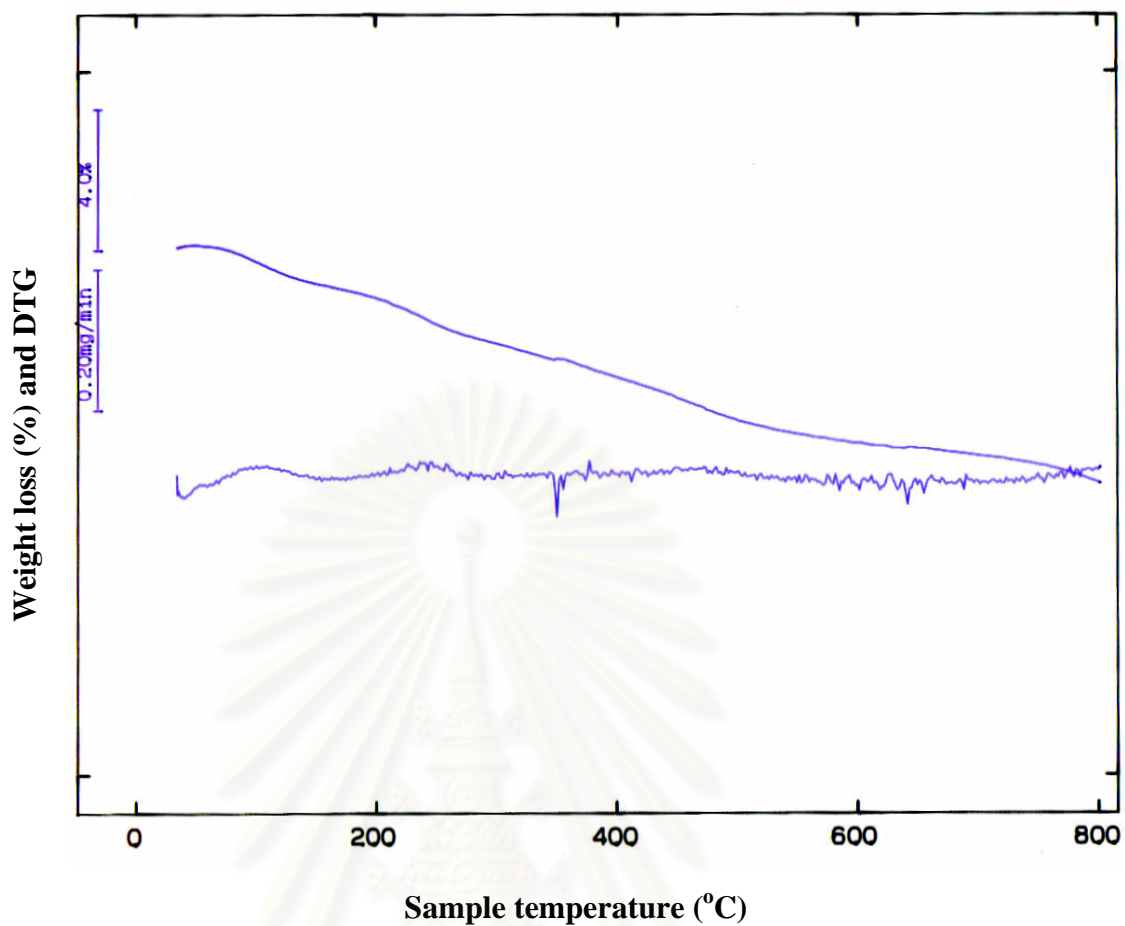


Figure 5.13 (a) Thermogravimetric analysis (TGA) experiments of Co/M-Ac in high temperature H_2 treatment.

สถาบันวิทยบริการ
จุฬาลงกรณ์มหาวิทยาลัย

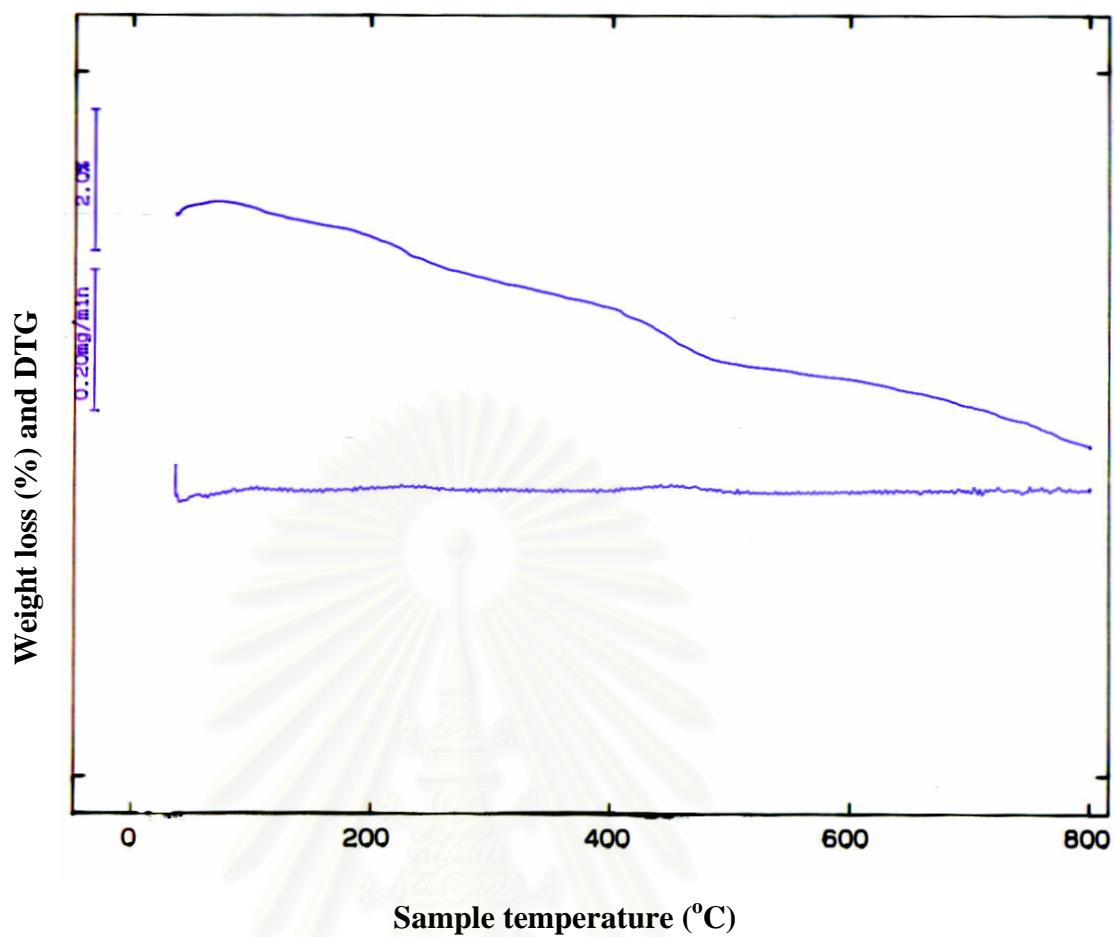


Figure 5.13 (b) Thermogravimetric analysis (TGA) experiments of Co/M-AA in high temperature H₂ treatment.

สถาบันวิทยบริการ
จุฬาลงกรณ์มหาวิทยาลัย

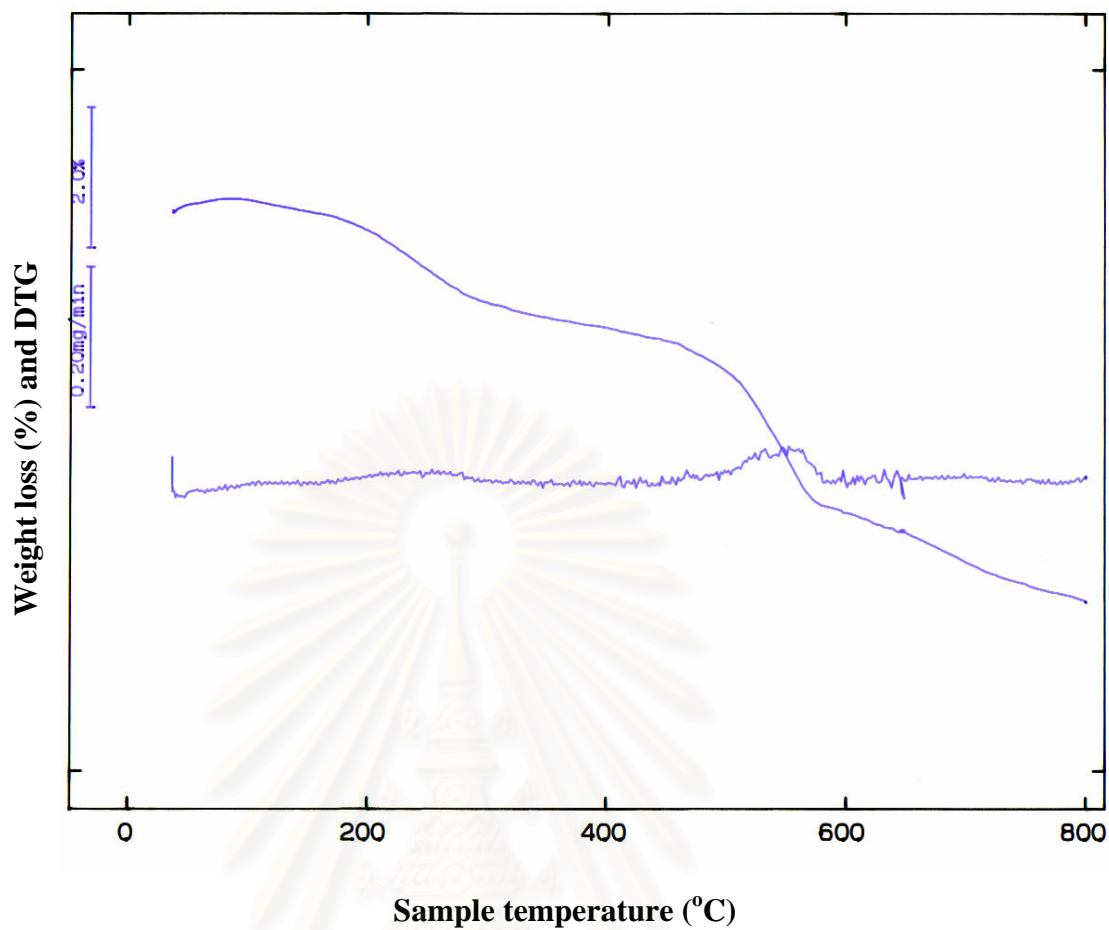


Figure 5.13 (c) Thermogravimetric analysis (TGA) experiments of Co/M-Cl in high temperature H_2 treatment.

สถาบันวิทยบริการ
จุฬาลงกรณ์มหาวิทยาลัย

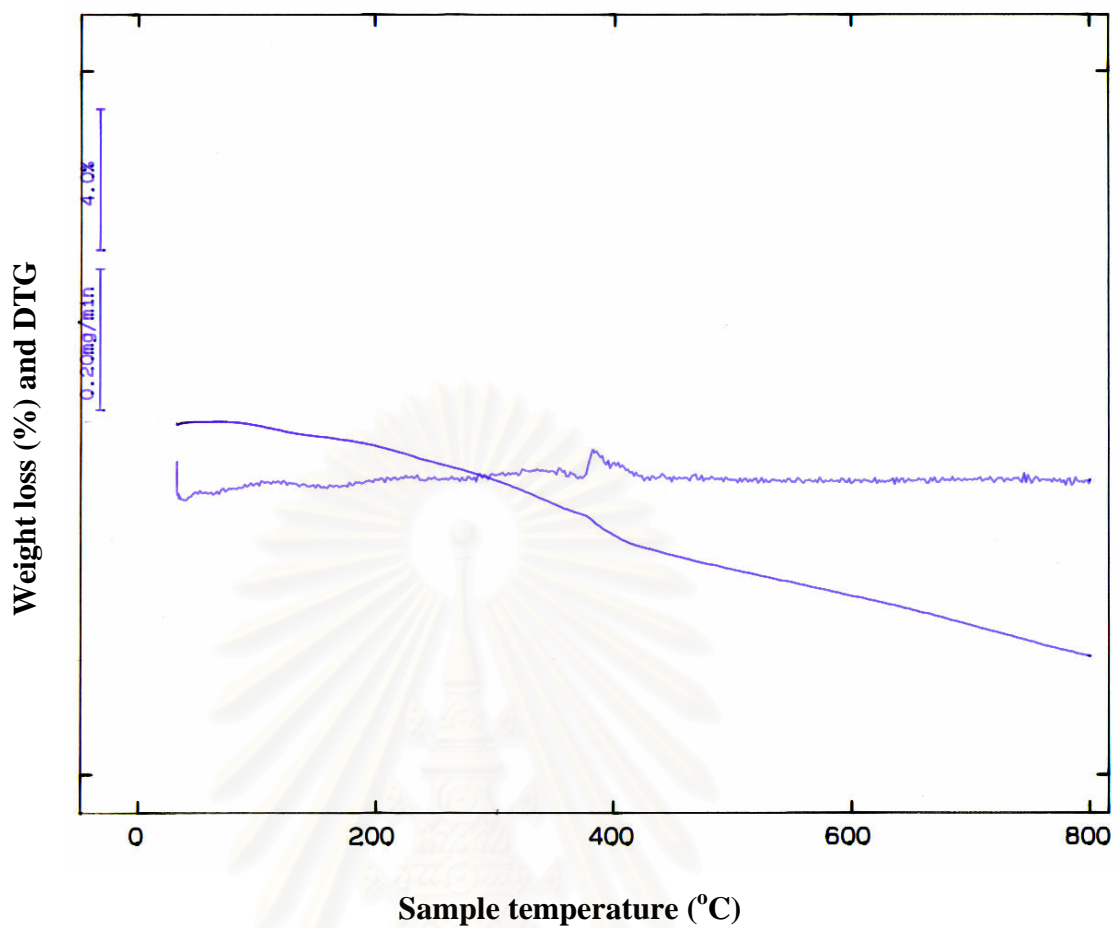


Figure 5.13 (d) Thermogravimetric analysis (TGA) experiments of Co/M-NO in high temperature H₂ treatment.

สถาบันวิทยบริการ
จุฬาลงกรณ์มหาวิทยาลัย

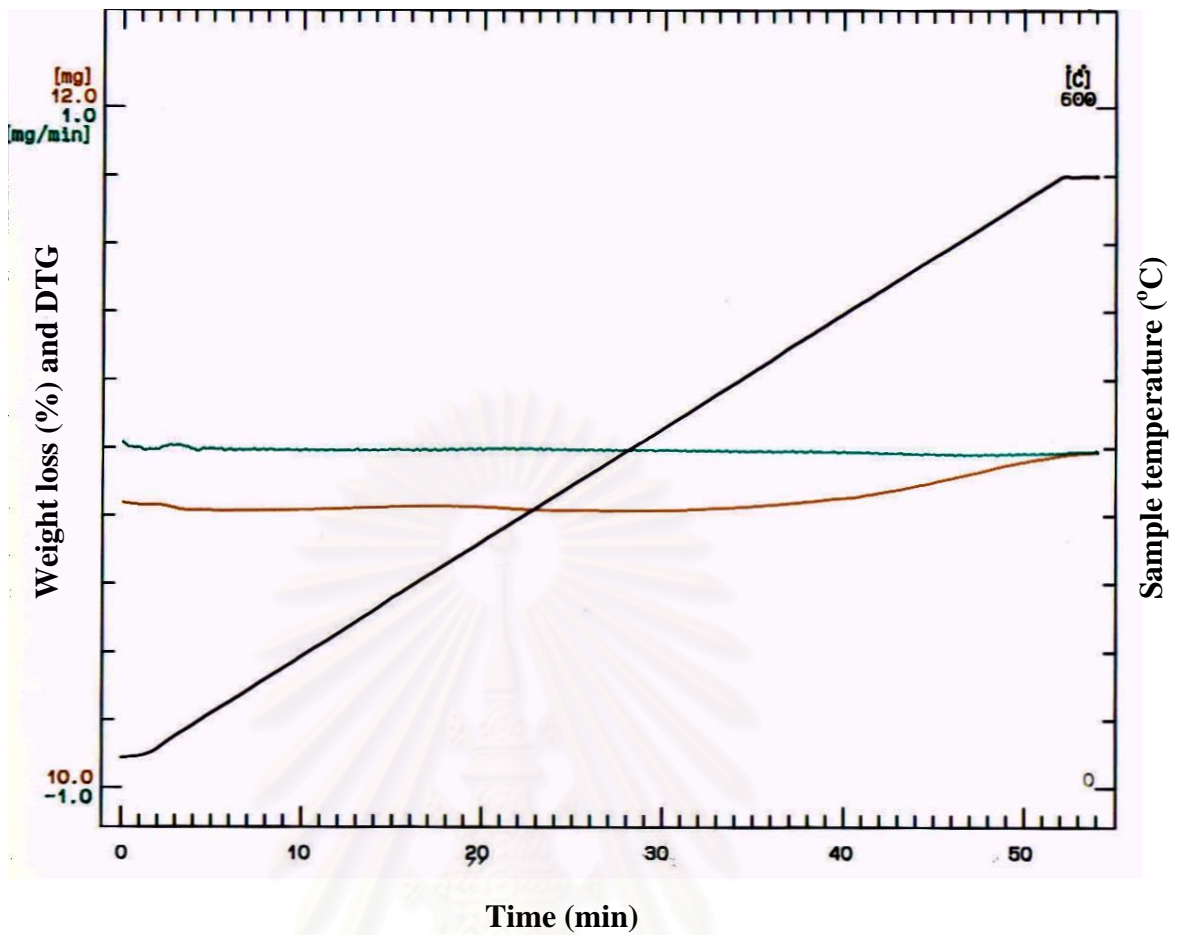


Figure 5.14 Thermogravimetric analysis (TGA) experiments for MCM-41 in air.

สถาบันวิทยบริการ
จุฬาลงกรณ์มหาวิทยาลัย

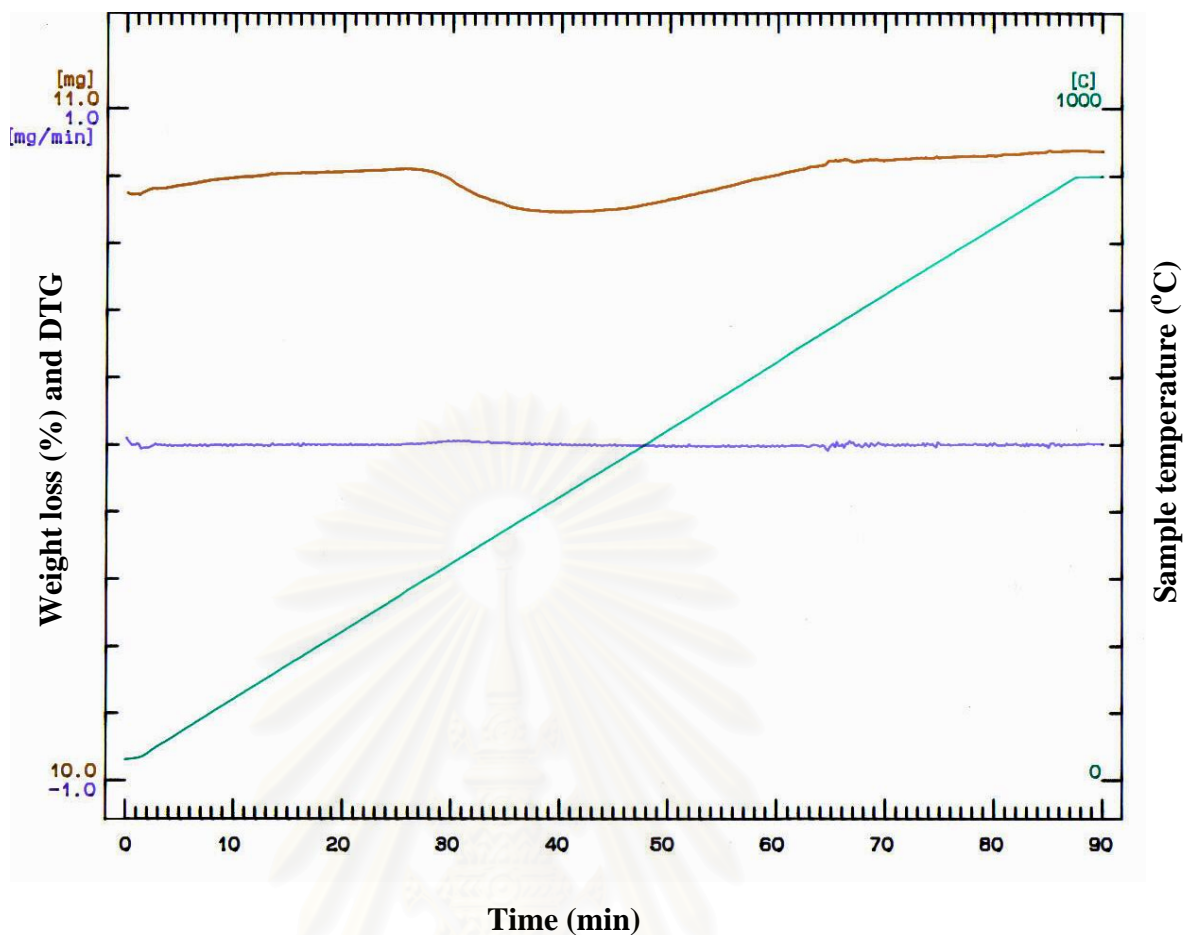


Figure 5.15 Thermogravimetric analysis (TGA) experiments for MCM-41 in high temperature H_2 treatment.

สถาบันวิทยบริการ
จุฬาลงกรณ์มหาวิทยาลัย

5.1.9 Raman Spectroscopy

Raman spectroscopy is one of vibrational spectroscopies that is used to study oxidation states and interactions of metal oxides. Vibration in Raman spectroscopy is excited by scattering of photons. Raman spectra of MCM-41 supported Co catalysts and Co_3O_4 are shown in Figure 5.16. Strong Raman bands for Co/M-NO catalyst were observed at 694, 528, and 488 cm^{-1} , which can be assigned to Co_3O_4 (Jongsomjit *et al.*, 2001). Raman bands for Co_3O_4 were not apparent for Co/M-Ac catalyst. This suggests that either (1) cobalt did not form Co_3O_4 crystallites but presented as an amorphous cobalt oxide or (2) the Co_3O_4 formed were located deep inside the MCM-41 pores which the photons were not able to scatter through. Typically, photons can scatter through surface of catalyst for less than 2 micron. The diameter size of our catalyst granules are ca. 30-50 μm . The existing of very small Co particles (amorphous or Co_3O_4) have been shown by XRD, SEM, and TEM. Raman results confirm that cobalt particles of Co/M-Ac were not deposited on outside surface of MCM-41. There was also little evidence of much formation of the highly dispersed Co “silicate” phase for the MCM-41-supported Co catalyst prepared from Co acetate. No peak for Co-Si was detected.

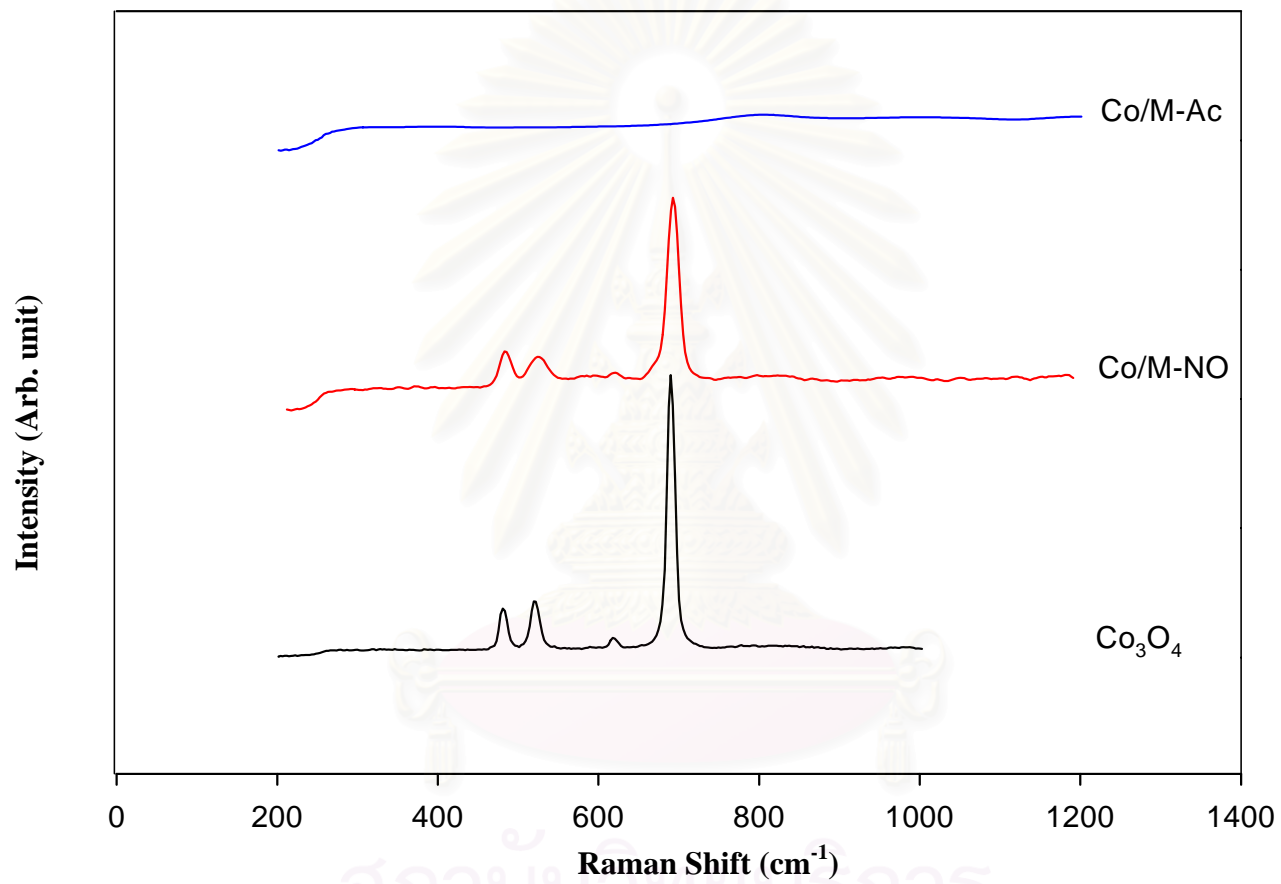


Figure 5.16 Raman spectra of different Co precursors of MCM-41 –supported Co catalysts.

5.1.10 Strong-Metal Support Interaction Effect

Normally, suppressing of chemisorption can be due to “strong-metal support interaction” (SMSI) effect which occurs in some partially reduced metal oxides (low chemisorption at high reduction temperature). The series of CO-pulse experiments were performed on Co/M-AA in order to observe SMSI effect in this catalyst. Table 5.8 shows percentages of Co dispersion of Co/M-AA after reduction in H₂ flow at 350°C and 500°C. Co/M-AA reduced at 350°C showed the same %Co dispersion as reduced at higher temperature (500°C). The catalyst was reduced at high reduction temperature but %Co dispersion did not change. Therefore, it was proved that this catalyst does not exhibit a strong metal-support interaction.

Table 5.8 Evidence for “non”-SMSI (strong-metal support interaction)

Catalyst	Co active sites ($\times 10^{17}$ CO molecule/g of cat.)	Total Co atoms present ($\times 10^{19}$ molecule/g of cat.)	Relative Co dispersion (CO/Co) ^a x 100
Co/M-AA (350°C) ^b	8.44	1.11	7.6
Co/M-AA (500°C) ^c	18.9	2.51	7.6

^a The relative %Co dispersion from pulse CO chemisorption experiments.

^b Co/M-AA was reduced in H₂ flow at 350°C.

^c Co/M-AA was reduced in H₂ flow at 500°C.

Overall, cobalt precursors were found to strongly affect the dispersion of Co on MCM-41. MCM-41 is known to have a restricted pore structure; however, using organic precursors such as cobalt acetate cobalt acetylacetonate resulted in very small cobalt particles and/or highly dispersed amorphous cobalt that could not be detected by XRD and Raman spectroscopy even for a cobalt loading as high as 8 wt%. These cobalt particles were small enough to fit into the pores of MCM-41. However, they were found to be inactive for H₂ chemisorption due probably to formation of cobalt silicates. No SMSI was found on such catalysts. The use of cobalt chloride resulted in very large cobalt particles/clusters and/or residual Cl⁻ blocking active sites. Consequently, very small active surface area was measurable. The use of cobalt nitrate resulted in a number of small cobalt particles dispersed throughout MCM-41 and some larger particles located on the external surface of MCM-41. Co/MCM-41 prepared from cobalt nitrate exhibited the highest H₂ chemisorption activity.

In the next section (section 5.2), CO hydrogenation was performed to determine the overall activity and selectivity of these catalysts under methanation conditions (220°C, 1 atm, and H₂/CO = 10).

5.2 CO Hydrogenation Activity over Co/MCM-41 Catalysts

Normally, cobalt catalyst is prepared in the form of cobalt oxide phase (Co_3O_4 or Co_2O_3). Cobalt oxide has to be reduced to cobalt metal (Co^0) prior to reaction since cobalt metal is known to be the most active phase for CO hydrogenation, not its oxides. Before reaction, cobalt oxide catalyst is reduced in H_2 at 500°C for 10 h in order to obtain metallic phase cobalt.

5.2.1 Temperature Programmed Reduction (TPR)

TPR or temperature programmed reduction is a powerful tool to study the reduction of metal oxide. %Reducibility of a catalyst can be calculated from areas under TPR peaks. The percentage of reducibility of a catalyst is important since it directly relates to the amount of active Co available for catalyzing reaction.

TPR profiles of the MCM-41-supported Co catalysts are shown in Figures 5.17. The TPR profile of bulk Co_3O_4 is also given in Figure 5.17. The reduction peak for bulk Co_3O_4 can be assigned to the two-step reduction of Co_3O_4 (Zhang *et al.*, 1999) as shown in reaction (1) and (2):



In general, TPR profiles are more complex for supported Co catalysts than for bulk Co_3O_4 due to various causes, such as variation in the metal particle size on the support, metal-support interaction, and influence of support porous structure, resulting in differently reducible cobalt species on the support (Reuel and Bartholomew, 1984; Ernst, 1999; Okamoto, 1991). The effects of particle size and support interaction, however, can superimpose on each other. Thus, while a decrease in metal oxide particle size can result in faster reduction due to a greater surface area/volume ratio, smaller particles may interact more with support slowing reduction.

The reduction profile of Co/M-NO was composed of two main reduction peaks at about 350°C ($T_{1\text{max}}$) and 785°C ($T_{2\text{max}}$), respectively. The first peak could be assigned to the two-step reduction of $\text{Co}_3\text{O}_4 \rightarrow \text{CoO} \rightarrow \text{Co}^0$. The second peak at

much higher temperature can be attributed to more difficult to reduce Co oxide species due to stronger interaction between small Co particle and MCM-41 support. The TPR spectrum of cobalt catalyst starting from chloride is essentially the same as for the unsupported cobalt salt showing negligible interaction between the support and the cobalt salt (Steen *et al.*, 1996). The peak was shifted to slightly higher temperature due probably to the extremely large cobalt oxide particle size.

The TPR profile of the Co/M-AA is composed of a small peak at about 390°C attributed to the reduction of Co_3O_4 to Co^0 , and a large reduction peak at about 765°C, attributed to difficult to reduce Co oxide species. However, the area under the first peak was much smaller than that of Co/M-NO. On the other hand, Co/M-Ac only showed an intense reduction peak centered at ca. 785°C, therefore Co oxide on Co/M-Ac could not be reduced under reduction condition used. Martinez *et al.*, 2003 also reported that the high-temperature peak could be assigned to the reduction of cobalt silicate species probably formed by reaction of Co^{2+} species strongly interacting with MCM-41 support.

The reducibilities of the catalysts during TPR 30-800°C and during TPR 30-500°C are reported in Table 5.9. The degrees of reduction of the catalysts in TPR from 30-800°C were different, ranging from 37-76%, and in the order of Co/M-Cl > Co/M-NO > Co/M-AA > Co/M-Ac. In a previous characterization study by Khodakov *et al.*, the hydrogen reduction properties of supported cobalt oxide particles were found to depend on the size of the Co_3O_4 crystallites, with larger particles being much easily reduced (Khodakov *et al.*, 1997; Khodakov *et al.*, 2001). Any Co not reducible during the H_2 reduction up to 800°C is identified as “non-reducible” Co silicates (Backman *et al.*, 1998; Kogelbauer *et al.*, 1995). In this study, the reducibilities during TPR 30-500°C for MCM-41-supported cobalt catalysts, especially for the ones prepared from organic cobalt precursors (Co/M-Ac and Co/M-AA) were found to be much less than the ones prepared from inorganic Co precursors (Co/M-Cl and Co/M-NO), with Co/M-NO showing the highest degree of reduction. The reducibility during TPR 30-500°C is especially important because it has been found to correlate with the reducibility of the catalysts during the optimum reduction procedure used (reduction at 500°C in flowing H_2 for 10 hours after ramping to that

temperature at 1°C/min). Using a reduction temperature too high during reduction step could result in fast catalyst deactivation (Ho, 1998; Jablonski *et al.*, 2003).

Table 5.9 Results from TPR

Catalyst	Reducibility ^a	
	During TPR 30 to 800°C	During TPR 30 to 500°C ^b
Co/M-Ac	37	0
Co/M-AA	47	16
Co/M-Cl	76	34
Co/M-NO	51	26

^a From TPR experiments.

^b Correlates to percentage of metal reduce during reduction procedure (ramp 1°C / min to 500°C, hold for 10 h)

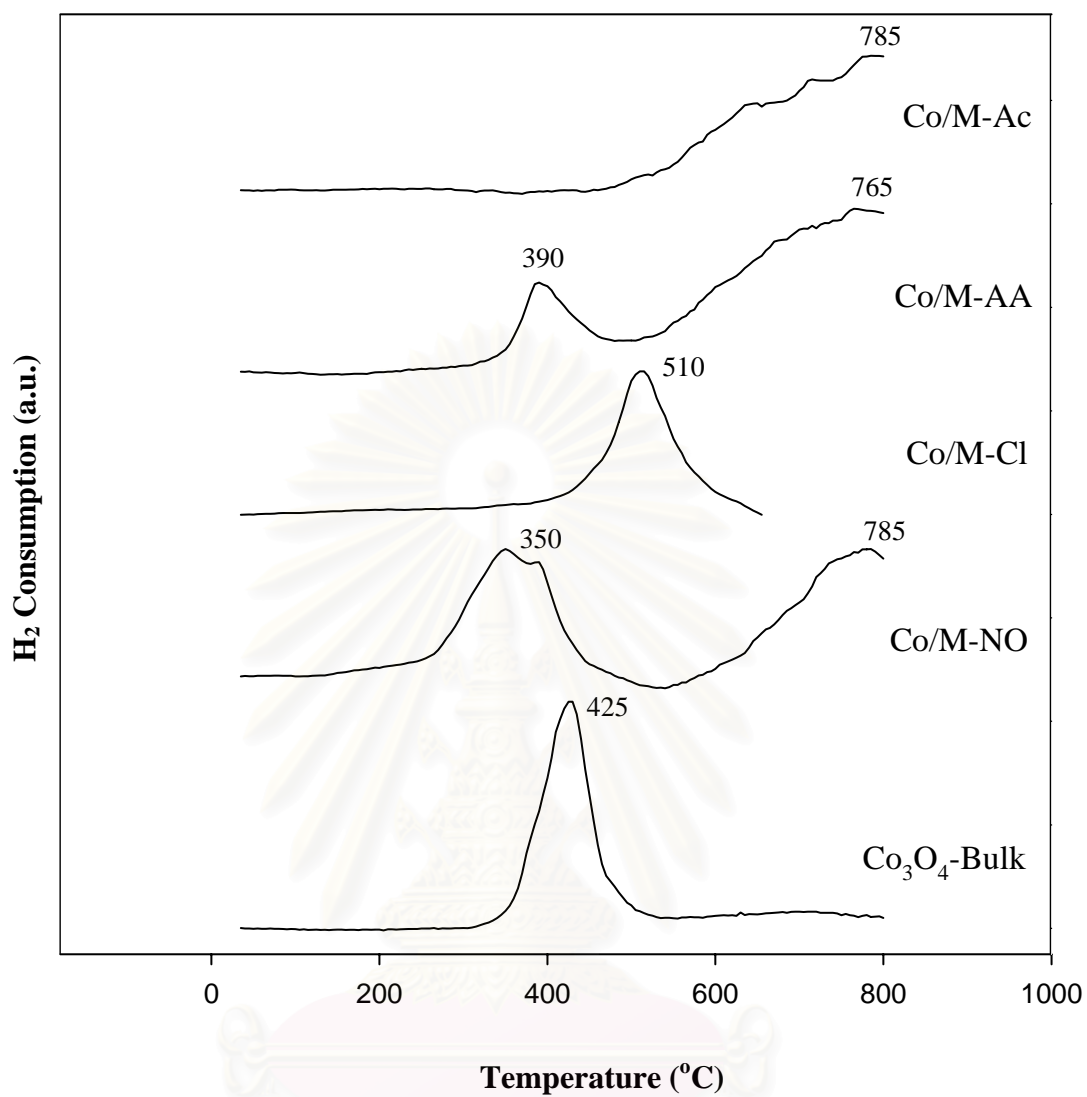


Figure 5.17 TPR profiles of the Co/MCM-41 catalysts with different Co precursors.

สถาบันวิทยบริการ
จุฬาลงกรณ์มหาวิทยาลัย

5.2.2 CO Hydrogenation

The CO hydrogenation reactions were carried out at 220°C, 1 atm, and H₂/CO ratio = 10 for all the catalyst samples. A relatively high H₂/CO ratio was used in order to minimize catalyst deactivation due to carbon deposition during reaction. Table 5.10 presents CO hydrogenation rates, %CO conversions, selectivities, and TOF of these catalysts. It was found that at the reaction conditions used, Co/M-NO exhibited a much higher CO hydrogenation rate than all other catalysts in this study. Co/M-Cl is due probably to very low Co dispersion as observed from XRD, TEM, SEM-Mapping, SEM-EDX and CO or H₂ chemisorption. In the case of Co/M-Ac and Co/M-AA, no H₂-chemisorption was detected suggesting that Co was not in an active form after standard reduction. It is not surprising that they exhibited very low CO hydrogenation activities. It has been reported that small Co particles on SiO₂, were unstable and could form Co silicates during reduction in H₂ (Kogelbauer *et al.*, 1995; Jablonski *et al.*, 1998).

Table 5.10 Results CO Hydrogenation Reaction at methanation conditions ^a.

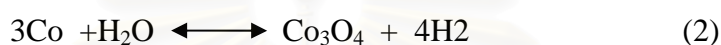
Catalyst	Rate (gCH ₂ / gcat./h)		CO Conversion (%)		%Selectivity			TOF ^b (1/S)
	Initial	Steady-state	Initial	Steady-state	CH ₄	C ₂	C ₃	
Co/M-Ac	0.0249	0.0179	3.2	2.4	91	7.0	2.0	nil
Co/M-AA	0.0132	0.0131	1.8	1.7	96	3.4	0.6	nil
Co/M-Cl	0.0244	0.0182	3.3	2.4	82	6.0	12.0	nil
Co/M-NO	0.449	0.323	59.8	47.6	97	2.5	0.5	0.26

^a CO hydrogenation was carried out at 220°C, 1 atm, H₂/CO = 10 (H₂/CO/Ar = 20/2/8 cc/min).

^b Turnover frequencies, based on total hydrogen chemisorption and the CO hydrogenation rate.

5.2.3 Catalysts Characterization after CO Hydrogenation

After CO hydrogenation reaction, the characteristics of the catalysts were investigated in order to observe any effect of cobalt precursors on catalyst deactivation. During CO hydrogenation, deactivation of supported cobalt catalysts is typically due to (1) sulphur poisoning, (2) blocking of pore and active surface by metal sintering and/or support collapse and/or condensation of hydrocarbon products (coking), and (3) oxidation of cobalt



From thermodynamic point of view, reactions (1) and (2) are unlikely to occur, whilst the oxidation to cobalt “silicate” is thermodynamically spontaneous.

Strong literature support exists in favor of cobalt catalyst oxidation during Fischer-Tropsch synthesis. Iglessia (Iglessia, 1997) concluded that rapid catalyst deactivation, as a result of cobalt oxidation, is to be anticipated in the case of supported Co catalysts with high cobalt dispersion (>15%).

In the present study, we focused only the deactivation by pore blocking due to metal sintering and/or support collapse and cobalt support compound formation because under the reaction conditions used, a relatively high H₂/CO ratio produce minimal carbon deposits and only high purity grade reaction gases were used, therefore, no sulphur was presented.

5.2.3.1 X-ray diffraction (XRD)

In order to observe any change in the pore structure of MCM-41 after CO hydrogenation by XRD, cobalt has to be first removed otherwise large Co particles can cause significant X-ray scattering. The metals were removed by acid leaching using a 30% HCl treatment for 2 days.

The results of the acid leached Co/MCM-41 after CO hydrogenation reaction are shown in Figure 5.18. It was found that the intensity of the MCM-41 reflection peak gradually decreased after reduction and 6 h CO hydrogenation and the peak became broadened. It is suggested that the long range order of the MCM-41 may have partially collapsed during reduction and reaction. This is probably due to an effect of water vapor produced during metal reduction and reaction. The instability of pure silica MCM-41 toward water vapor has also been found by others (Ribeiro Carrott *et al.*, 1999; Kruk *et al.*, 1999).

The XRD results at higher diffraction angles of Co/MCM-41 after reduction and reaction without and with re-calcination treatment state were display in Figure 5.19 and 5.20, respectively. Surprisingly, only Co/M-Cl exhibited diffraction peaks at 2θ of ca. 44.5° which indicate formation of large Co metal. After re-calcination treatment at 500°C 2 hrs, the spent Co/M-Cl catalyst exhibited XRD peak at 36.8° 2θ , the major peak of Co_3O_4 spinel. The average cobalt oxide crystallite sizes of Co/M-Cl after reduction and reaction with and re-calcination treatment are shown in Table 5.12. These cobalt oxide particle sizes are much smaller than cobalt oxide particle sizes of Co/M-Cl before reaction. It is indicated that the residual Cl⁻ was removed when water vapor is present, during CO hydrogenation.

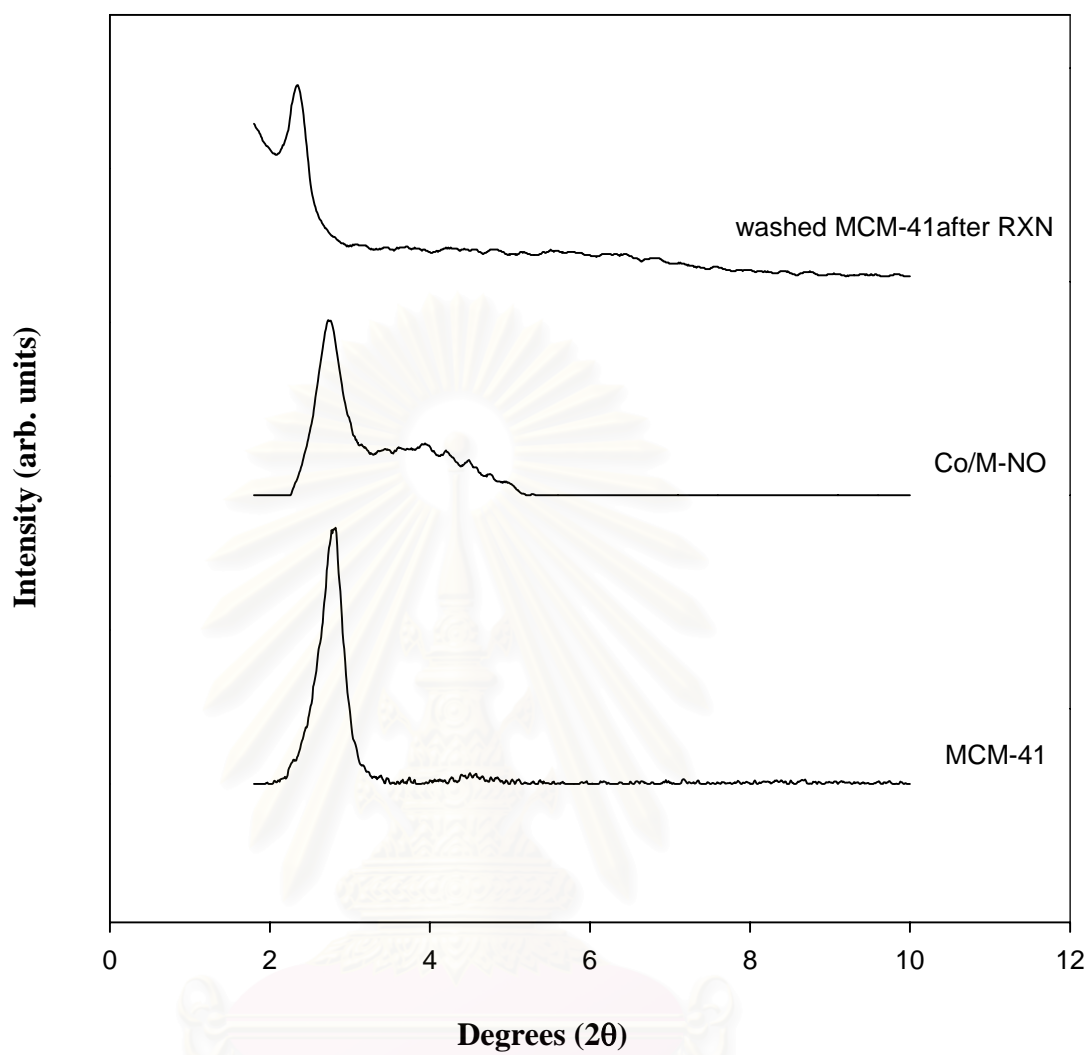


Figure 5.18 XRD results for acid-leached MCM-41-supported Co catalysts.

สถาบันวิทยบริการ
จุฬาลงกรณ์มหาวิทยาลัย

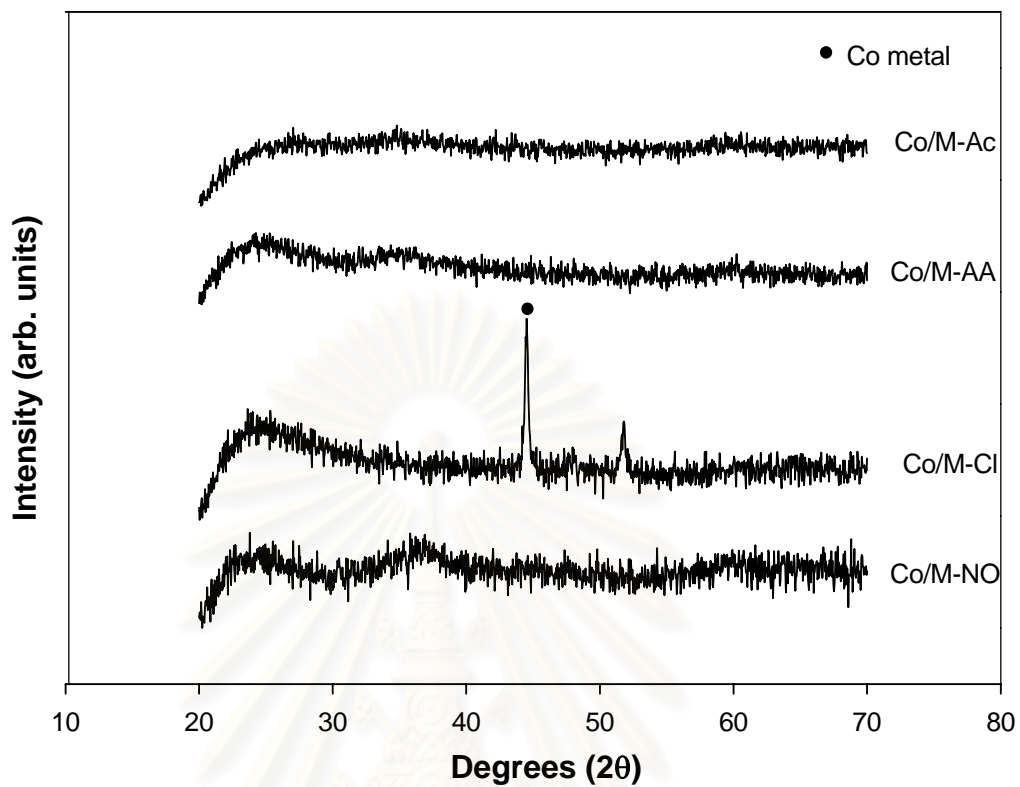


Figure 5.19 XRD results for the spent MCM-41 supported Co catalysts after reduction and reaction without re-calcination treatment.

สถาบันวิทยบริการ
จุฬาลงกรณ์มหาวิทยาลัย

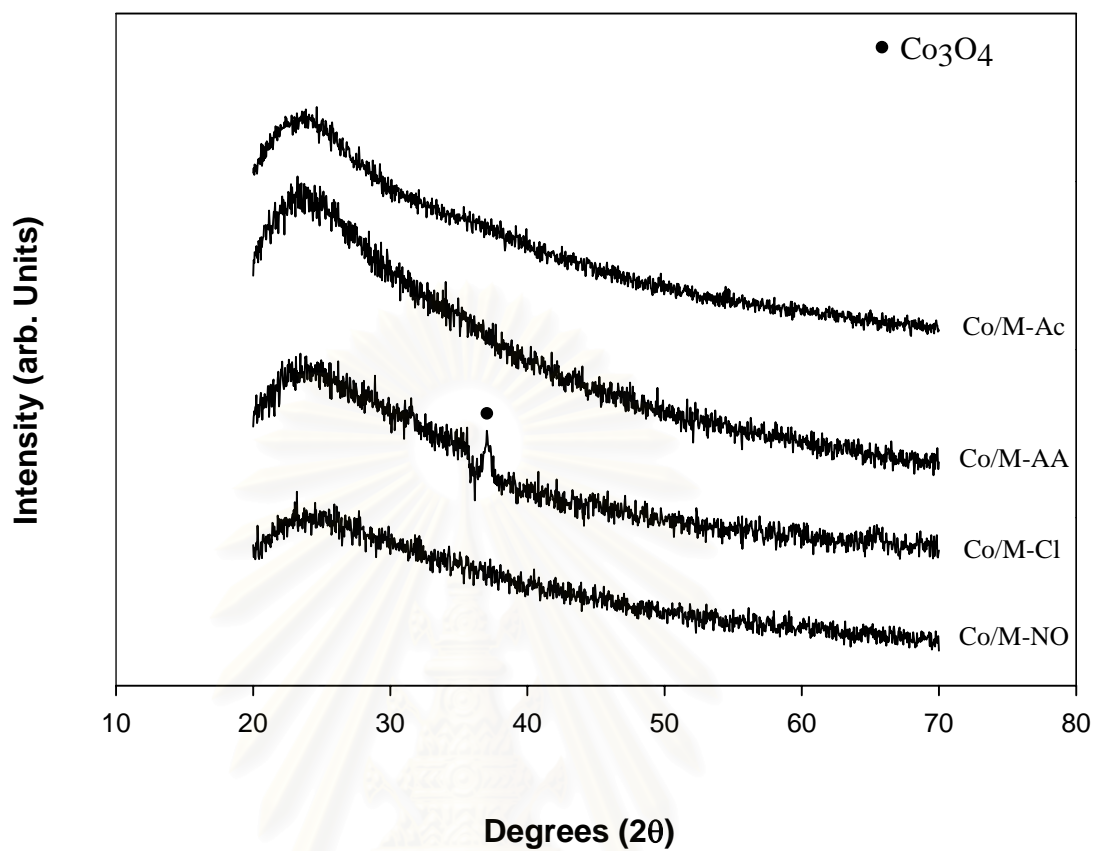


Figure 5.20 XRD results for spent Co/MCM-41 catalysts after reduction and reaction with re-calcination treatment at 500°C 2 hrs.

สถาบันวิทยบริการ
จุฬาลงกรณ์มหาวิทยาลัย

5.2.2.2 H₂ Chemisorption

The results from H₂ chemisorption on the spent catalysts with and without re-calcination treatment were presented in Table 5.11. The %Co dispersion which only measurable for Co/M-NO decreased by approximately 80% of the fresh catalyst. This is probably the consequence of destruction of the MCM-41 support pore structure after reaction blocking Co active sites.

Table 5.11 Results from H₂ chemisorption of the spent catalysts with and re-calcination treatment

Catalyst	H ₂ chemisorption	
	Total ($\mu\text{mol H}_2/\text{gcat.}$)	% Co Dispersion
Spent Co/M-Ac	nil	nil
Spent Co/M-AA	nil	nil
Spent Co/M-Cl	nil	nil
Spent Co/M-NO	1.71	0.25

5.2.2.3 Transmission Electron Microscopy (TEM)

TEM micrographs were taken for all the spent catalysts after CO hydrogenation reaction in order to physically observe any change in the size of cobalt oxide particles after reaction. The TEM micrographs for spent MCM-41-supported Co catalysts are shown in Figure 5.21. Table 5.12 also shows the average cobalt oxide crystallite sizes that are measured from TEM micrographs. TEM images were found quite similar Co oxide particles size to fresh catalysts especially Co/M-NO, Co/M-AA, and Co/M-Ac. Much smaller particle size of Co/M-Cl was clearly seen by TEM, confirming that the residual Cl⁻ was removed during CO hydrogenation reaction. Sintering of metal particles were not observed for all the catalysts.

Table 5.12 Co₃O₄ average particle size of Co/MCM-41 catalyst after reduction and reaction with and re-calcination treatment

Catalyst	Co ₃ O ₄ Average Particle Size (nm)			
	TEM		XRD	
	Fresh	Spent	Fresh	Spent
Co/M-Ac	6.7	5.6	<5	<5
Co/M-AA	12.5	8.3	<5	<5
Co/M-Cl	60.0	16.7	46.1	17.9
Co/M-NO	18.4	12.5	13.3	<5

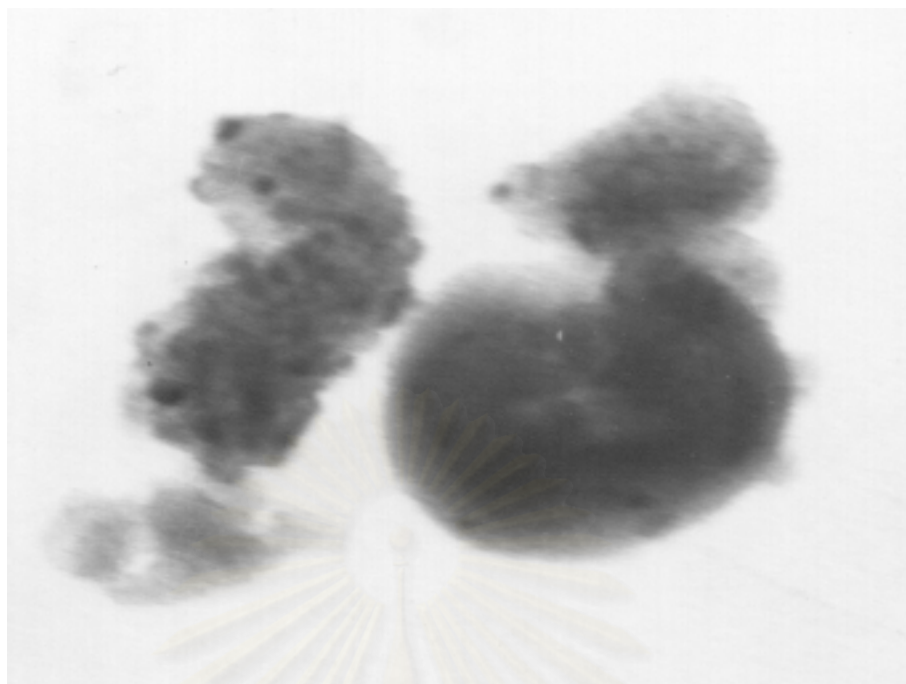


Figure 5.21 (a) TEM micrographs of calcined spent Co/M-Ac ($d_p=5.6\text{nm}$)

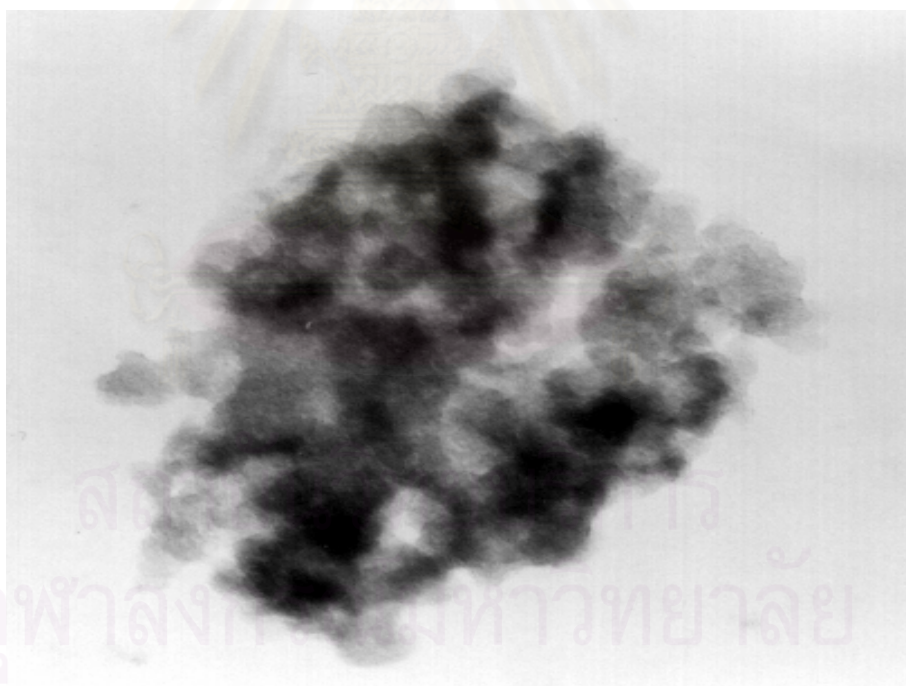


Figure 5.21 (b) TEM micrographs of calcined spent Co/M-AA ($d_p=8.3\text{nm}$)

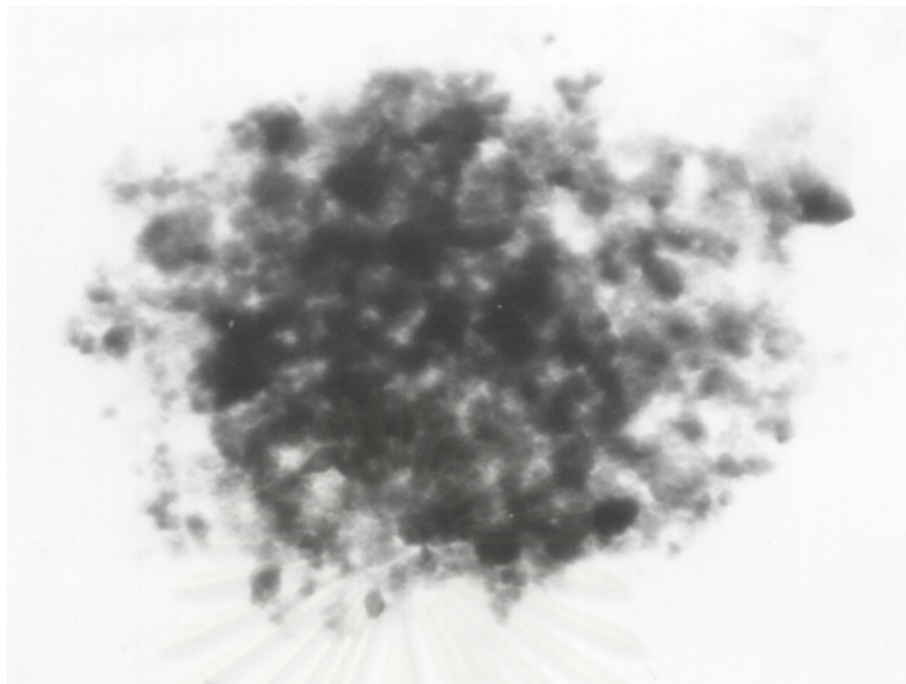


Figure 5.21 (c) TEM micrographs of calcined spent Co/M-Cl ($d_p=16.7\text{nm}$)

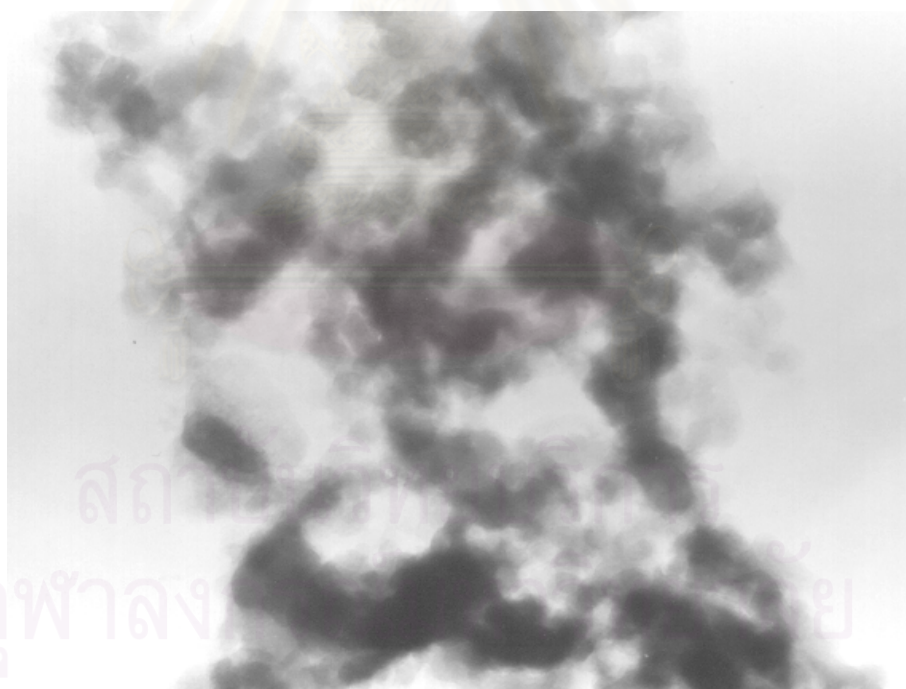


Figure 5.21 (d) TEM micrographs of calcined spent Co/M-NO ($d_p=12.5\text{nm}$)

From XRD, H₂ chemisorption, and TEM results, the catalyst was found to deactivate primarily by partial collapse of MCM-41 structure and not by metal sintering.

An existence of metal-support compounds were shown by higher reduction peaks in the TPR profiles discussed earlier in section 5.2.1. However, Co “silicate” formed could not be detected by characterization techniques such as XRD and Raman spectroscopy (Figure 5.22 showed Raman spectroscopy of Co/M-Ac after reduction at 500°C 10h.) suggesting that the highly dispersed Co “silicate” may be formed, possibly, by Co atom migration into the silica matrix as occurred in the case of Co/Al₂O₃ catalysts (Jongsomjit *et al.*, 2001).

From this section, it can be summarized that the effect of cobalt precursors on the characteristics and catalytic properties of supported catalysts is different from typically observed on commercial catalysts when restricted pore structure supports such as MCM-41 are used. In the literature (Jentys *et al.*, 1998; Suvanto *et al.*, 2000; Loosdrecht *et al.*, 1997; Kraum and Baerns, 1999; Rosynek and Polansky, 1991), the influence of cobalt precursors on SiO₂, TiO₂, and Al₂O₃ supported Co Fischer-Tropsch catalysts have been reported. Using organic precursors such as cobalt acetate or cobalt acetylacetonate, instead of inorganic ones such as cobalt nitrate or cobalt chloride result in very small cobalt particles, high Co dispersion and usually higher FTS activity. However, in this study it was found that Co particles small enough to fit into the pores of MCM-41, showed relatively small amount of CO or H₂ chemisorption and low activities for CO hydrogenation. It should be emphasized that a balance between dispersion-enhancing, strong support-precursor interaction and loss of metallic Co as a result of metal-support compound formation in order to obtain high activity supported Co catalysts is needed. The type of cobalt precursor must be carefully chosen, especially when restricted pore structure supports such as MCM-41 are used. Co particles small enough to fit into the pores of MCM-41 could be unstable at commercially relevant synthesis conditions and thus have limited practical use.

In the next section (section 5.3), the characteristics and catalytic activities of MCM-41-supported Co catalysts were compared to SiO₂-supported Co catalysts. The

SiO₂ used is a high surface area chromatographic grade silica that possesses a narrow pore size distribution of an average pore diameter of ca. 3 nm.

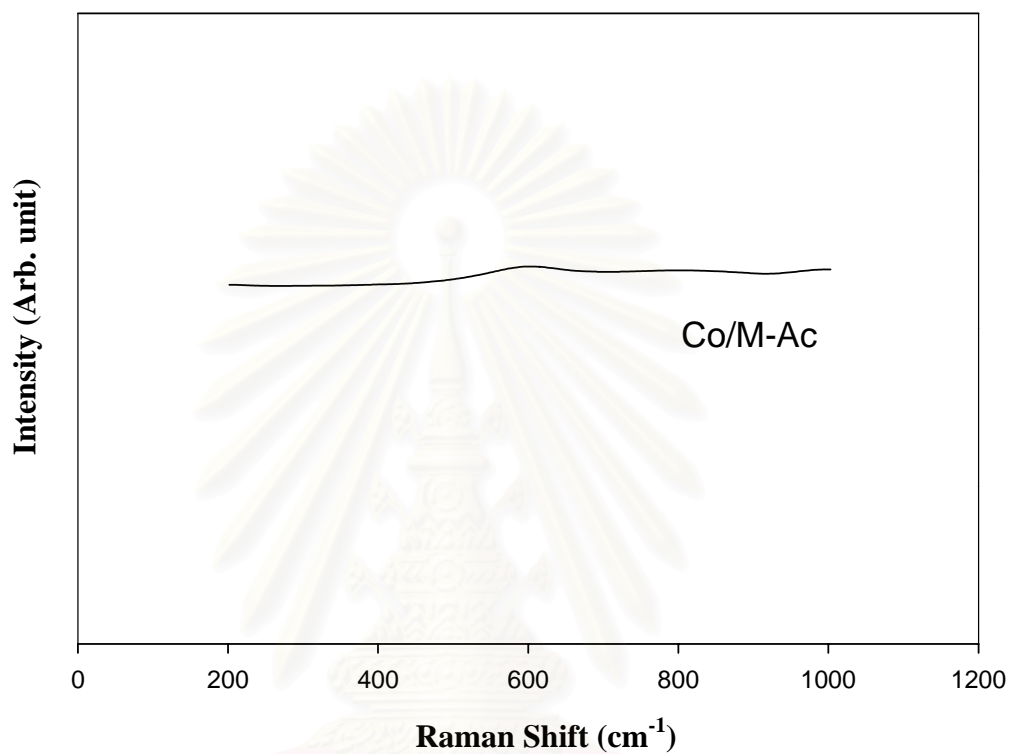


Figure 5.22 Raman spectra of Co/M-Ac after reduction in H₂ flow at 500°C for 10 h.

สถาบันวิทยบริการ
จุฬาลงกรณ์มหาวิทยาลัย

5.3 A Comparative Study of Co/MCM-41 and Co/SiO₂ Catalysts in CO Hydrogenation

In the previous sections, it was shown that Co on MCM-41 support exhibited different characteristics and catalytic properties to other supported Co catalyst reported in the literatures. Therefore, the effect of MCM-41 structure on the characteristics and catalytic activity for CO hydrogenation was extensively investigated in this section. And in order to distinguish the effect of pore size and pore structure of the support, high surface area silica with average pore diameter of 3 nm (similar to that of MCM-41) was employed as the catalyst support for preparation of supported Co catalysts and was compared to MCM-41-supported ones.

5.3.1 Characterization of Co/SiO₂ Catalysts

5.3.1.1 N₂ Physisorption

BET surface areas, pore volumes, and average pore diameters of Co/SiO₂ catalysts are given in Table 5.13. The SiO₂ support before cobalt impregnation had a BET surface area of 717 m²/g, and a pore volume of 0.39 cm³/g. They were slightly less than MCM-41. The BET surface areas of the SiO₂-supported cobalt catalysts prepared with different cobalt precursors had BET surface areas between 500-600 m²/g and in the order of Co/M-AA > Co/M-NO > Co/M-Ac > Co/M-Cl. The pore size distributions of MCM-41 and SiO₂ support are shown in Figure 5.23. Both series of supported Co catalysts had narrow pore size distributions. The average pore diameters for MCM-41 and SiO₂ were determined to be approximately 3 nm. This high surface area SiO₂, however, has much lower pore volume compared to MCM-41 (0.39 vs. 0.77 cm³/g), due to SiO₂ is an amorphous material while MCM-41 possesses cylindrical pore structure. No macropore was observed on both materials.

Table 5.13 N₂ physisorption results of Co/SiO₂ catalysts

Catalysts	BET S.A. (m ² /g)
SiO ₂	717
Co/S-Ac	562 ^a
Co/S-AA	595 ^a
Co/S-Cl	517 ^a
Co/S-NO	571 ^a

^a From Single point BET in our laboratory

5.3.1.2 Atomic Adsorption Spectroscopy (AAS)

The amounts of cobalt loading for the SiO₂-supported Co catalysts were measured by atomic adsorption spectroscopy and are given in Table 5.14. Cobalt loading on the catalyst samples was approximately 7-8 wt% similar to those of Co/MCM-41 catalysts.

Table 5.14 Atomic adsorption results of Co/SiO₂ catalysts

Catalyst	Co (wt%)
Co/S-Ac	7.9
Co/S-AA	7.7
Co/S-Cl	7.1
Co/S-NO	8.4

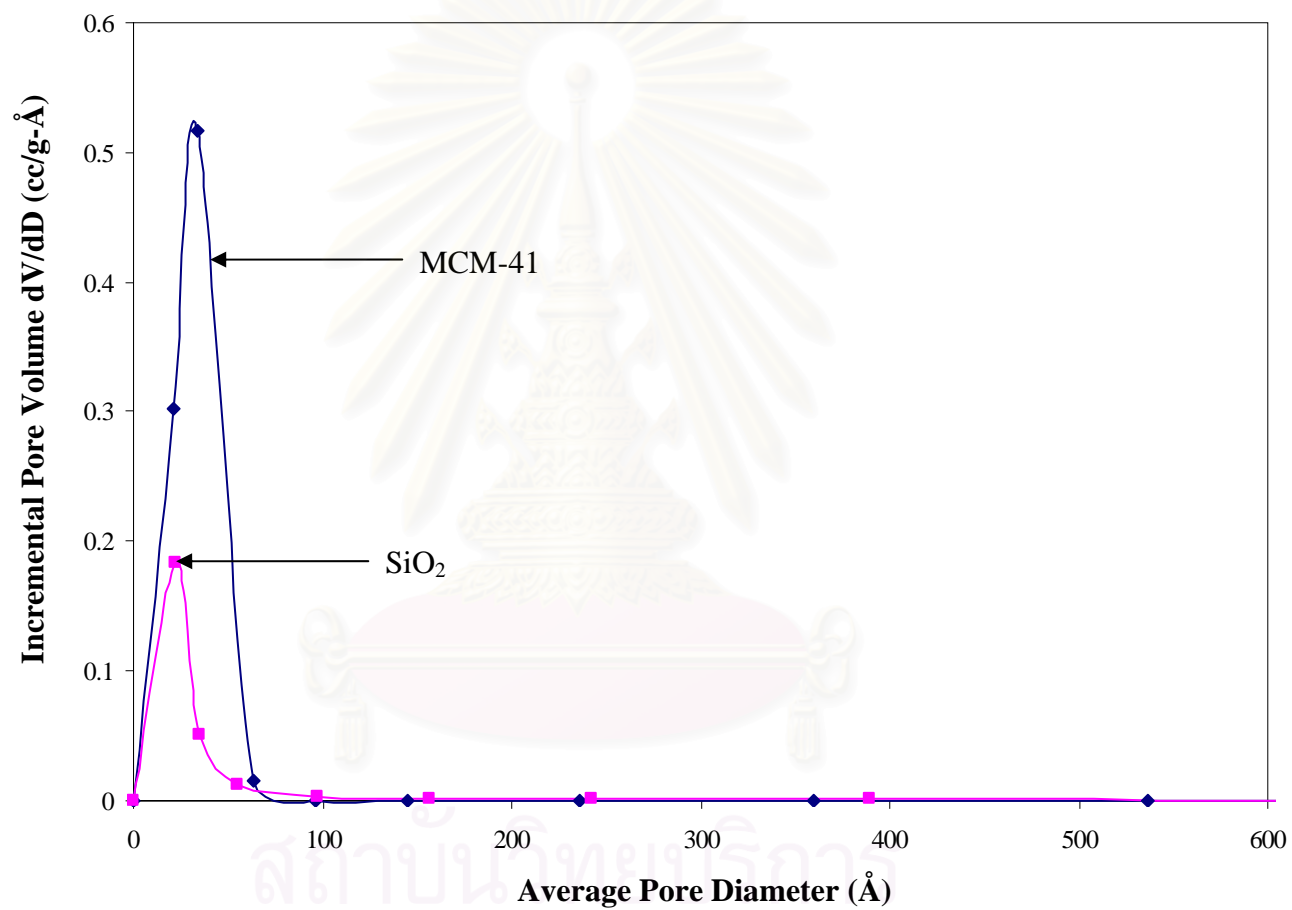


Figure 5.23 Pore size distribution of MCM-41 and SiO₂ support.

5.3.1.3 X-ray diffraction (XRD)

The XRD patterns at higher diffraction angles of the SiO₂-supported cobalt catalysts prepared with different cobalt precursors in the calcined state are shown in Figures 5.24. Co/S-NO and Co/S-Cl exhibited diffraction peaks at 2θ of ca. 31.3°, 36.8°, 45.1°, 59.4°, and 65.4° indicate that after calcinations at 500°C, cobalt was primarily in the form of Co₃O₄ spinel in the catalyst particles. Similar to MCM-41-supported Co catalysts, Co/S-Ac and Co/S-AA did not exhibit any distinct XRD patterns. This suggests that the crystallite size of cobalt oxide prepared from cobalt acetate and cobalt acetylacetonate on SiO₂ was also very small or an amorphous cobalt oxide were presented. The average cobalt oxide crystallite sizes calculated using the Scherrer's equation are given in Table 5.15. Larger average Co particles were observed on Co/S-NO and Co/S-Cl. The average Co particle sizes on Co/S-Cl was much smaller than Co/M-Cl suggesting that use of SiO₂ as a support resulted in less amount of residual Cl⁻ compared to MCM-41 supports.

Table 5.15 Comparison of Co₃O₄ Average Particle Size between Co/SiO₂ and Co/MCM-41.

Catalyst	Co ₃ O ₄ Average Particle Size (nm)		SEM
	TEM	XRD	avg. catalyst granule size (μm)
Co/S-Ac	8.3	<5	142
Co/S-AA	9.7	<5	136
Co/S-Cl	16.7	17.6	134
Co/S-NO	14.0	16.4	138
Co/M-Ac	6.7	<5	28
Co/M-AA	12.5	<5	30
Co/M-Cl	60.0	46.1	30
Co/M-NO	18.4	13.3	31

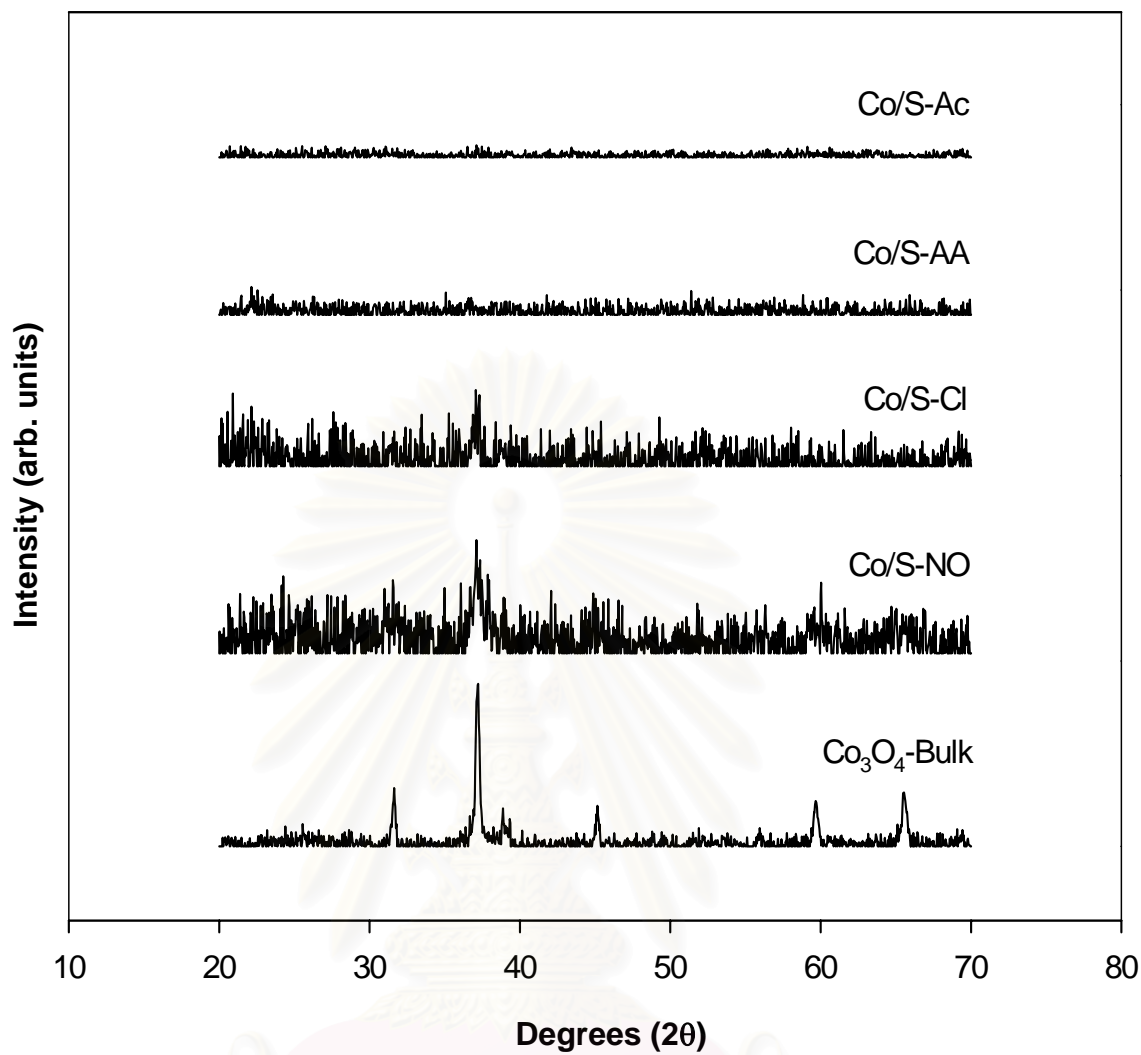


Figure 5.24 Effect of cobalt precursors on the XRD patterns of Co/SiO₂ catalysts (high degree 2θ)

สถาบันวิทยบริการ
จุฬาลงกรณ์มหาวิทยาลัย

5.3.1.4 Scanning Electron Microscopy (SEM) and Elemental Mapping

SEM micrographs of catalyst granules for SiO_2 are shown in Figure 5.25. The catalyst granule size distribution of Co/SiO_2 catalysts was obtained by measuring the catalyst granule size of a hundred primary particles from SEM micrograph and is shown in Figure 5.26. Typical SEM micrographs of catalyst granules for SiO_2 are shown in Figure 5.27. The average catalyst granules sizes for Co/SiO_2 catalysts are reported in Table 5.15. The SEM micrographs of catalyst granules for Co/SiO_2 prepared with different cobalt precursors show similar catalyst granule sizes of 130-150 microns. Use of SiO_2 as a Co catalyst support resulted in much larger catalyst granule size than use of MCM-41 (30-50 μm). The elemental mappings of cobalt on Co/SiO_2 are shown in Figure 5.28.

Distribution of Co on SiO_2 can be clearly seen from SEM micrographs. Large Co clusters and low Co dispersion was observed on Co/S-Cl while a uniform Co clusters of about 2.5 micron was well-dispersed on the surface of Co/S-NO . Smaller cobalt clusters were found to be non-uniformly distributed on both Co/S-Ac and Co/S-AA .

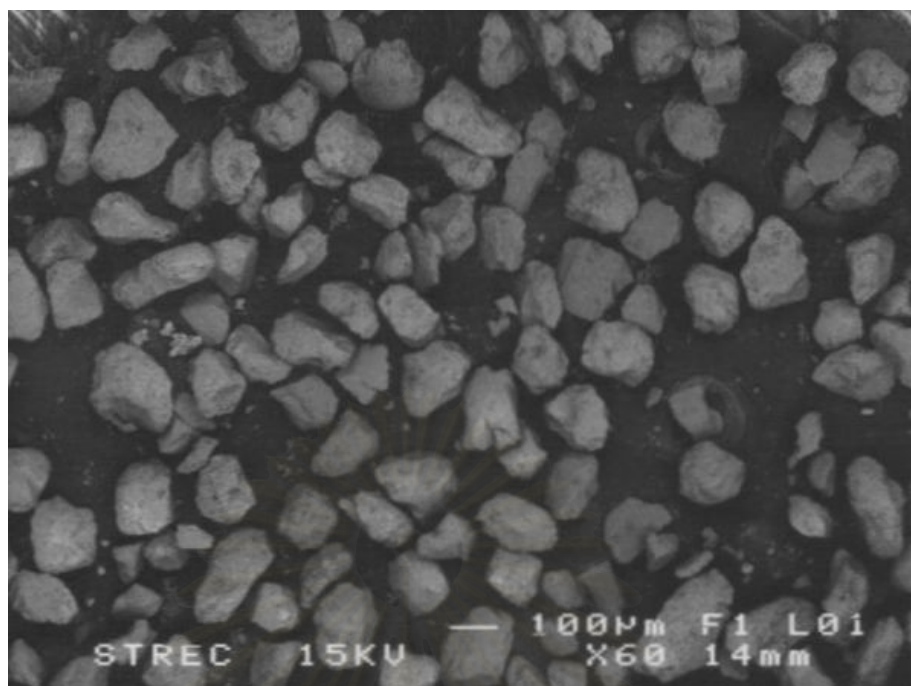


Figure 5.25 (a) SEM micrograph of catalyst granules for Co/S-Ac

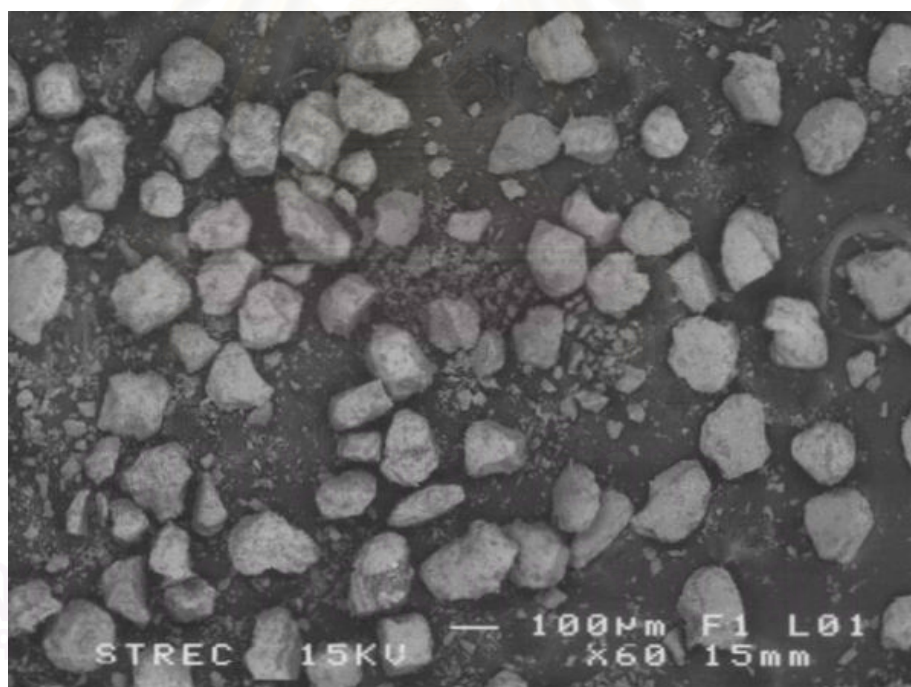


Figure 5.25 (b) SEM micrograph of catalyst granules for Co/S-AA

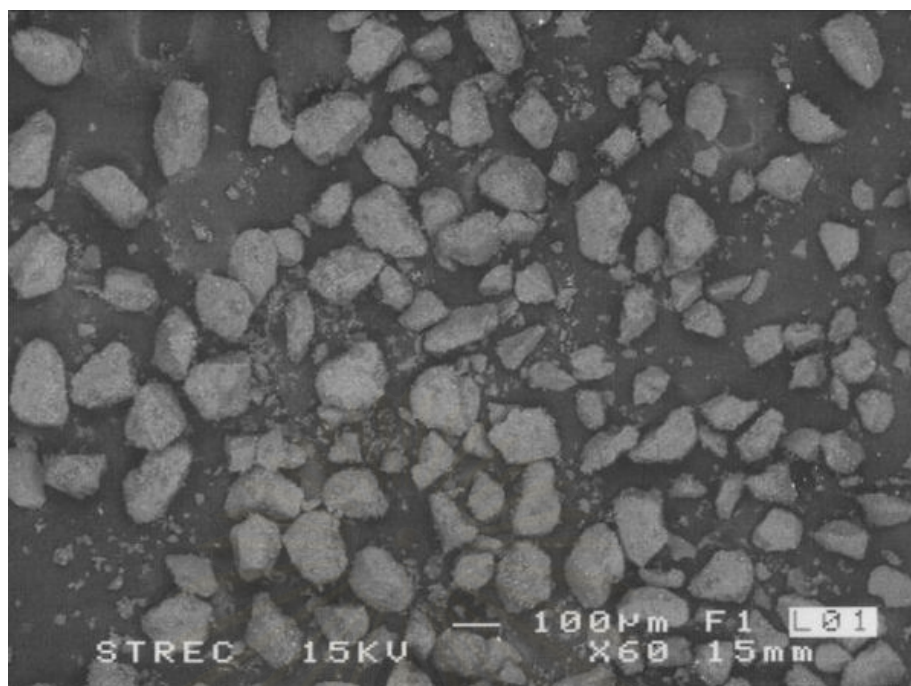


Figure 5.25 (c) SEM micrograph of catalyst granules for Co/S-Cl

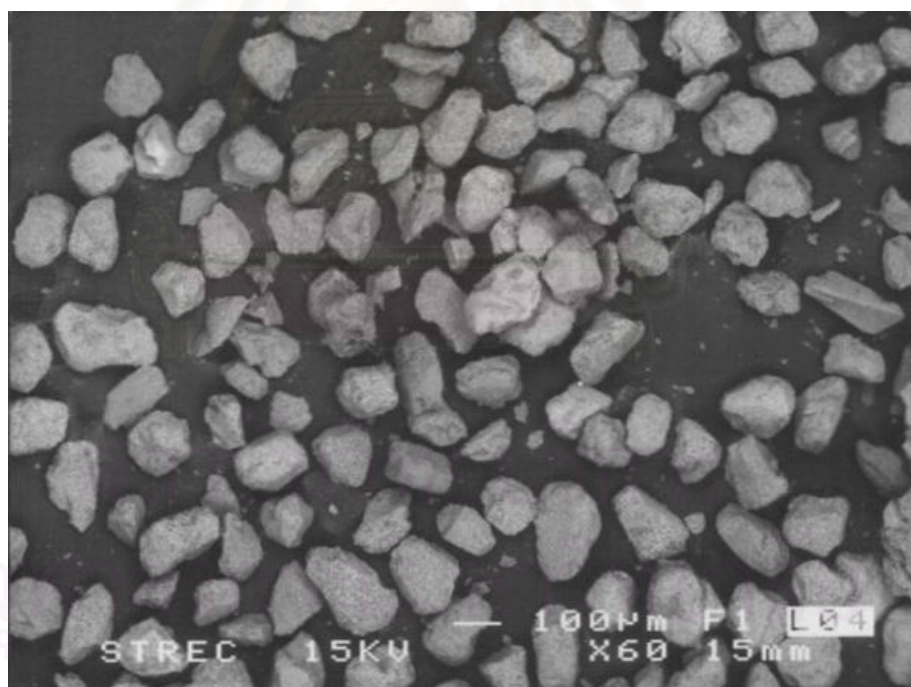


Figure 5.25 (d) SEM micrograph of catalyst granules for Co/S-NO

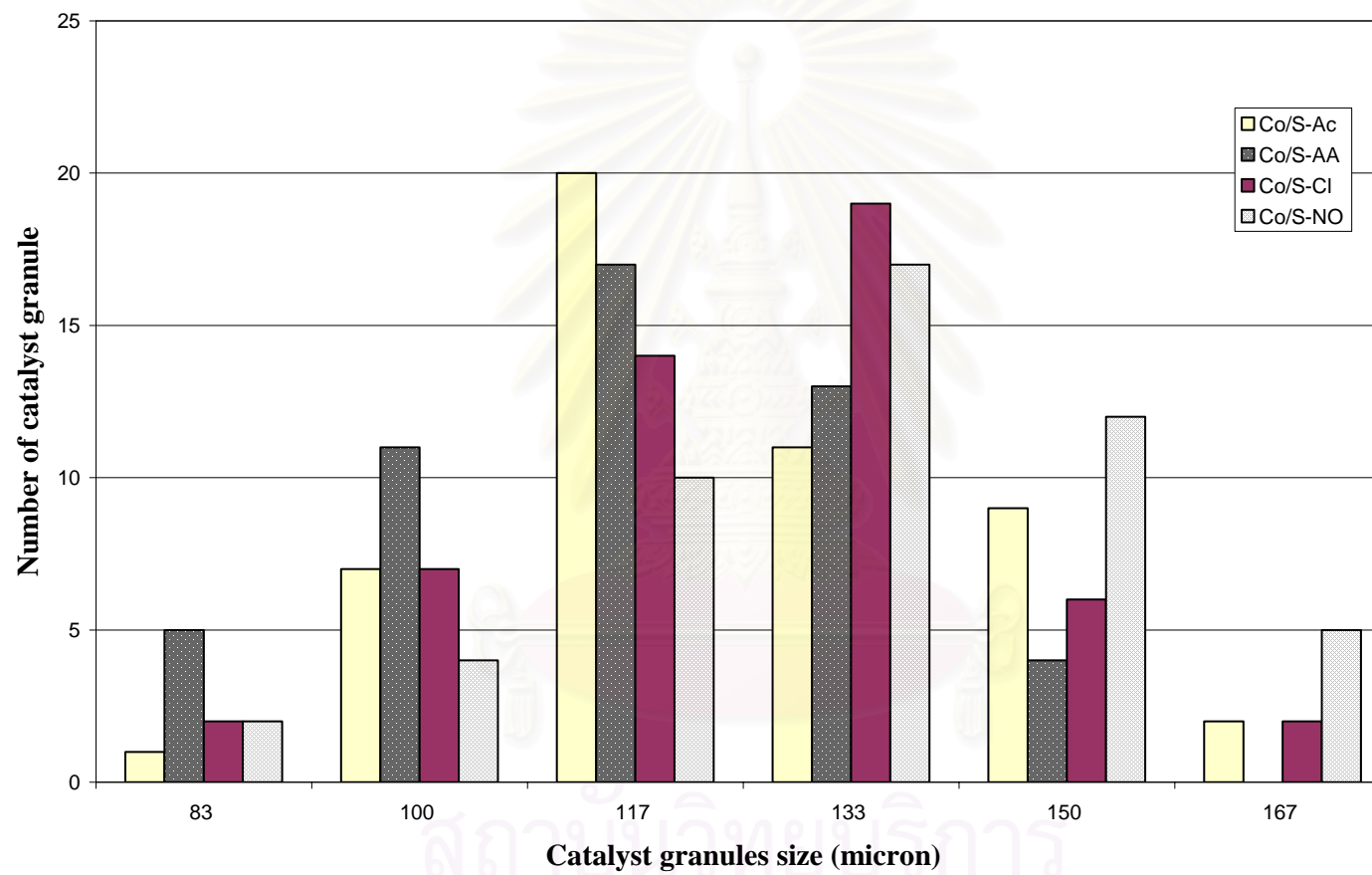


Figure 5.26 Catalyst granule size distribution of SiO₂ supported cobalt catalysts.

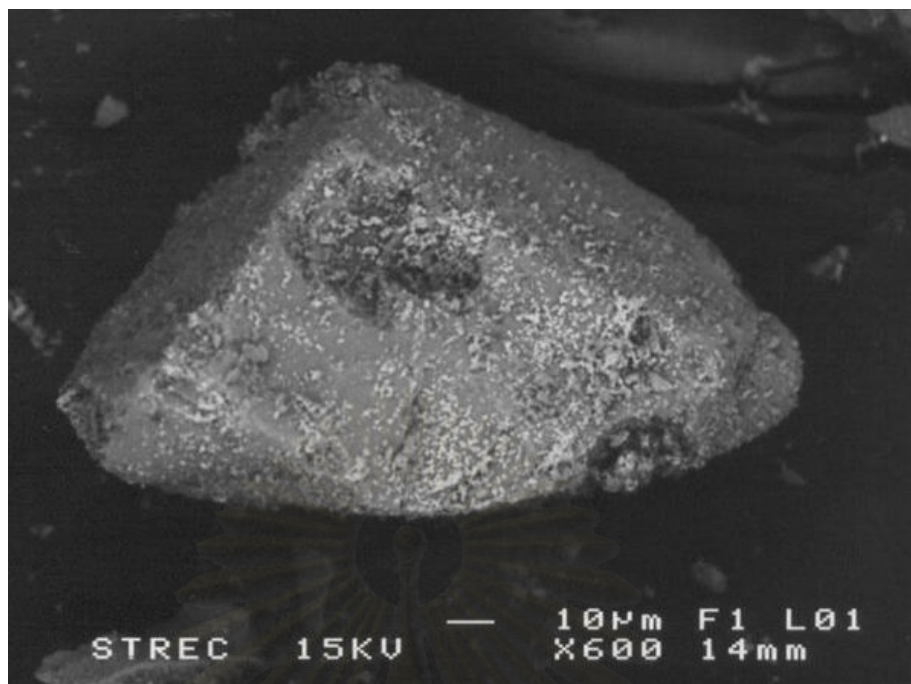


Figure 5.27 (a) SEM micrograph of Co/S-Ac

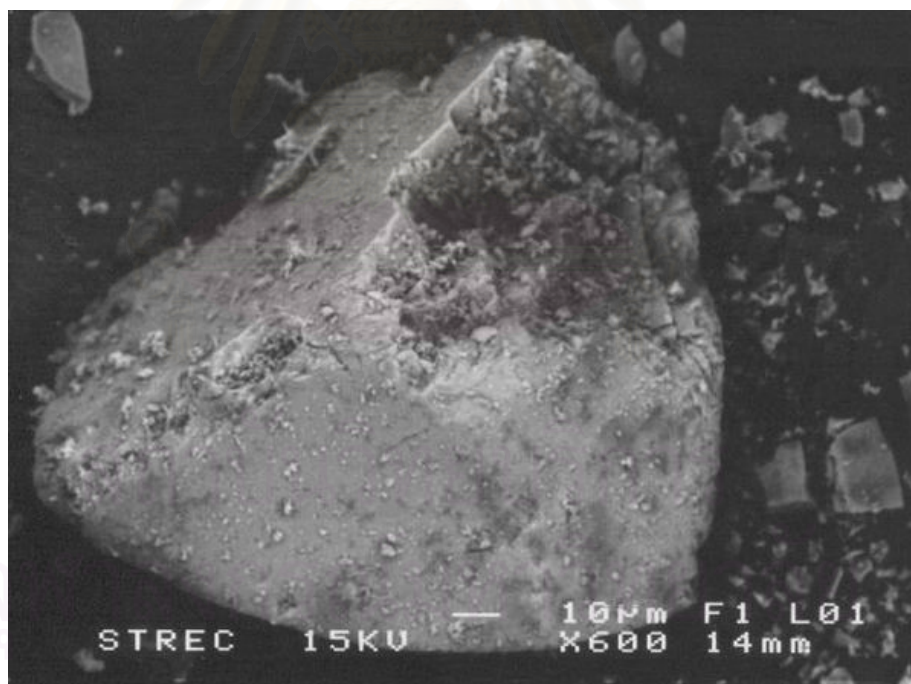


Figure 5.27 (b) SEM micrograph of Co/S-AA

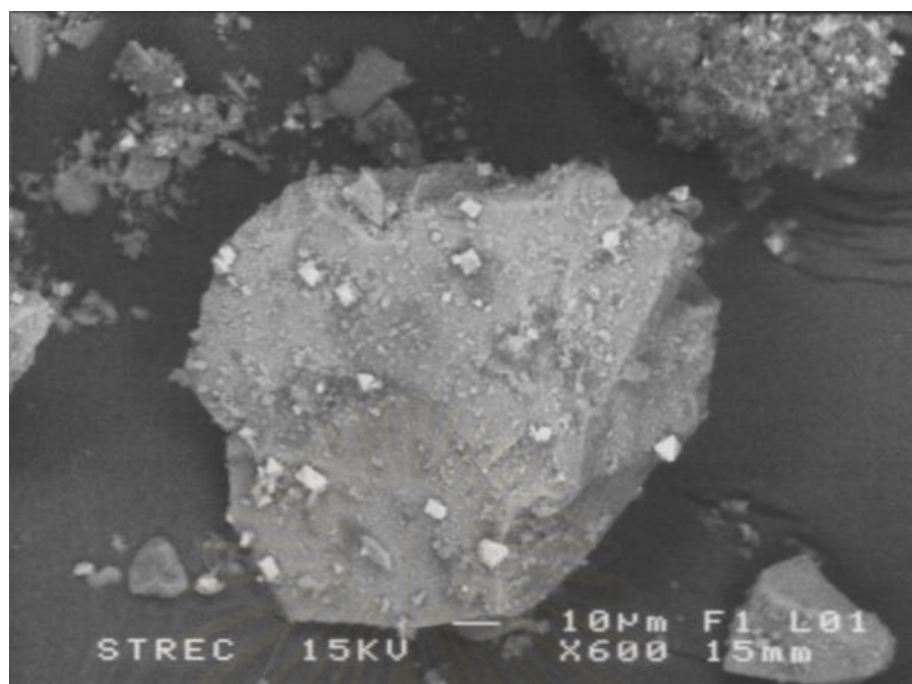


Figure 5.27 (c) SEM micrograph of Co/S-Cl

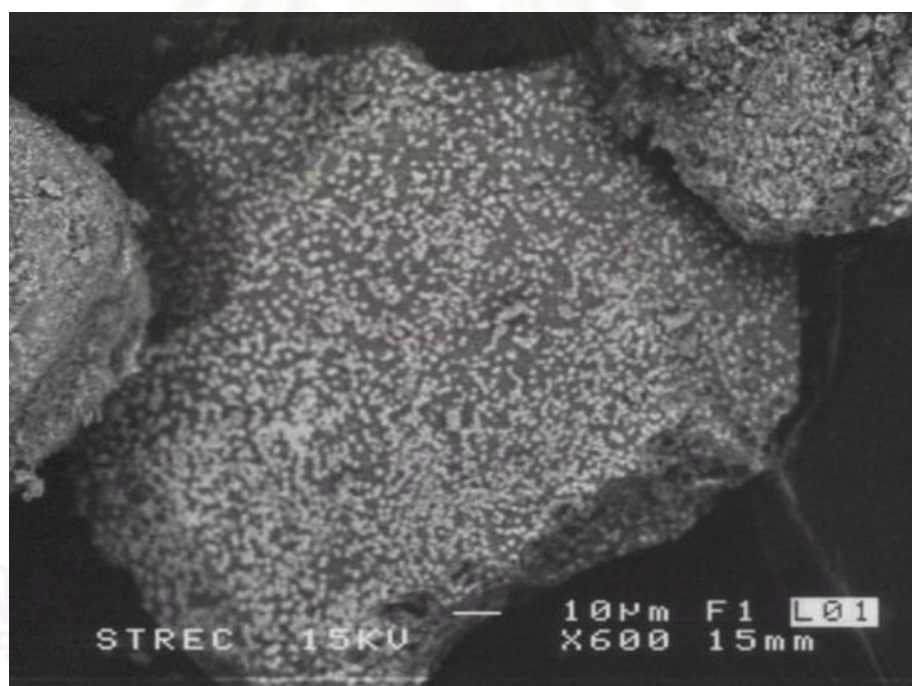


Figure 5.27 (d) SEM micrograph of Co/S-NO

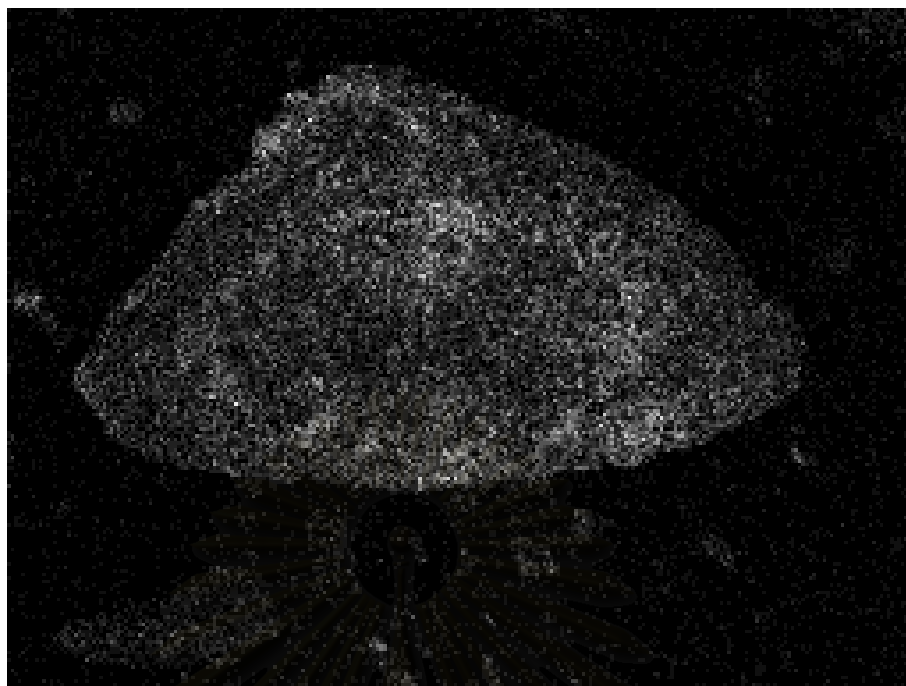


Figure 5.28 (a) SEM elemental mappings of cobalt on the exteriors of Co/S-Ac



Figure 5.28 (b) SEM elemental mappings of cobalt on the exteriors of Co/S-AA

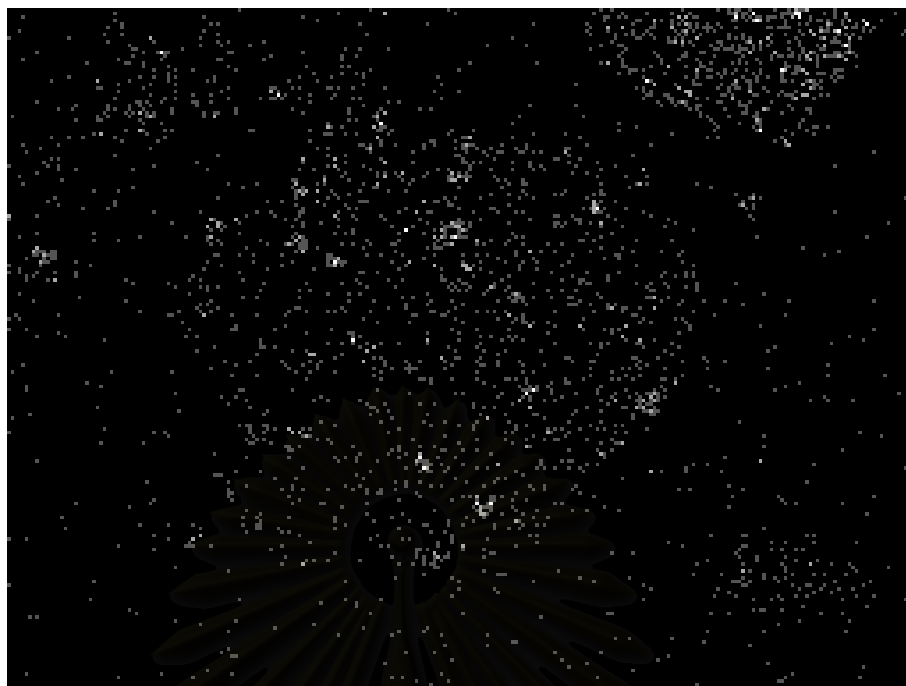


Figure 5.28 (c) SEM elemental mappings of cobalt on the exteriors of Co/S-Cl

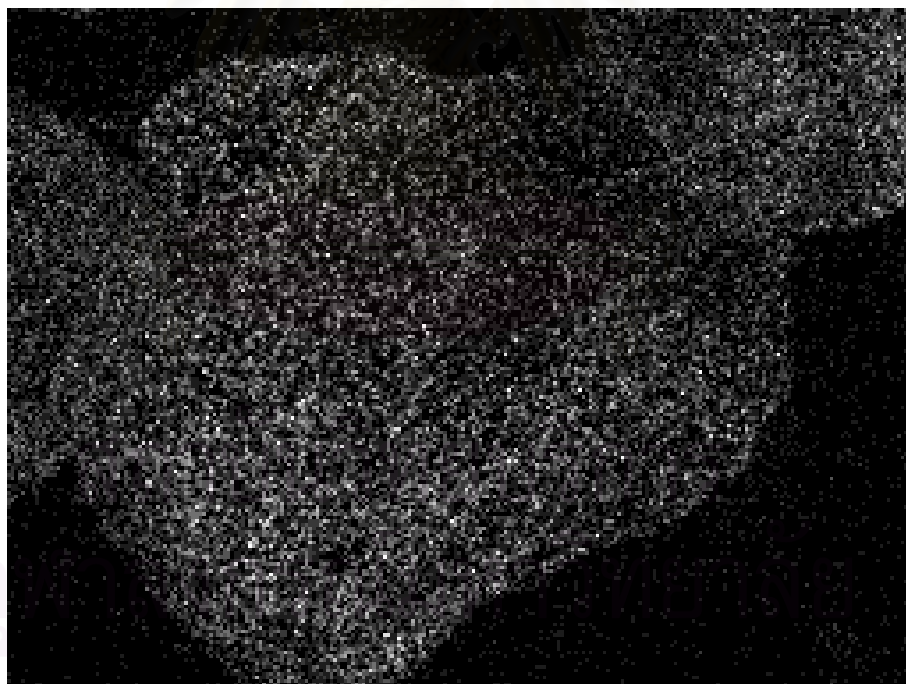


Figure 5.28 (d) SEM elemental mappings of cobalt on the exteriors of Co/S-NO

5.3.1.5 Transmission Electron Microscopy (TEM)

TEM micrographs were taken for all the catalysts in order to physically measure the size of cobalt oxide particles and/or cobalt clusters. The TEM micrographs for SiO₂-supported Co catalysts are shown in Figure 5.29. The particle size of Co₃O₄ measured from TEM micrographs are reported in Table 5.15. The results are in an agreement with the XRD results. TEM images show quite similar dispersion of cobalt for all Co/SiO₂ catalysts. However, it is difficult to draw any conclusion based on TEM measurement because only a small portion of each catalyst was tested and a low contrast of the images.



สถาบันวิทยบริการ
จุฬาลงกรณ์มหาวิทยาลัย

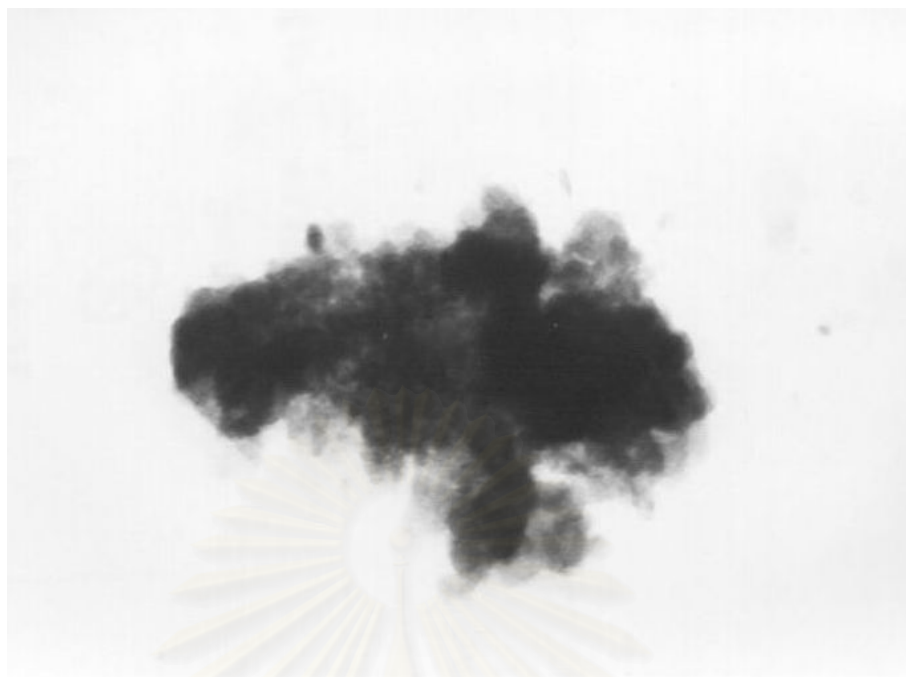


Figure 5.29 (a) TEM micrograph of Co/S-Ac



Figure 5.29 (b) TEM micrograph of Co/S-AA



Figure 5.29 (c) TEM micrograph of Co/S-Cl



Figure 5.29 (d) TEM micrograph of Co/S-NO

5.1.1.7 H₂ Chemisorption

The total hydrogen uptakes and the percentages of cobalt dispersion are reported in Table 5.16. Similar to MCM-41-supported catalysts, it was found that H₂ chemisorption was only measurable for Co/S-NO. The total H₂ chemisorption for Co/S-NO, however, was almost 2 times lower than that of Co/M-NO (8.73 $\mu\text{mol H}_2/\text{gcat}$) due to lower Co dispersion.

Table 5.16 Results from H₂ chemisorption

Catalyst	H ₂ chemisorption	
	Total ($\mu\text{mol H}_2/\text{gcat}$)	% Co Dispersion
Co/S-Ac	nil	nil
Co/S-AA	nil	nil
Co/S-Cl	nil	nil
Co/S-NO	4.46	0.65

5.3.2 CO Hydrogenation Results over Co/SiO₂

5.3.2.1 CO Hydrogenation

CO hydrogenation rates, CO conversion, product selectivities, and TOF for SiO₂ supported cobalt catalysts were presents in Table 5.17. It was found that at the reaction conditions used, Co/S-NO exhibited a much higher CO hydrogenation rate than all other SiO₂-supported catalysts. Formation of Co silicates during reduction in H₂ may also present in Co/S-Ac and Co/S-AA catalysts due to the water vapor generated (Kogelbauer *et al.*, 1995; Jablonski *et al.*, 1998). The SiO₂-supported cobalt catalysts prepared with cobalt chloride precursor were exhibited lower methane selectivity than the other catalysts. The results were in similar order of the activities of MCM-41-supported catalysts; Co/S-NO >> Co/S-AA ≈ Co/S-Ac ≈ Co/S-Cl. The methane selectivity of the SiO₂ supported cobalt catalysts prepared with cobalt nitrate precursor, however, was found to be less than the others. It is typical for active Co catalyst that has high activity for making long chain paraffin. However, in all cases Co supported on MCM-41 have shown higher CO hydrogenation activity than SiO₂-supported catalysts due to a better dispersion of cobalt in mesoporous structure. Figure 5.30 shows the time-on-stream rates for all the catalysts (MCM-41 and SiO₂ supported Co catalysts).

Table 5.17 Results CO Hydrogenation Reaction at methanation conditions ^a.

Catalyst	Rate (gCH ₂ / gcat./h)		CO Conversion (%)		%Selectivity			TOF ^b (1/S)
	Initial	Steady-state	Initial	Steady-state	CH ₄	C ₂	C ₃	
Co/S-Ac	0.012	0.01	2.1	1.4	95	4.5	0.5	nil
Co/S-AA	0.013	0.012	1.7	1.6	96	3.5	0.5	nil
Co/S-Cl	0.007	0.006	0.9	0.8	95	5.0	-	nil
Co/S-NO	0.176	0.167	23.4	22.7	84	13.0	-	0.2

^a CO hydrogenation was carried out at 220°C, 1 atm, H₂/CO = 10 (H₂/CO/Ar = 20/2/8 cc/min).

^b Turnover frequencies, based on total hydrogen chemisorption and the CO hydrogenation rate.

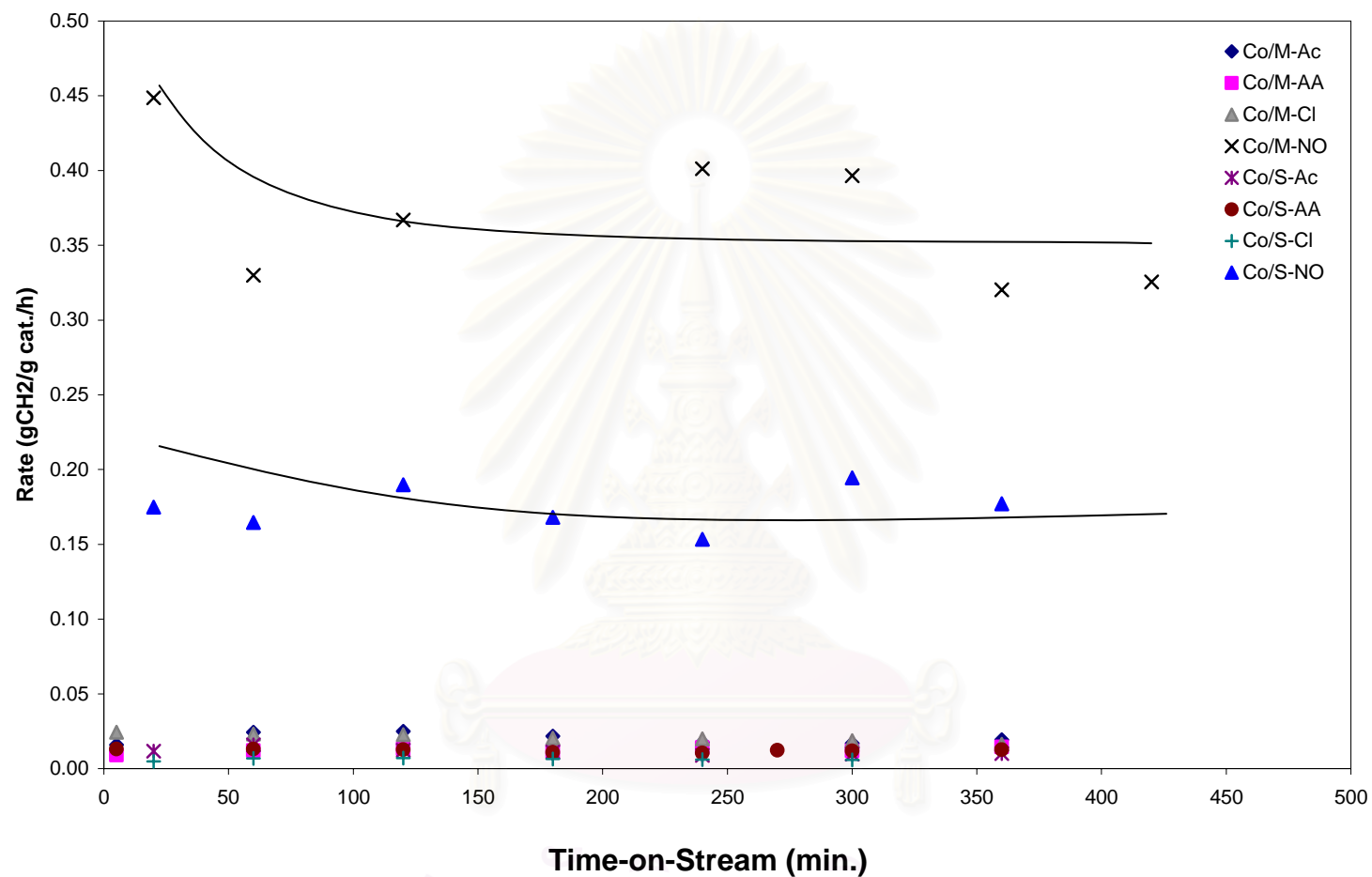


Figure 5.30 CO hydrogenation activities at 220°C, 1 atm, H₂/CO = 10 (H₂/CO/Ar = 20/2/8 cc/min).

5.3.2.1 Temperature Programmed Reduction (TPR)

TPR profiles of the SiO₂-supported Co catalysts and bulk Co₃O₄ are shown in Figures 5.31. The reduction profile of Co/S-NO is composed of two main reduction peaks with temperature maxima at about 375°C (T_{1max}) and 600°C (T_{2max}), respectively. The first peak could be assigned to the reduction of Co₃O₄ to Co⁰, and the second peak at much higher temperature can be attributed to more difficult to reduce Co oxide species due to interaction between small Co particle and SiO₂ support. The TPR profile of the Co/S-AA is presented by a small peak at about 415°C attributed to the reduction of Co₃O₄ to Co⁰, and a large reduction peak centered at about 750°C attributed to difficult to reduce Co oxide species. The TPR profile of Co/S-Cl was almost identical to that of pure Co₃O₄, having a single peak at 545°C. By contrast, Co/S-Ac only showed an intense reduction peak centered at ca. 800°C that could be assigned to reduce cobalt silicate species. Overall, the SiO₂-supported Co catalysts exhibited quite similar TPR profiles to the MCM-41-supported Co catalysts for the same Co precursors. The peaks for Co/SiO₂, however, were located at slightly higher temperatures. High surface area SiO₂ with almost the same pore size distribution as MCM-41 showed similar metal-support interaction to MCM-41-supported catalysts (Figure 5.32).

The reducibilities of the SiO₂-supported catalysts during TPR 30-800°C and during TPR 30-500°C are reported in Table 5.18. The degrees of reduction of the catalysts in TPR from 30-800°C were different, ranging from 38-75%, and in the order of Co/S-Cl > Co/S-NO > Co/S-AA > Co/S-Ac. However, the reducibilities during TPR 30-500°C for SiO₂-supported cobalt catalysts, especially for organic cobalt precursors (Co/S-Ac and Co/S-AA) were much less than the inorganic one (Co/S-Cl and Co/S-NO), with Co/S-NO showing the highest degree of reduction. These trends are in agreement with the results of reaction activities. Co/S-NO showed much higher CO hydrogenation rate than all the other catalysts and the highest % reducibility.

Table 5.18 A comparison of %reducibility of Co/SiO₂ and Co/MCM-41 from TPR experiments

Catalyst	%Reducibility ^a	
	During TPR 30 to 800°C	During TPR 30 to 500°C ^b
Co/S-Ac	38	17
Co/S-AA	52	19
Co/S-Cl	84	25
Co/S-NO	75	27
Co/M-Ac	37	0
Co/M-AA	47	16
Co/M-Cl	76	34
Co/M-NO	51	26

^a From TPR experiments.

^b Correlates to percentage of metal reduce during standard reduction procedure (ramp 1°C / min to 500°C, hold for 10 h)

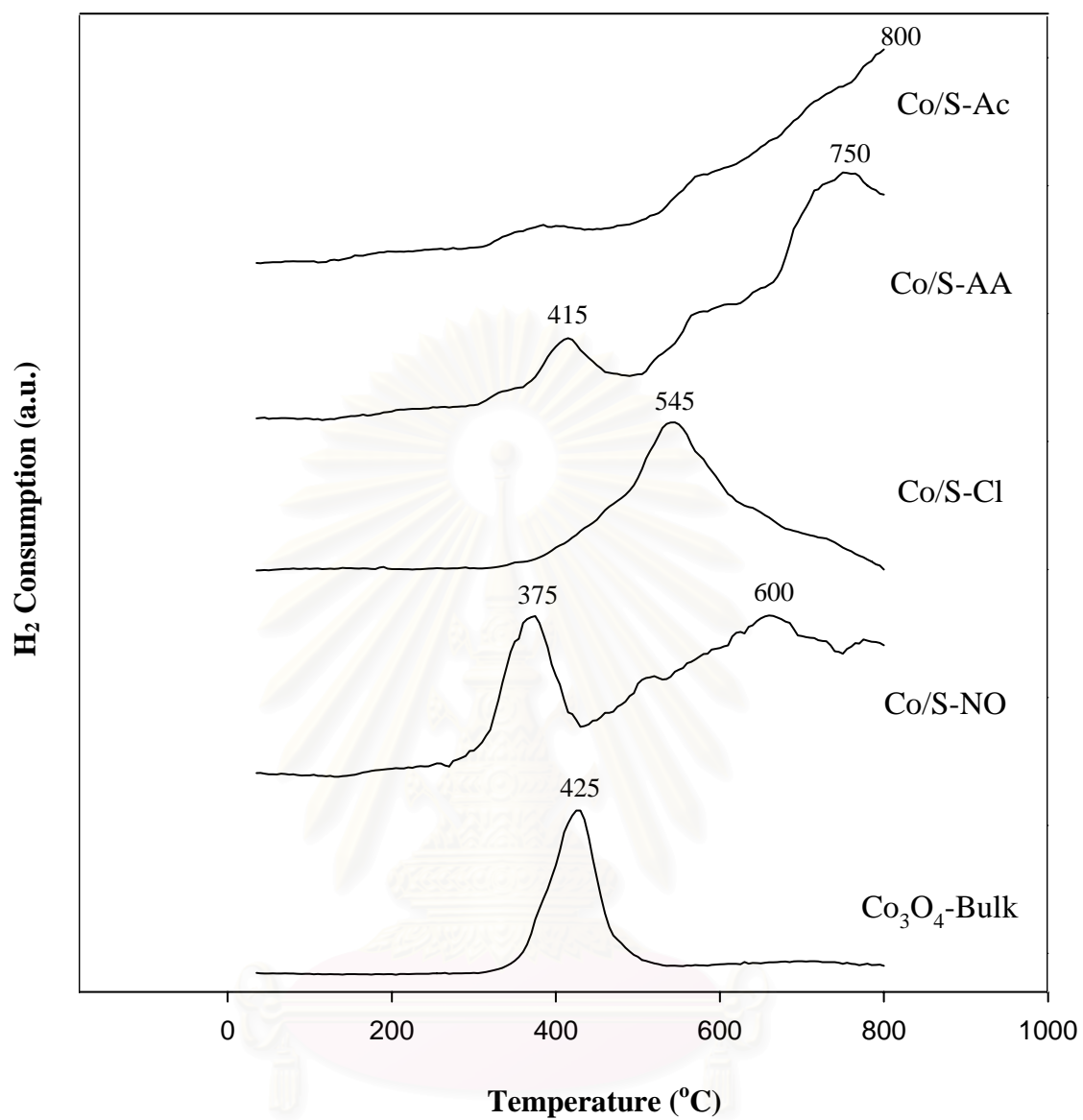


Figure 5.31 TPR profiles of the Co/SiO₂ catalysts with different Co precursors.

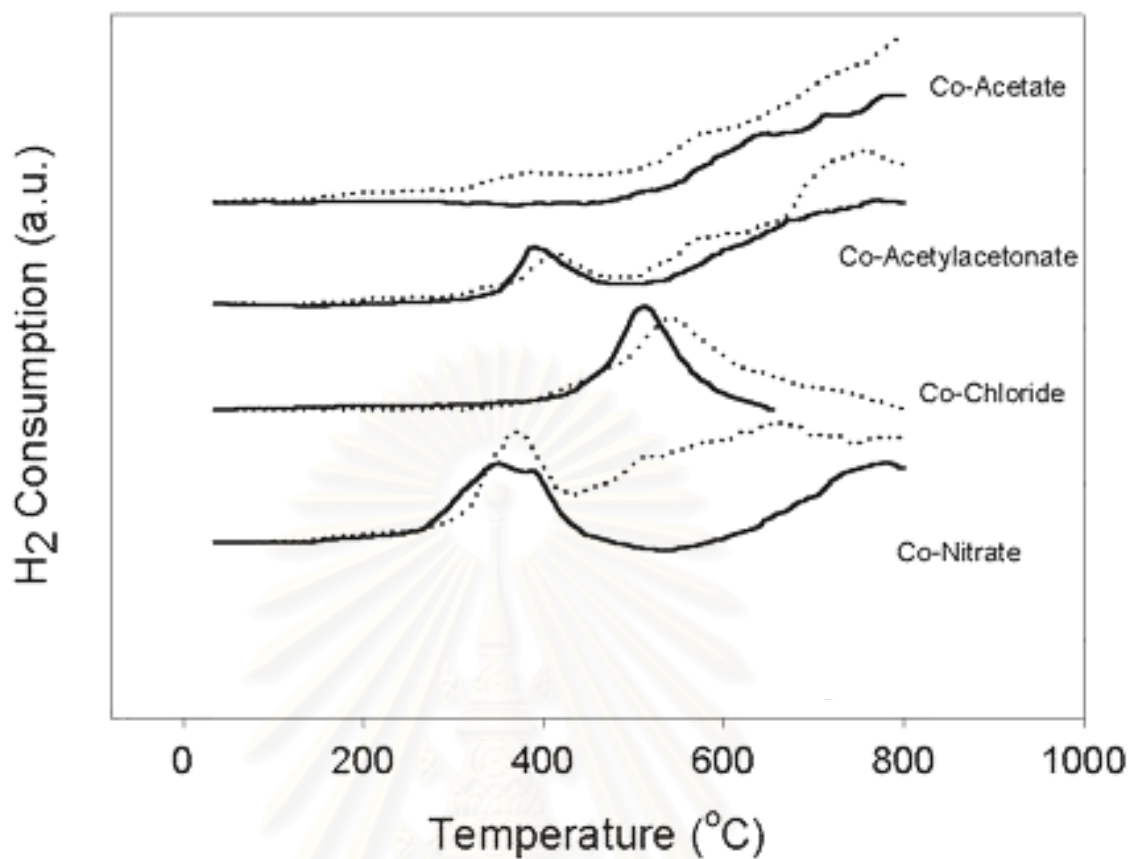


Figure 5.32 Temperature program reduction (TPR) profiles of — Co/MCM-41 and Co/SiO₂ catalysts prepared with different cobalt precursors.

สถาบันวิทยบริการ
จุฬาลงกรณ์มหาวิทยาลัย

A number of publications have appeared dealing with the study of the interaction between metal and support on silica and alumina-supported cobalt catalysts (Backman *et al.*, 2000). It has been reported that metal-support interaction is dependent on the size of cobalt oxide particles, pore size of support, and nature of support. The larger cobalt particles would interact less with the support and would be easier to reduce (Rosynek and Polansky, 1991). Metal-support interaction was found to decrease with increasing pore diameter of the support for SiO₂ supports with an average pore diameter larger or equal to 40Å (Saib *et al.*, 2002).

Nevertheless, the effect of catalyst structure for similar support compositions has not been studied to much of a degree. In this study, it was shown that pore structure of support silica (MCM-41 versus SiO₂) had little effect on metal-support interaction. The small pore size has much effect in metal-support interaction, while MCM-41 and SiO₂ pore structure showed similar results. The higher CO hydrogenation activity of Co/MCM-41 was due primarily to a better dispersion of cobalt in mesoporous structure.

CHAPTER VI

CONCLUSIONS AND RECOMMENDATIONS

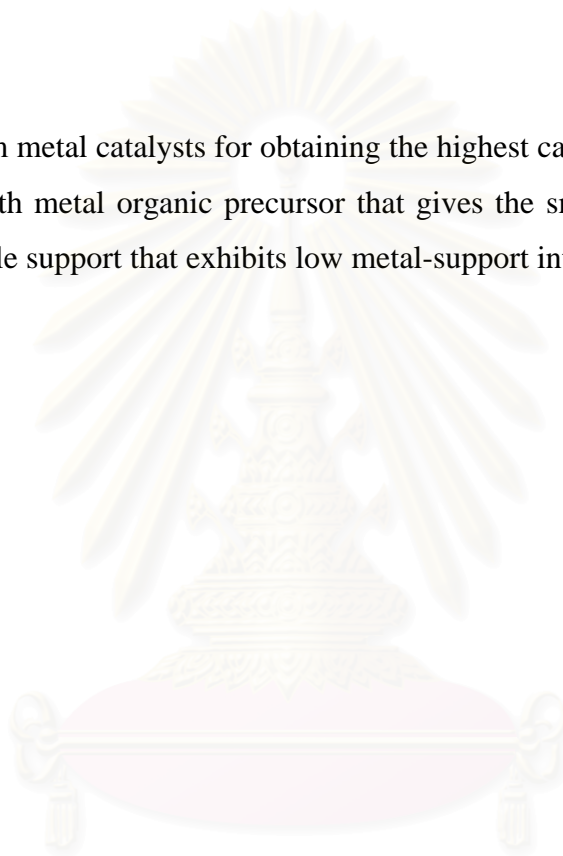
6.1 Conclusions

With careful experimental works, the effects of Co precursors on the dispersion of Co on MCM-41, the physico-chemical properties of Co/MCM-41 catalysts, and the catalytic activities for CO hydrogenation were extensively investigated. The properties of Co/MCM-41 catalysts prepared from different Co precursors were then compared to high surface area amorphous Co/SiO₂ catalysts with similar support pore size. The following conclusions can be drawn:

1. Using organic precursors such as cobalt acetate or cobalt acetylacetonate, instead of inorganic ones such as cobalt nitrate or cobalt chloride results in very small cobalt particles uniformly distributed throughout the pore structure of MCM-41. Extremely large cobalt particles/clusters are evident on Co/MCM-41 prepared from cobalt chloride. The results suggest, however, that there may be an optimum Co particle size and dispersion to maximize surface Co availability since Co-silicate formation during reduction may occur (especially for highly dispersed Co) and result in lower CO hydrogenation activity. Only surface Co metal atoms are active for CO hydrogenation. Among the four types of cobalt compounds used in this study, cobalt nitrate seems to be the best (optimum) cobalt precursor to prepare MCM-41-supported Co catalysts with significant CO hydrogenation activity at commercially relevant synthesis conditions.
2. Co particle size as well as support interaction have an influence on the reduction behavior of cobalt catalysts as shown by the observation of different locations of the reduction peaks in TPR profiles. The effects of particle size and support interaction, however, can superimpose on each other. Thus, while a decrease in metal oxide particle size can result in faster reduction due to a greater surface

area/volume ratio, smaller particles may interact more with the support slowing reduction.

3. The pore structure of silica supports (MCM-41 versus SiO_2) does not affect the metal-support interaction in supported Co catalysts since similar TPR profiles were observed. High activities for Co/MCM-41 catalysts were due primarily to higher Co dispersion in mesoporous structure of MCM-41 than in amorphous SiO_2 .
4. The optimum metal catalysts for obtaining the highest catalytic activities should be prepared with metal organic precursor that gives the smallest metal particle size and a suitable support that exhibits low metal-support interaction.



สถาบันวิทยบริการ
จุฬาลงกรณ์มหาวิทยาลัย

6.2 Recommendations

1. MCM-41 has shown to be a suitable support for preparing a high activity supported Co catalyst but the type of cobalt precursor must be carefully chosen. The effect of metal precursors for other metals (base or noble metals) supported on MCM-41 should also be studied.
2. The metal-support interaction on other supported metal catalyst systems should be investigated because there may be an optimum metal particle size for each metal on a catalyst support.
3. More characterization techniques such as X-ray photoelectron spectroscopy (XPS) and extended X-ray absorption fine structure (EXAFS) should be applied in order to gain more information of cobalt species on the support. XPS could confirm the existence of cobalt silicate that probably formed during catalyst preparation, reduction, and/or CO hydrogenation reaction. EXAFS is especially useful for investigation of the environment of amorphous phases and small metal particles which are very difficult to study by other techniques.
4. The reaction study under commercial Fischer-Tropsch synthesis conditions using Co/MCM-41 catalysts is also recommended.

REFERENCES

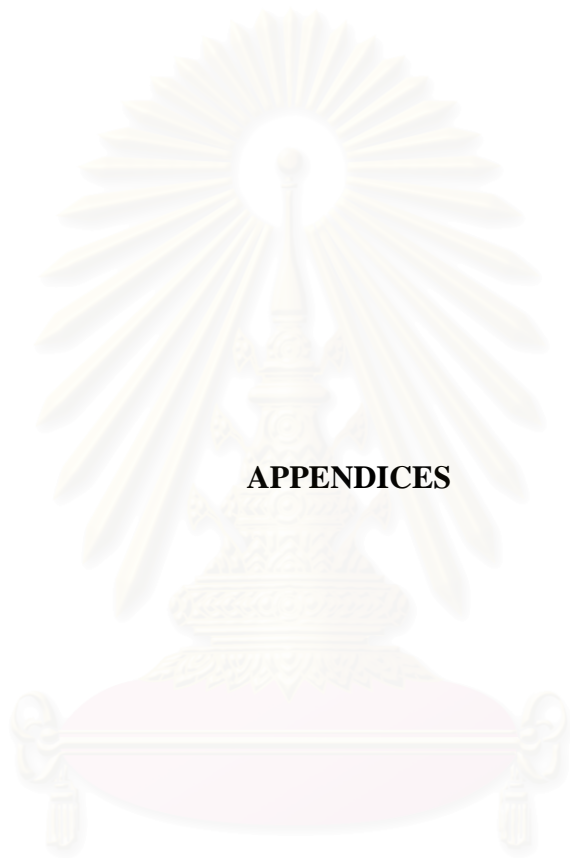
- Backman, L.B., Rautiainen, A., Krause, A. O. I., and Lindblad, M. A novel Co/SiO₂ catalyst for hydrogenation. Catal. Today. 43 (1998): 11-19.
- Backman, L.B., Rautiainen, A., Krause, A. O. I., and Lindblad, M. Effect of support and calcination on the properties of cobalt catalysts prepared by gas phase deposition. Appl. Catal. A. 191 (2000): 55-68.
- Beck, J. S., Vartuli, J. C., Roth, W. J., Leonowicz, M. E., Kresge, C. T., Schmitt, K. D., Chu, C. T., Oslon, D. H., Sheppard, E. W., McCullen, S. B., Higgins, J. B., and Schlemker, J. L. A New Family of Mesoporous Molecular Sieves Prepared with liquid Crystal Templates. J. Am. Chem. Soc. 114 (1992): 10834-10843.
- Bessell, S. Supports effects in cobalt-based Fischer-Tropsch catalysis. Appl. Catal. A. 96 (1993): 253-268.
- Brady, R. C., and Petit, R. J. On the Mechanism of the Fischer-Tropsch Reaction. The Chain Propagation Step. J. Am. Chem. Soc. 103(1981): 1287-1289.
- Carrott, M. M. L. R., Candeias, A. J. E., Carrott, P. J. M., and Unger, K. K. Evaluation of the Stability of Pure Silica MCM-41 toward Water Vapor. Langmuir. 15 (1999): 8895-8901.
- Cho, D. H., Chang, T. S., Ryu, S. K., and Lee, Y. K. Characterization and catalytic activities of MoMCM-41. Catal. Lett. 64 (2000): 227-232.
- Corma, A. From Microporous to Mesoporous Molecular Sieve Materials and Their Use in Catalysis. Chem. Rev. 97 (1997): 2373-2419.
- Ernst, B., Lib, S., Chaumette, P., and Kiennemann, A. Preparation and characterization of Fischer-Tropsch active Co/SiO₂ catalysts Appl. Catal. A. 186 (1999): 145-168.
- Farrauto, R. J., and Bartholomew, C. H. Fundamentals of Industrial Catalytic Processes UK: Chapman & Hall, 1997.
- Haddad, G. J., and Goodwin, J.G., Jr. The Impact of Aqueous Impregnation on the Properties of Prereduced vs Precalcined Co/SiO₂. J. Catal. 157 (1995): 25-34.
- Ho, S. W. Metal-support interaction in silica-supported cobalt catalyst. J. Chinese Chem. Soc. 45 (1998): 569-575.

- Huang, C. J., Fei, J. H., Wang, D. J., and Zheng, X. M. The Dramatic Effect of Metal Precursor on the Catalytic Performance of Co/SiO₂ Catalyst for CO₂ Reforming of CH₄. Chinese Chem. Lett. 11 (2000): 181-184.
- Iglesia, E., Soled, S. L., and Fiato, R. A. Fischer-Tropsch Synthesis on Cobalt and Ruthenium: Metal Dispersion and Support Effects on Reaction Rate and Selectivity J. Catal. 137 (1992): 212-224.
- Iglesia, E., Soled, S. L., Fiato, R. A., and Via, G. H. Bimetallic Synergy in Cobalt Ruthenium Fischer-Tropsch Synthesis Catalysts J. Catal. 143 (1993): 345-368.
- Iwasaki, T., Reinikainen, M., Onodera, Y., Hayashi, H., Ebina, T., Nagase, T., Tori, K., Kataja, K., and Chatterjee, A. Use of silicate crystallite mesoporous material as catalyst support for Fischer-Tropsch reaction. Appl. Surf. Sci. 130-132 (1998): 845-850.
- Jablonski, J. M., Wolcyrz, M., and Krajczyk, L. On Cobalt Silicate Formation during High-Temperature Calcination of Impregnated Cobalt/Silica Catalysts. J. Catal. 137 (1992):
- Jablonski, J. M., Okal, J., Potoczna-Petru, D., and Krajczyk, L. High temperature reduction with hydrogen, phase composition, and activity of cobalt/silica catalysts. J. Catal. 173 (1998): 530-534.
- Jentys, A., Pham, N.H., Vinek, H., Englisch, M., and Lercher, J.A. Synthesis and characterization of mesoporic materials containing highly dispersed cobalt. Microporous and Mesoporous Mater. 6 (1996): 13-17.
- Jentys, A., Pham, N.H., Vinek, H., Englisch, M., and Lercher, J.A. Struc of Co and Co clusters in MCM-41. Catal. Today 39 (1998): 311-315.
- Jess, A., Popp, R., and Hedden, K. Fischer-Tropsch-synthesis with nitrogen-rich syngas: Fundamentals and reactor design aspects. Appl. Catal. A. 186 (1999): 321-342.
- Johnston, P., and Joyner, R. W. Influence of Chlorine on the Lability of Small Rhodium Particles in Carbon-Monoxide. J. Chem. Soc. Faraday Trans. 89 (1993): 863-864.
- Jongsomjit, B., Panpranot, J., and Goodwin, J. G., Jr. Co-Support Compound Formation in Alumina-Supported Cobalt Catalysts. J. Catal. 204 (2001): 98-109.
- Karandikar, P., Dhanya, K.C., Deshpande, Chandwadkar, A.J., Sivasanker, S., and Agashe, M. Cu/Co-salen immobilized MCM-41: characterization and catalytic reactions. Catal. Communications. 5(2004): 69-74.

- Khodakov, A.Y., Lynch, J., Bazin, D., Rebours, B., Zanier, N., Moisson, B., and Chaumette, P. Reducibility of Cobalt Species in Silica-Supported Fischer-Tropsch Catalysts. J. Catal. 168 (1997): 16-25.
- Khodakov, A.Y., Constant, A. G., Bechara, R., and Villain, F. Pore-Size Control of Cobalt Dispersion and Reducibility in Mesoporous Silicas. J. Phys. Chem. B. 105 (2001): 9805-9811.
- Khodakov, A.Y., Constant, A. G., Bechara, R., Zholobenko, V. L. Pore Size Effects in Fischer Tropsch Synthesis over Cobalt-Supported Mesoporous Silicas. J. Catal. 206 (2002): 230-241.
- Khodakov, A.Y., Bechara, R., and Constant, A.G. Fischer-Tropsch synthesis over silica supported cobalt catalysts: mesoporous structure versus cobalt surface density. Appl. Catal. A. 254 (2003): 273-288.
- Kogelbauer, A., Webber, J.C., and Goodwin, J.G. Jr. The formation of cobalt silicates on Co/SiO₂ under hydrothermal conditions. Catal. Lett. 34 (1995): 259-267.
- Zhou, Y., Wood, M. C., and Winograd, N. A time-of-flight SIMS study of the chemical nature of highly dispersed Pt on alumina. J. Catal. 146 (1994):82-86.
- Kim, S. W., Son, S. U., Lee, S. I., Hyeon, T., and Chung, Y. K. Cobalt on Mesoporous Silica: The first Heterogeneous Pauson-Khand Catalyst. J. Am. Chem. Soc. 122 (2000): 1550-1551.
- Klug, H. P., and Alexander, L. E. X-ray diffraction procedures for polycrystalline amorphous materials 2nd ed. New York: Wiley, 1974.
- Koh, D. J., Chung, J. S., and Kim, Y. G. Selective Synthesis and Chain Growth of Linear Hydrocarbons in the Fischer-Tropsch Synthesis over Zeolite-Entrapped Cobalt Catalysts. Ind. Eng. Chem. Res. 34 (1995): 1969-1975.
- Kraum, M., and Baerns, M. Fischer-Tropsch synthesis: the influence off various cobalt compounds applied in the preparation of supported cobalt catalysts on their performance. Appl. Catal. A. 186 (1999): 189-200.
- Kresge, C. T., Leonowicz, M. E., Roth, W. J., and Vartuli, J. C. US Patent No. 5,098,684 (1992).
- Kruk, M., Jaroniec, M.,and Sayari, A. Influence of hydrothermal restructuring conditions on structural properties of Mesoporous molecular sieves. Microporous and Mesoporous Mater. 27(1999): 217-229.

- Loosdrecht, J. V., Haar, M. V., Kraan, A. M. V., Dillen, A. J. V., and Geus, J. W. Preparation and properties of supported cobalt catalysts for Fischer-Tropsch synthesis. Appl. Catal. A. 150 (1997): 365-376.
- Mahata, N. and Vishwanathan, V. Influence of Palladium Precursors on Structural Properties and Phenol Hydrogenation Characteristics of Supported Palladium Catalysts. J. Catal. 196 (2000): 262-270.
- Martinez, A., Lopez, C., Marquez, F., and Diaz, I. Fischer-Tropsch synthesis of hydrocarbons over mesoporous Co/SBA-15 catalysts: the influence of metal loading, cobalt precursor, and promoters. J. Catal. 220 (2003): 486-499.
- Niemela, M. K., Krause, A.O.I, Vaara, T., Kiviahho, J.J., and Reinikainen, M.K.O. The effect of the precursor on the characteristics of Co/SiO₂ catalysts. Appl. Catal. A. 147 (1996): 325-345.
- Okamoto, Y., Nagata, K., Adachi, T., Imanaka, T., Inamura, K., and Takyu, T. Preparation and characterization of highly dispersed cobalt oxide and sulfide catalysts supported on silica. J. Phys. Chem. 95 (1991): 310-319.
- Panpranot, J., Goodwin, J. G., Jr., and Sayari, A. CO Hydrogenation on Ru-Promoted Co/MCM-41 Catalysts. J. Catal. 211 (2002): 530-539.
- Panpranot, J., Goodwin, J. G., Jr., and Sayari, A. Synthesis and characteristics of MCM-41 supported CoRu catalysts. Catal. Today. 77 (2002): 269-284.
- Panpranot, J., Goodwin, J. G., Jr., and Sayari, A. Effect of H₂ partial pressure on surface reaction parameters during CO hydrogenation on Ru-promoted silica-supported Co catalysts. J. Catal. 213 (2003): 78-85.
- Parvulescu, V., and Su, B. L. Iron, cobalt or nickel substituted MCM-41 molecular sieves for oxidation of hydrocarbons. Catal. Today. 69 (2001): 315322.
- Parvulescu, V., Constantin, C., and Su, B. L. Liquid phase oxidation of aromatic hydrocarbons using highly ordered Nb an NbCo-MCM-41 nanoreactors. J. Molecular Catal. A. 202 (2003): 171-178.
- Pasqua, L., Testa, F., Aiello, R., Renzo, F. D., and Fajula, F. Microporous and Mesoporous Mater. 44-45 (2001): 111-117.
- Reuel, R.C., and Bartholomew, C.H. Effects of Support and Dispersion on the CO Hydrogenation Activity/Selectivity Properties of Cobalt. J. Catal. 85 (1984): 78-88.
- Rosynek, M. P., and Polansky, C. A. Effect of cobalt source on the reduction properties of silica-supported cobalt catalysts. Appl. Catal. 73 (1991): 97-112.

- Saib, A.M., Claeys, M., and Steen, E.V. Silica supported cobalt Fischer-Tropsch catalysts: effect of pore diameter of support. Catal. Today. 71 (2002): 395-402.
- Schieber, W., Vinek, H., and Jentys, A. Catalytic reduction of NO_x over transition-metal-containing MCM-41. Catal. Lett. 56 (1998): 189-194.
- Schulz, H. Short history and present trends of Fischer-Tropsch synthesis. Appl. Catal. A. 186(1999): 3-12.
- Sie, S. T., Senden, M. M. G., and Van Wechem, H. M. H. Conversion of natural gas to transportation fuels via the shell middle distillate synthesis process (SMDS) Catal. Today. 8 (1991): 371-394.
- Song, C., and Reddy, K. M. Mesoporous molecular sieve MCM-41 supported Co-Mo catalyst for hydrodesulfurization of dibenzothiophene in distillate fuels. Appl. Catal. A. 176 (1999): 1-10.
- Steen, E.V., Sewell, G.S., Makhothe, R.A., Micklethwaite, C., Manstein, H., Lange, M.D., and O'Connor, C.T. TPR Study on the Preparation of Impregnated Co/SiO₂ Catalysts. J. Catal. 162 (1996): 220-229.
- Suvanto, S., Hukkamaki, J., Pakkanen, T. T., and Pakkanen, T. A. High-Cobalt-Loaded MCM-41 via the Gas-Phase Method. Langmuir 16 (2000): 4109-4115.
- Suvanto, S., and Pakkanen, T. A. Temperature programmed studies off Co on MCM-41 and SiO₂. J. Molecular Catal. A. 164 (2002): 273-280.
- Turaga, U.T., and Song, C. MCM-41-supported Co-Mo catalysts for deep hydrodesulfurization of light cycle oil. Catal. Today. 86 (2003): 129-140.
- Yin, D., Li, W., Yang, W., Xiang, H., Sun, Y., Zhong, B., and Peng, S. Mesoporous HMS molecular sieves supported cobalt catalysts for Fischer-Tropsch synthesis. Microporous and Mesoporous Mater. 47 (2001): 15-24.
- Zhang, Y., Wei, D., Hammache, S., and Goodwin, Jr., J.G. Effect of Water Vapor on the Reduction of Ru-Promoted Co/Al₂O₃. J. Catal. 188 (1999): 281-290.
- Zhao, X. S., Lu, G. Q. (Max), and Millar, Graeme J. Advances in Mesoporous Molecular Sieve MCM-41. Ind. Eng. Chem. Res. 35 (1996): 2075-2090.



APPENDICES

สถาบันวิทยบริการ
จุฬาลงกรณ์มหาวิทยาลัย

APPENDIX A

CALCULATION FOR CATALYST PREPARATION

Preparation of 10%Co/MCM-41 and 10%Co/SiO₂ catalysts by the incipient wetness impregnation method are shown as follows:

- Reagent:
- Cobalt (II) nitrate hexahydrate [Co(NO₃)₂ · 6H₂O]
Molecular weight = 291.03 g
 - Cobalt (II) chloride. hexahydrate [CoCl₂ · 6H₂O]
Molecular weight = 237.9 g
 - Cobalt (II) acetyl acetonate [Co(CH₃COCH=COCH₃)₂]
Molecular weight = 256.9 g
 - Cobalt (II) acetate tetrahydrate [Co(CH₃COO)₂ · 4H₂O]
- Molecular weight = 249.09 g
 - Support: - MCM-41 and SiO₂

Example Calculation for the preparation of 10% Co/MCM-41 catalyst with Co(NO₃)₂ · 6H₂O as Co precursor (Co/M-NO)

Based on 100 g of catalyst used, the composition of the catalyst will be as follows:

$$\begin{aligned} \text{Cobalt} &= 10 \text{ g} \\ \text{MCM-41} &= 100-10 = 90 \text{ g} \end{aligned}$$

For 1 g of catalyst

$$\text{Cobalt required} = 1 \times (10/100) = 0.1 \text{ g}$$

Cobalt 0.1 g was prepared from Co(NO₃)₂ · 6H₂O and molecular weight of Co is 58.93

$$\begin{aligned} \text{the Co(NO}_3)_2 \cdot 6\text{H}_2\text{O content} &= \frac{\text{MW of Co(NO}_3)_2 \cdot 6\text{H}_2\text{O} \times \text{cobalt required}}{\text{MW of Co}} \\ &= (291.03/58.93) \times 0.1 = 0.49 \text{ g} \end{aligned}$$

Since the pore volume of the pure silica support is 1.8 ml/g and 0.78 ml/g for MCM-41 and SiO₂, respectively. Thus, the total volume of impregnation solution

which must be used is 1.62 ml for MCM-41 and 0.7 ml for SiO₂ by the requirement of incipient wetness impregnation method, the de-ionised water is added until equal pore volume for dissolve Cobalt (II) nitrate hexahydrate.

The calculation for the preparation of other catalysts, Co/M-Ac, Co/M-AA, Co/M-Cl, Co/S-Ac, Co/S-AA, Co/S-Cl, and Co/S-NO, is the same as the preparation of Co/M-NO catalyst.



สถาบันวิทยบริการ
จุฬาลงกรณ์มหาวิทยาลัย

APPENDIX B

CALCULATION OF THE CRYSTALLITE SIZE

Calculation of the crystallite size by Debye-Scherrer equation

The crystallite size was calculated from the half-height width of the diffraction peak of XRD pattern using the Debye-Scherrer equation.

From Scherrer equation:

$$D = \frac{K\lambda}{\beta \cos \theta} \quad (\text{B.1})$$

- where
- D = Crystallite size, Å
 - K = Crystallite-shape factor = 0.9
 - λ = X-ray wavelength, 1.5418 Å for CuK α
 - θ = Observed peak angle, degree
 - β = X-ray diffraction broadening, radian

The X-ray diffraction broadening (β) is the pure width of a powder diffraction free from all broadening due to the experimental equipment. α -Alumina is used as a standard sample to observe the instrumental broadening since its crystallite size is larger than 2000 Å. The X-ray diffraction broadening (β) can be obtained by using Warren's formula.

From Warren's formula:

$$\beta = \sqrt{B_M^2 - B_S^2} \quad (\text{B.2})$$

- Where
- B_M = The measured peak width in radians at half peak height.
 - B_S = The corresponding width of the standard material.

Example: Calculation of the crystallite size of Co/M-Cl

$$\begin{aligned} \text{The half-height width of 111 diffraction peak} &= 0.31^\circ \text{ (from the figure B.1)} \\ &= (2\pi \times 0.31)/360 \\ &= 0.00541 \text{ radian} \end{aligned}$$

The corresponding half-height width of peak of α -alumina (from the B_s value at the 2θ of 37.04° in figure B.2) = 0.00438 radian

$$\begin{aligned} \text{The pure width, } \beta &= \sqrt{B_M^2 - B_S^2} \\ &= \sqrt{0.00541^2 - 0.00438^2} \\ &= 0.00318 \text{ radian} \end{aligned}$$

$$B = 0.0318 \text{ radian}$$

$$2\theta = 37.04^\circ$$

$$\theta = 18.52^\circ$$

$$\lambda = 1.5418 \text{ \AA}$$

$$\begin{aligned} \text{The crystallite size} &= \frac{0.9 \times 1.5418}{0.00318 \cos 18.52} = 460.63 \text{ \AA} \\ &= 46.06 \text{ nm} \end{aligned}$$

สถาบันวิทยบริการ
จุฬาลงกรณ์มหาวิทยาลัย

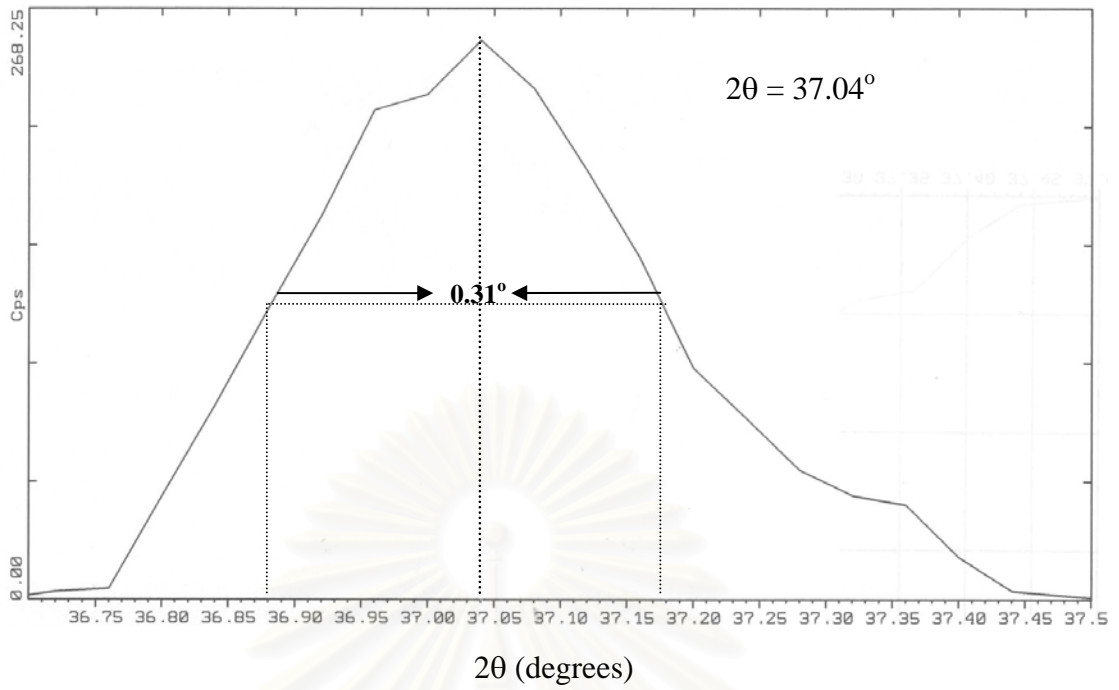


Figure B.1 The 111 diffraction peak of Co/M-Cl for calculation of the crystallite size

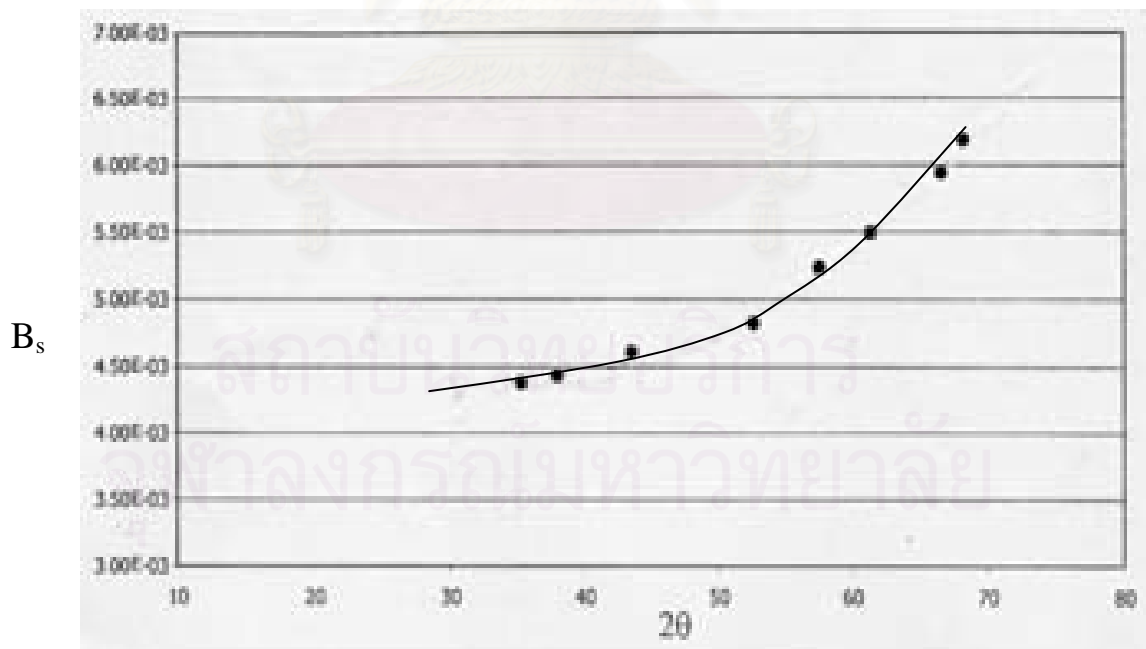


Figure B.2 The plot indicating the value of line broadening due to the equipment.

The data were obtained by using α -alumina as a standard

APPENDIX C

CALCULATION FOR METAL ACTIVE SITES AND DISPERSION

Calculation of the metal active sites and metal dispersion of the catalyst measured by CO adsorption is as follows:

Let the weight of catalyst used	= W	g
Integral area of CO peak after adsorption	= A	unit
Integral area of 40 μ l of standard CO peak	= B	unit
Amounts of CO adsorbed on catalyst	= B-A	unit
Volume of CO adsorbed on catalyst	= $40 \times [(B-A)/B]$	μ l
Volume of 1 mole of CO at 30°C	= 24.86×10^6	μ l
Mole of CO adsorbed on catalyst	= $[(B-A)/B] \times [40/24.86 \times 10^6]$	mole
Molecule of CO adsorbed on catalyst	= $[1.61 \times 10^{-6}] \times [6.02 \times 10^{23}] \times [(B-A)/B]$ molecules	
Metal active sites	= $9.68 \times 10^{17} \times [(B-A)/B] \times [1/W]$ molecules of CO/g of catalyst	
Molecules of Co loaded	= $[\% \text{ wt of Co}] \times [6.03 \times 10^{23}] / [\text{MW of Co}]$ molecules/g of catalyst	
Metal dispersion (%)	= $100 \times [\text{molecules of Co from CO adsorption} / \text{molecules of Co loaded}]$	

สถาบันวิทยบริการ
จุฬาลงกรณ์มหาวิทยาลัย

APPENDIX D

CALCULATION FOR TOTAL H₂ CHEMISORPTION AND DISPERSION

Calculation of the total H₂ chemisorption and metal dispersion of the catalyst, a stoichiometry of H/Co = 1, measured by H₂ chemisorption is as follows:

Let the weight of catalyst used	=	W	g
Integral area of H ₂ peak after adsorption	=	A	unit
Integral area of 45 μl of standard H ₂ peak	=	B	unit
Amounts of H ₂ adsorbed on catalyst	=	B-A	unit
Concentration of Co (by AAS)	=	C	% wt
Volume of H ₂ adsorbed on catalyst	=	45×[(B-A)/B]	μl
Volume of 1 mole of H ₂ at 100°C	=	28.038	μl
Mole of H ₂ adsorbed on catalyst	=	[(B-A)/B]×[45/28.038]	μmole
Total hydrogen chemisorption	=	[(B-A)/B]×[45/28.038]×[1/W]	μmole /g of catalyst
	=	N	μmole /g of catalyst
Molecular weight of cobalt	=	58.93	
Metal dispersion (%)	=	$\frac{2 \times H_{2 \text{ tot}} / \text{g of catalyst} \times 100}{\text{No } \mu\text{mole Co}_{\text{tot}} / \text{g of catalyst}}$	
	=	$\frac{2 \times N \times 100}{\text{No } \mu\text{mole Co}_{\text{tot}}}$	
	=	$\frac{2 \times N \times 58.93 \times 100}{C \times 10^6}$	
	=	$\frac{1.179 \times N}{C}$	

APPENDIX E

CALCULATION FOR REDUCIBILITY

For supported cobalt catalyst, it can be assumed that the major species of calcined Co catalysts is Co_3O_4 . H_2 consumption of Co_3O_4 is calculated as follows:

$$\begin{aligned} \text{Molecular weight of Co} &= 58.93 \\ \text{Molecular weight of } \text{Co}_3\text{O}_4 &= 240.79 \end{aligned}$$

Calculation of the calibration of H_2 consumption using cobalt oxide (Co_3O_4)

$$\begin{aligned} \text{Let the weight of } \text{Co}_3\text{O}_4 \text{ used} &= 0.01 \text{ g} \\ &= 4.153 \times 10^{-5} \text{ mole} \end{aligned}$$

From equation of Co_3O_4 reduction;



$$\begin{aligned} \text{H}_2 &= 4 \text{ Co}_3\text{O}_4 \\ &= 4 \times 4.153 \times 10^{-5} = 1.661 \times 10^{-4} \text{ mole} \end{aligned}$$

$$\text{Integral area of } \text{Co}_3\text{O}_4 \text{ after reduction} = 396572.5 \text{ unit}$$

Thus, the amount of H_2 that can be consumed at 100 % reducibility is 1.661×10^{-4} mole which related to the integral area of Co_3O_4 after reduction 396572.5 unit.

Calculation of reducibility of supported cobalt catalyst

$$\begin{aligned} \text{Integral area of the calcined catalyst} &= X \text{ unit} \\ \text{The amount of } \text{H}_2 \text{ consumption} &= [1.661 \times 10^{-4} \times (X) / 396572.5] \text{ mole} \\ \text{Let the weight of calcined catalyst used} &= W \text{ g} \\ \text{Concentration of Co (by AAS)} &= Y \text{ \% wt} \\ \text{Mole of Co} &= [(W \times Y) / 58.93] \text{ mole} \\ \text{Mole of } \text{Co}_3\text{O}_4 &= [(W \times Y) / 3 \times 58.93] \text{ mole} \end{aligned}$$

$$\begin{aligned} \text{Mole of H}_2 \text{ can be consumed} &= [(W \times Y) \times 4/3 \times 58.93] \text{ mole} \\ \text{Reducibility (\% of supported Co catalyst)} &= \frac{[1.661 \times 10^{-4} \times (X) / 396572.5] \times 100}{[(W \times Y) \times 4/3 \times 58.93]} \end{aligned}$$



สถาบันวิทยบริการ
จุฬาลงกรณ์มหาวิทยาลัย

APPENDIX F

CALIBRATION CURVES

This appendix shows the calibration curves for calculation of composition of reactant and products in CO hydrogenation reaction. The reactant is CO and the main product is methane. The other products are linear hydrocarbons of heavier molecular weight that are C₂-C₄ such as ethane, ethylene, propane, propylene and butane. Mol of reagent in y-axis and area reported by gas chromatography in x-axis are shown in the curves.



สถาบันวิทยบริการ
จุฬาลงกรณ์มหาวิทยาลัย

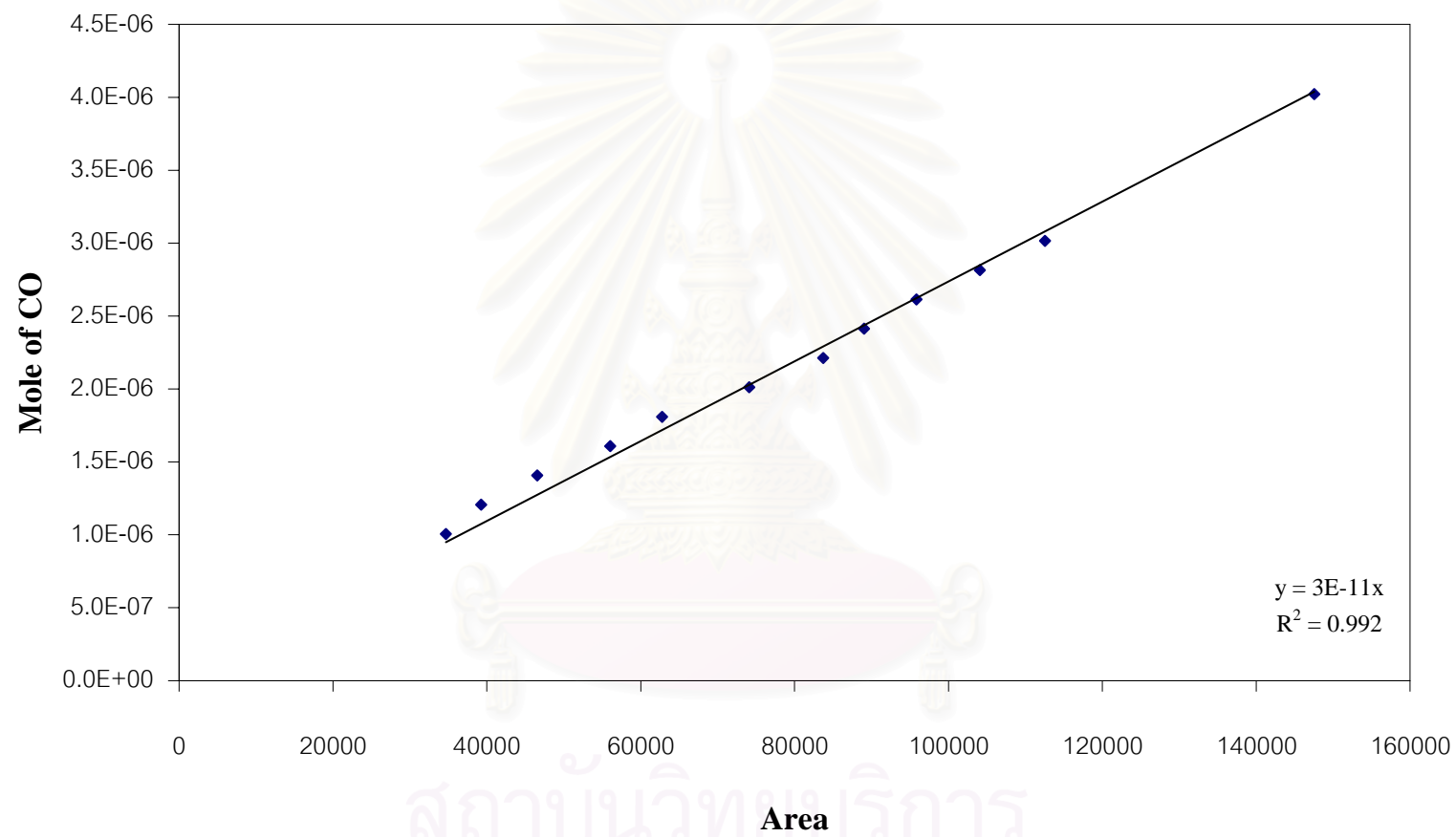


Figure F.1 Calibration curve of CO

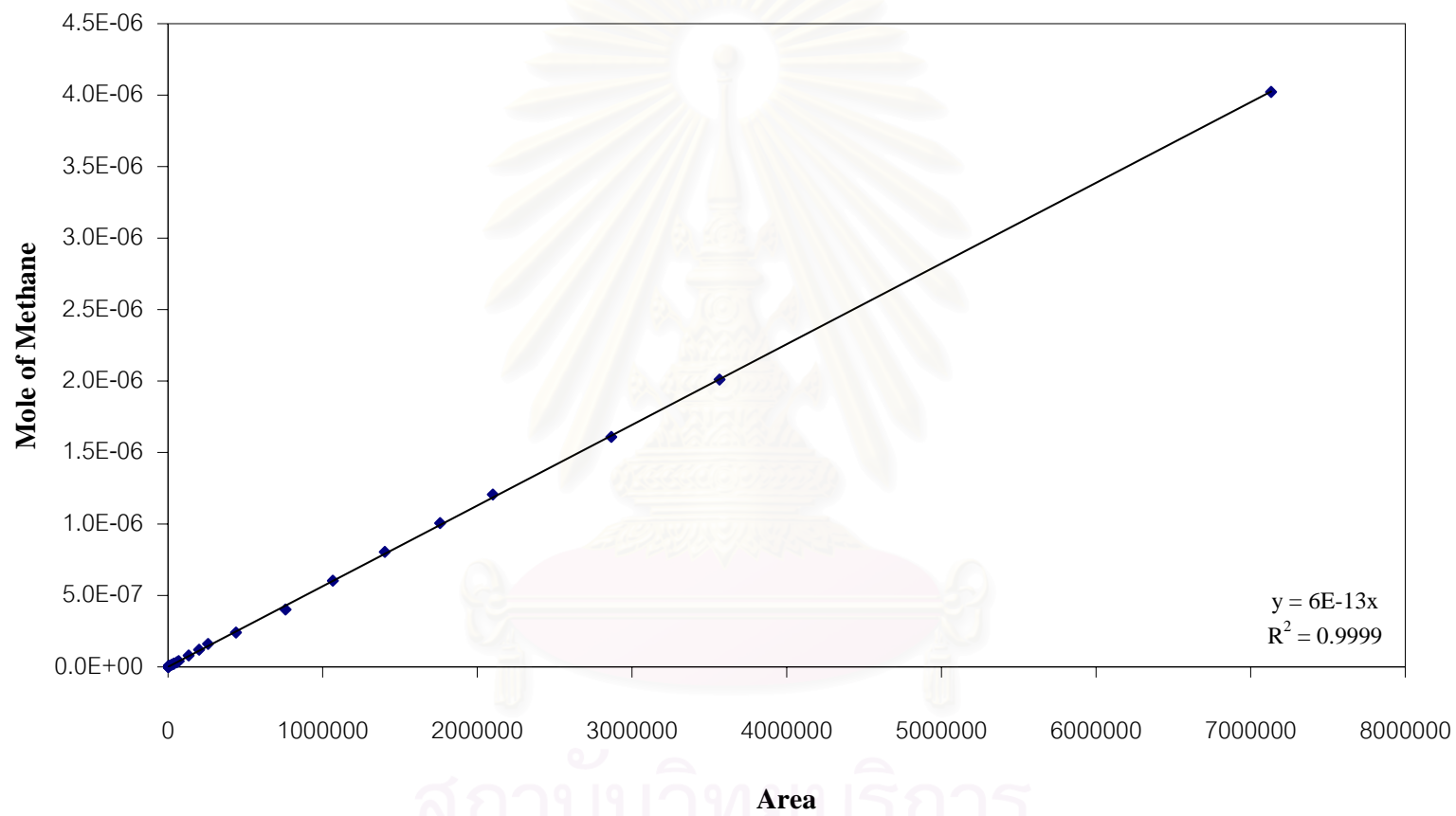


Figure F.2 Calibration curve of methane

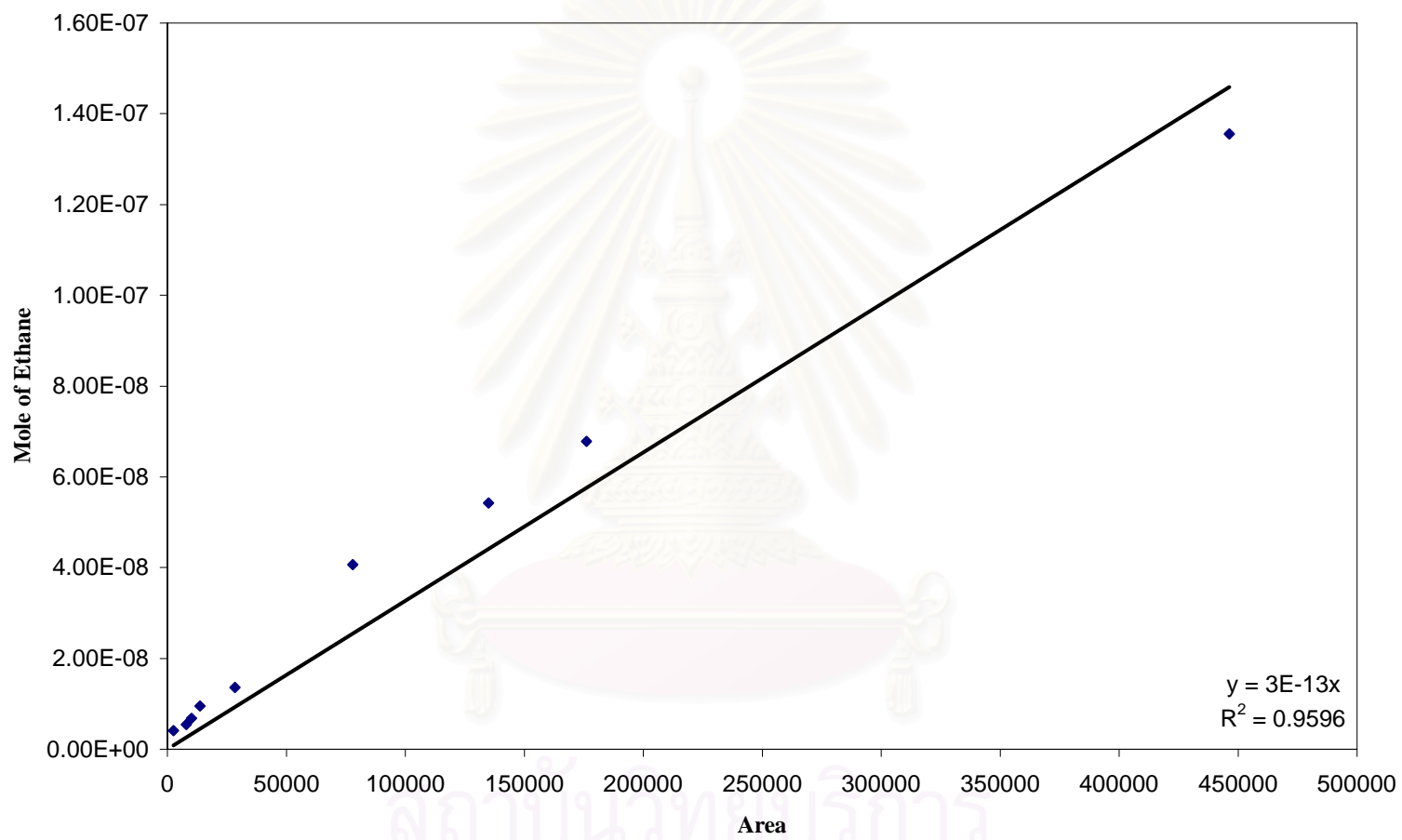


Figure F.3 Calibration curve of ethane

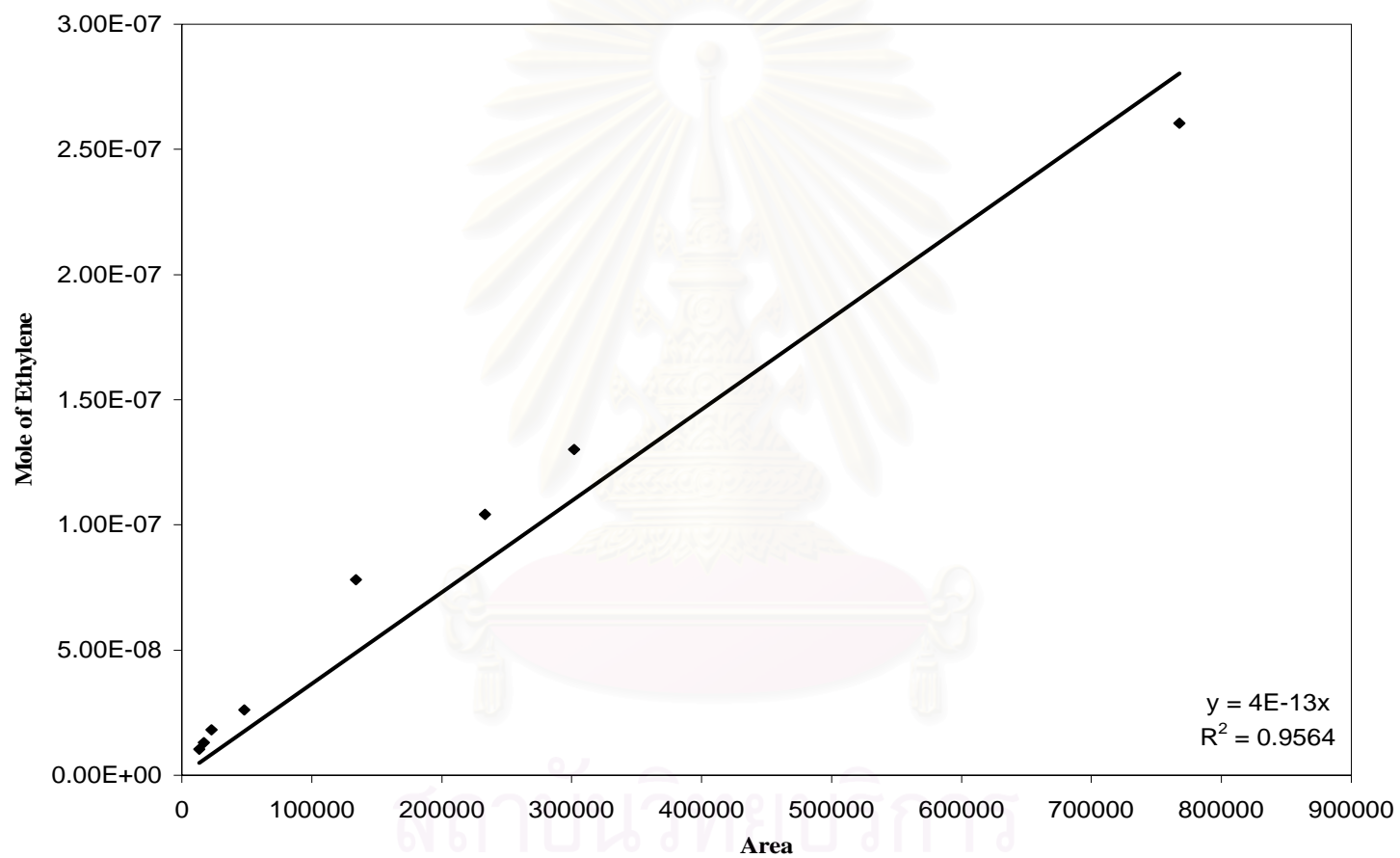


Figure F.4 Calibration curve of ethylene

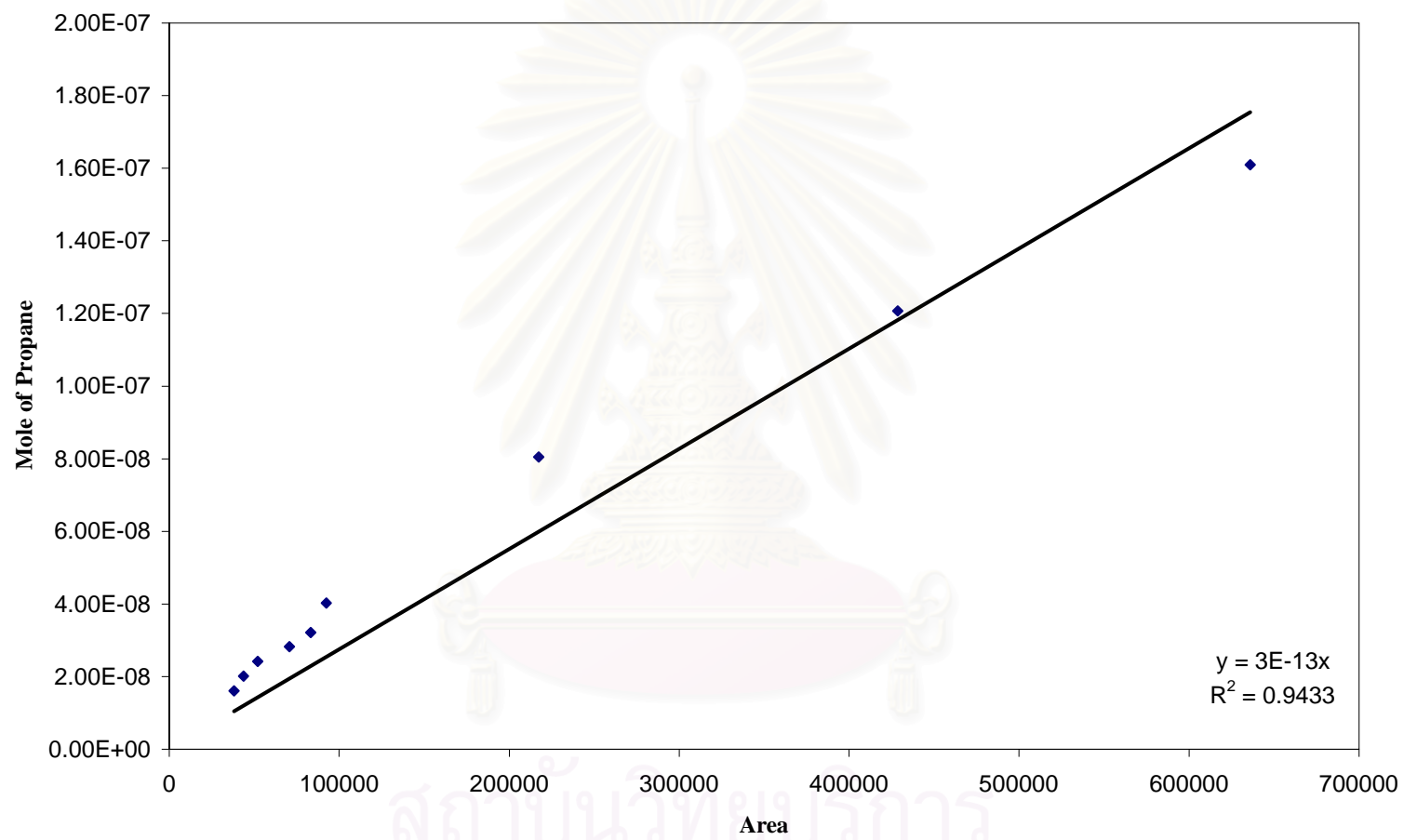


Figure F.5 Calibration curve of propane

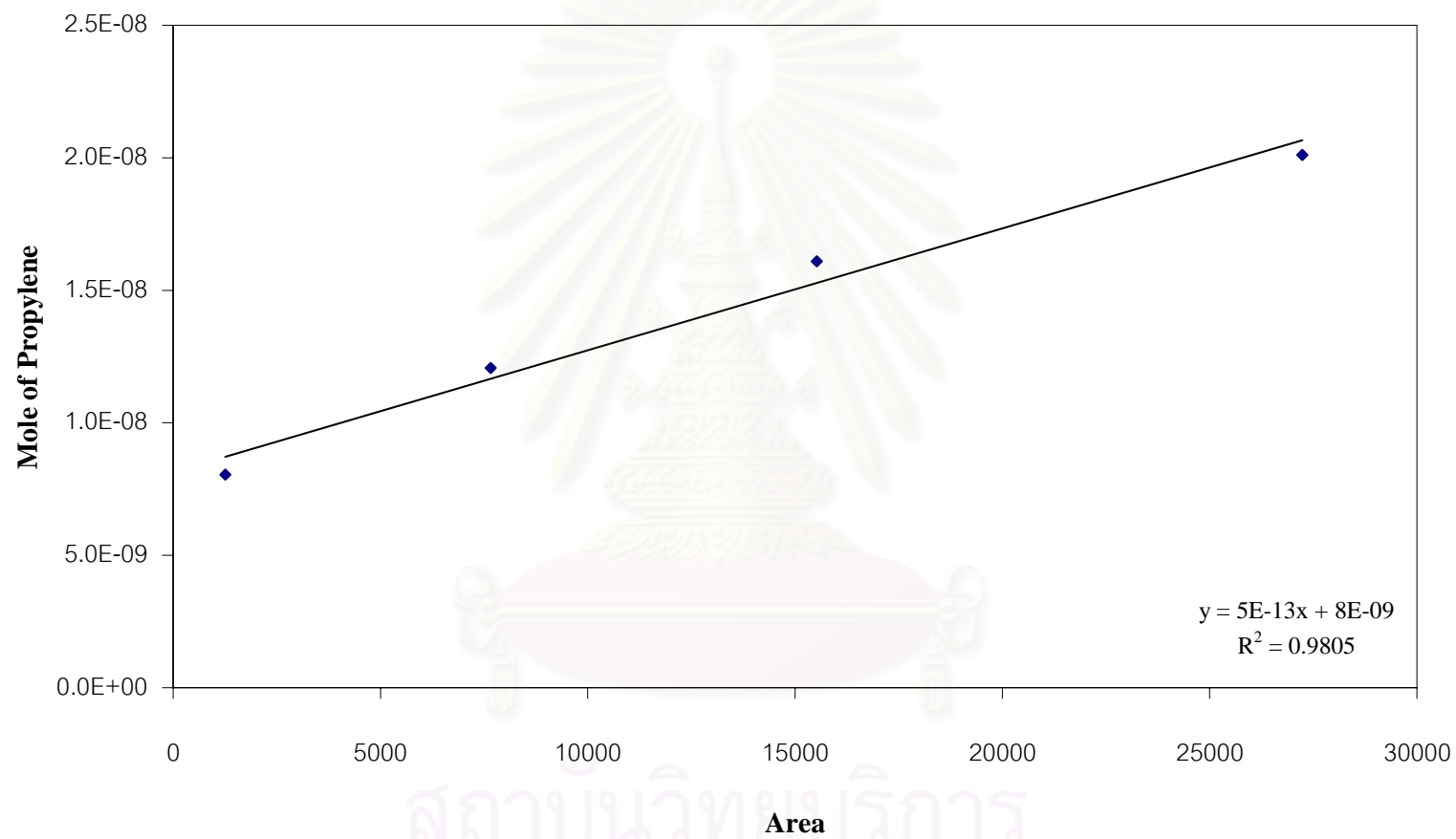


Figure F.6 Calibration curve of propylene

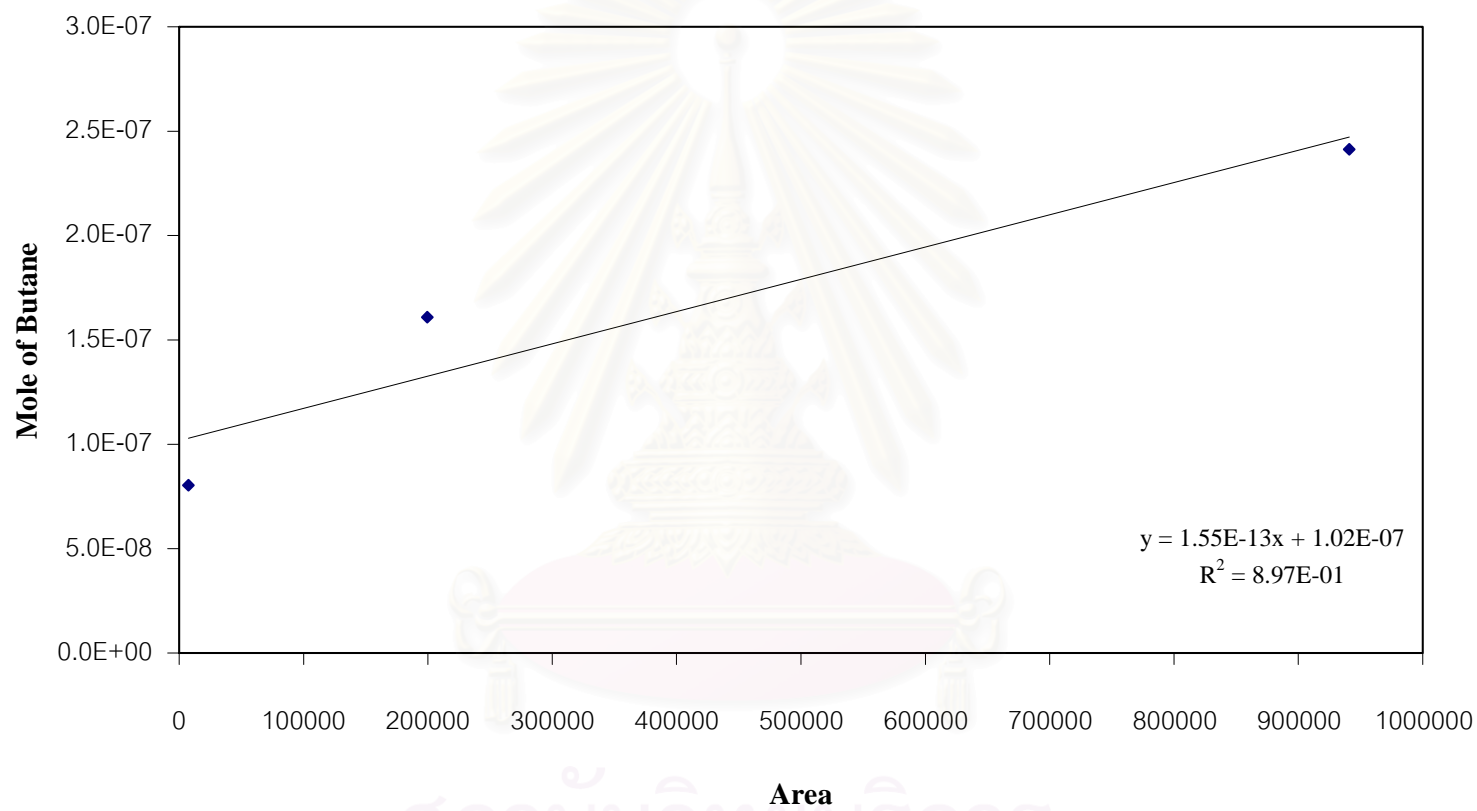


Figure F.7 Calibration curve of butane

APPENDIX G

CALCULATION OF CO CONVERSION, REACTION RATE AND SELECTIVITY

The catalyst performance for the CO hydrogenation was evaluated in terms of activity for CO conversion reaction rate and selectivity.

Activity of the catalyst performed in term of carbon monoxide conversion and reaction rate. Carbon monoxide conversion is defined as moles of CO converted with respect to CO in feed:

$$\text{CO conversion (\%)} = \frac{100 \times [\text{mole of CO in feed} - \text{mole of CO in product}]}{\text{mole of CO in feed}} \quad (\text{i})$$

where mole of CO can be measured employing the calibration curve of CO in Figure F.1, Appendix F., i.e.,

$$\text{mole of CO} = (\text{area of CO peak from integrator plot on GC-8A}) \times 3 \times 10^{-11}$$

Reaction rate was calculated from CO conversion that is as follows:

Let the weight of catalyst used	=	W	g
Flow rate of CO	=	2	ml/min
Reaction time	=	60	min
Weight of CH ₂	=	14	g
Volume of 1 mole of gas at 1 atm	=	22400	ml
Reaction rate (g CH ₂ /g of catalyst/h)	=	$\frac{[\% \text{ conversion of CO}/100] \times 60 \times 14 \times 2}{W \times 22400} \quad (\text{ii})$	

Selectivity of product is defined as mole of product (B) form with respect to mole of CO converted:

$$\text{Selectivity of D (\%)} = 100 \times [\text{mole of D form}/\text{mole of CO converted}] \quad (\text{iii})$$

Or;

$$\text{Selectivity of D (\%)} = 100 \times \frac{\text{mole of D form}}{\text{mole of CO converted}} \times \frac{\text{no. of C atom of B}}{\text{no. of C atom of CO}} \quad (\text{iv})$$

Where D is product, mole of D can be measured employing the calibration curve of products such as methane, ethane, ethylene, propane, propylene and butane in Figure F.2-F.7, Appendix F. Appendix F.,i.e.,

$$\text{mole of CH}_4 = (\text{area of CH}_4 \text{ peak from integrator plot on GC-14B}) \times 6 \times 10^{-13} \quad (\text{v})$$



สถาบันวิทยบริการ
จุฬาลงกรณ์มหาวิทยาลัย

APPENDIX H**LIST OF PUBLICATION**

1. Panpranot, J., Kaewkun, S., Prasertdam, P., and Goodwin, J. G., Jr. (2003). Effect of Cobalt Precursors on the Dispersion of Cobalt on MCM-41. *Catalysis Letters* Volume 91 no. 1-2 pages 95-102.
2. Sujaree Kaewkun, Joongjai Panpranot, and Piyasan Prasertdam, “Influence of cobalt Precursors on the characteristics and Catalytic Properties of Co/MCM-41 Catalysts”, Proceedings of the Regional Symposium on Chemical Engineering 2003, Metro Manila, Philippines, Dec. 1-3, 2003, 14.



สถาบันวิทยบริการ
จุฬาลงกรณ์มหาวิทยาลัย

Effect of cobalt precursors on the dispersion of cobalt on MCM-41

Joongjai Panpranot^{a,*}, Sujaree Kaewkun^a, Piyasan Praserttham^a, and James G. Goodwin, Jr.^b

^aCenter of Excellence on Catalysis and Catalytic Reaction Engineering, Department of Chemical Engineering, Chulalongkorn University, Bangkok, 10330 Thailand

^bDepartment of Chemical Engineering, Clemson University, South Carolina, 29634 USA

Received 26 June 2003; accepted 5 September 2003

Co/MCM-41 catalysts were prepared using the incipient wetness impregnation technique with aqueous solutions of different cobalt compounds such as cobalt nitrate, cobalt chloride, cobalt acetate, and cobalt acetylacetonate. MCM-41 is known to have a restricted pore structure; however, using organic precursors such as cobalt acetate and cobalt acetylacetonate resulted in very small cobalt oxide particles that could not be detected by XRD even for a cobalt loading as high as 8 wt%. These cobalt particles were small enough to fit into the pores of MCM-41. However, they were found to chemisorb CO in only relatively small amounts and to have low activities for CO hydrogenation—probably due to the formation of cobalt silicates. The use of cobalt chloride resulted in very large cobalt particles/clusters and/or residual Cl⁻-blocking active sites, and, consequently, very small active surface area was measurable. The use of cobalt nitrate resulted in a number of small cobalt particles dispersed throughout MCM-41 and some larger particles located on the external surface of MCM-41. Cobalt nitrate appeared to be the best precursor for preparing high-activity MCM-41-supported cobalt Fischer–Tropsch synthesis catalysts.

KEY WORDS: cobalt catalyst preparation; cobalt precursors; MCM-41; CO hydrogenation.

1. Introduction

Co-based catalysts are widely used in CO hydrogenation or Fischer–Tropsch synthesis (FTS), especially when high molecular weight paraffins are preferred [1–3]. To increase their activity, cobalt is usually deposited on a high surface area support to obtain a high metal dispersion. The commonly used supports include silica [4–6], alumina [7–9], and titania [10,11]. Recently, attention has been focused on the use of ordered mesoporous materials such as MCM-41 as catalyst supports. MCM-41 possesses excellent support properties such as high BET surface area and well-ordered hexagonal pore structures that can be tailor-made in the pore-diameter range of 1.5–10 nm [12,13]. Their thermal and hydrothermal stability have also been improved by changing the synthesis chemicals and/or reaction conditions [14,15]. Many studies have reported significant improvements when these mesoporous materials were used as supports for catalyst preparation compared to conventional and commercial catalysts. For example, Song and Reddy [16] reported that Co–Mo supported on aluminosilicate MCM-41 prepared by impregnation showed higher hydrogenation and hydrocracking activities than conventional Co–Mo supported on γ -Al₂O₃. Schuth *et al.* [17] reported that Fe₂O₃/MCM-41 exhibited a superior performance for the conversion of SO₂ to SO₃ compared to Fe₂O₃ supported on conventional silica.

In a previous study [18], we reported the high Fischer–Tropsch activity of Ru-promoted MCM-41-supported cobalt catalysts. However, using incipient wetness impregnation with cobalt nitrate as the precursor resulted in cobalt being nonuniformly distributed on the MCM-41 support.

Besides the conventional impregnation technique, direct synthesis in which the metal ion source is introduced as a reactant into the synthesis gel and ion exchange has been widely used [19,20]. These methods, however, are limited by only small amounts of metal being able to be loaded and low metal dispersions [6]. Suvanto and coworkers reported high metal-loaded, well-dispersed Co/MCM-41 prepared using a gas-phase method and a fluidized-bed reactor [21]. This method is, however, more complicated than the conventional incipient wetness impregnation technique and may not be suitable for the preparation of commercial catalysts.

It is known that cobalt dispersion depends on the type of cobalt precursors. van de Loosdrecht *et al.* [22] showed that alumina-supported cobalt catalysts prepared by incipient wetness impregnation using cobalt EDTA and cobalt citrate precursors resulted in smaller cobalt oxide particles compared to the one prepared from cobalt nitrate. The use of cobalt oxalate, cobalt acetate, or cobalt acetylacetonate as cobalt precursors for titania-supported cobalt catalysts has been found to give higher cobalt dispersions than the catalysts prepared from cobalt nitrate [23]. Rosenek and Polansky [24] reported that use of cobalt acetate yields higher dispersion than cobalt chloride on silica. Sun *et al.* [25]

* To whom correspondence should be addressed.
E-mail: Joongjai.P@eng.chula.ac.th

concluded that catalysts prepared by mixed impregnation of cobalt nitrate and cobalt acetate result in higher Fischer–Tropsch synthesis activity than catalysts prepared from either monoprecursor. And recently, Soled *et al.* [26] has presented a comprehensive model for how precursor-support interactions influence the morphology and reducibility of the fresh cobalt catalysts. A balance between dispersion-enhancing strong support–precursor interaction and metal loss by retarded reduction was suggested.

However, less is known about the influence of cobalt precursors on the dispersion of cobalt when restricted pore-structure supports such as MCM-41 are used. The purpose of this study was to investigate the impact of different organic and inorganic cobalt precursors on cobalt dispersion in a restricted pore-structure support—in this case mesoporous MCM-41.

2. Experimental

2.1. Catalyst preparation

Pure silica MCM-41 was prepared in the same manner as that of Kruk *et al.* [27] using the following gel composition: $(1.0 \text{ SiO}_2) : (0.317 \text{ TMAOH}) : (0.45 \text{ CTMABr}) : (66.7 \text{ H}_2\text{O})$, where TMAOH denotes tetramethylammonium hydroxide and CTMABr denotes cetyltrimethyl ammonium bromide. The Co/MCM-41 catalysts were prepared by the incipient wetness impregnation of the supports with aqueous solution of different cobalt precursors such as cobalt nitrate (Aldrich), cobalt acetate (APS), cobalt acetylacetonate (Aldrich) and cobalt chloride (Fluka). Cobalt loading was approximately 8% by weight of catalyst. The samples were dried at 110 °C for 1 day and were then calcined in air at 500 °C for 2 h. These catalysts with different cobalt precursors are respectively designated as Co/M-NO, Co/M-Cl, Co/M-AA, and Co/M-Ac, where Co/M refers to cobalt supported on MCM-41 and the last two letters reflect the type of the cobalt precursor used: NO for cobalt nitrate, Cl for cobalt chloride, AA for cobalt acetylacetonate, and Ac for cobalt acetate.

2.2. Catalyst characterization

2.2.1. Atomic adsorption spectroscopy

The bulk composition of cobalt was determined using a Varian Spectra A800 atomic adsorption spectrometer.

2.2.2. N_2 physisorption

The BET surface area, pore volume, average pore diameter, and pore-size distribution of the catalysts were determined by N_2 physisorption using a Micromeritics ASAP 2000 automated system. Each sample was degassed in the Micromeritics ASAP 2000 at 150 °C for 4 h prior to N_2 physisorption.

2.2.3. X-ray diffraction (XRD)

The XRD spectra of the catalysts were measured using a SIEMENS D5000 X-ray diffractometer, using $\text{Cu K}\alpha$ radiation with a nickel filter in the 2–8° or 10–80° 2θ angular regions.

2.2.4. Scanning electron microscopy (SEM)

Catalyst granule morphology and elemental distribution were obtained using a JEOL JSM-35CF scanning electron microscope. The SEM was operated at 20 kV. After the SEM micrographs were taken, elemental mappings were performed to determine the elemental concentration distribution on the catalyst granules using Link Isis 300 software. The catalyst samples were cut using an ultramicrotome in order to perform SEM-EDX on different spots of cross-sectioned catalyst granules.

2.2.5. Transmission electron microscopy (TEM)

The cobalt oxide particle size and the distribution of cobalt on MCM-41 were observed using a JEOL-TEM 200CX transmission electron microscope operated at 100 kV.

2.2.6. CO-pulse experiment

Relative percentages of cobalt dispersion were determined by pulsing carbon monoxide over the reduced catalyst. Approximately 0.2 g of catalyst was placed in a quartz tube, incorporated in a temperature-controlled oven and connected to a thermal conductivity detector (TCD). Prior to chemisorption, the catalyst was reduced in a flow of hydrogen (50 cc/min) at 400 °C for 2 h. Afterward, the sample was purged with helium at 400 °C for 1 h and finally cooled down to room temperature. Carbon monoxide was pulsed at 25 °C over the reduced catalyst until the TCD signal was constant.

2.2.7. Reaction test

CO hydrogenation was carried out at 220 °C and 1 atm total pressure in a fixed-bed stainless steel reactor under differential conversion conditions. A flow rate of $\text{H}_2/\text{CO}/\text{Ar} = 20/2/8 \text{ cm}^3/\text{min}$ was used. Typically, 0.2 g of the catalyst samples was reduced *in situ* in flowing H_2 (50 cc/min) at 350 °C for 10 h prior to the reaction. The product samples were taken at 1-h intervals and analyzed by gas chromatography. Steady state was reached after 6 h time onstream in all cases.

3. Results and discussion

To determine a suitable temperature for calcination of all cobalt precursors, thermogravimetric analysis (TGA) experiments were performed with bulk cobalt nitrate, cobalt acetate, cobalt acetyl acetonate, and cobalt chloride (figure 1). All cobalt precursors appeared to be fully decomposed for calcination

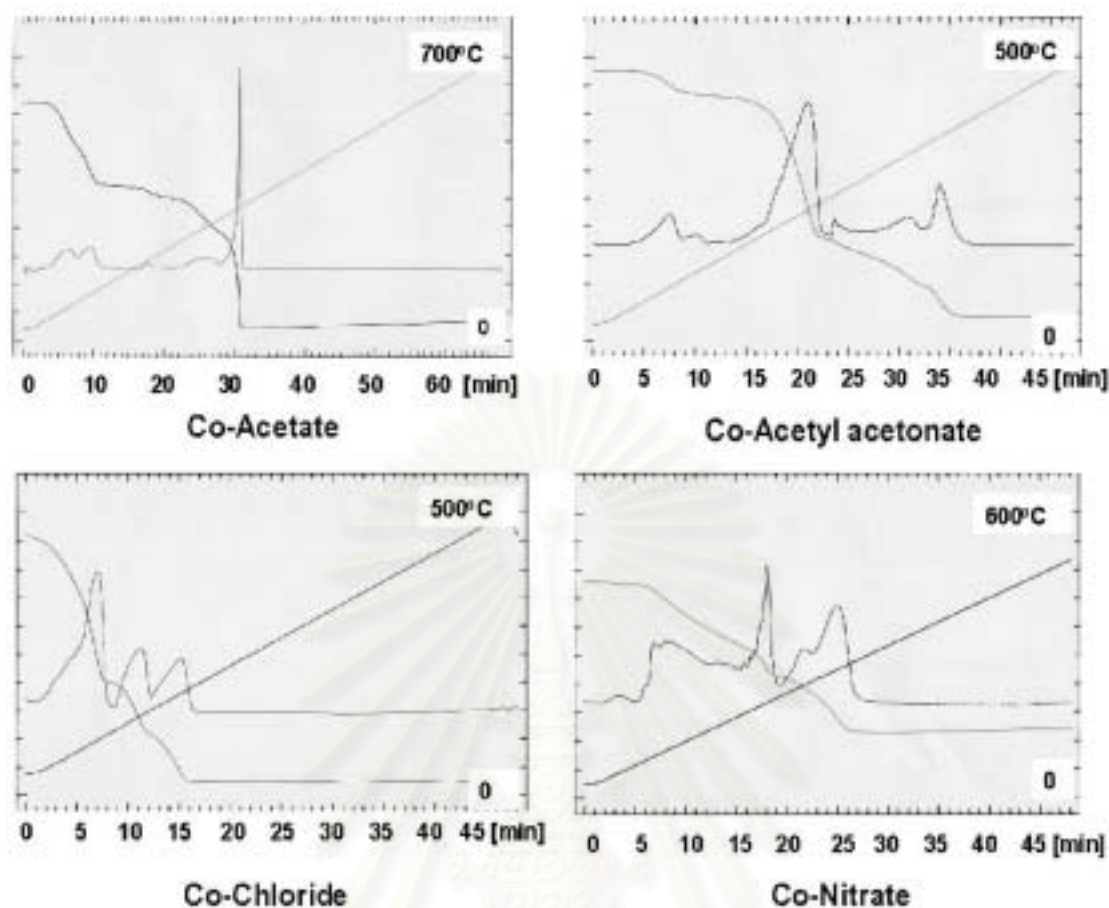


Figure 1. Thermogravimetric analysis (TGA) experiments for different cobalt precursors (bulk).

temperatures above 400 °C. Thus, a calcination procedure using 500 °C for 2 h was used to produce the cobalt oxide phase in all the various catalysts prepared.

The actual amounts of cobalt loading (determined by atomic adsorption spectroscopy), the BET surface areas, and the cobalt crystallite sizes (derived from XRD line broadening) for the catalyst samples are given in table 1. In this study, cobalt loading on the catalyst samples was approximately 7–8 wt% in order to make it close to that required for a commercial catalyst. The pure silica MCM-41 support before cobalt impregnation had a

BET surface area of 1234 m²/g and a pore volume of 0.85 cm³/g. The BET surface areas of the cobalt catalysts prepared with different cobalt precursors were found to be in the range of 646–756 m²/g and in the order of Co/M-Ac > Co/M-NO > Co/M-AA > Co/M-Cl. The significant decrease in surface area of the original support material suggests that cobalt was deposited significantly in the pores of MCM-41. The cobalt precursor did not have a significant impact on the average pore diameter of MCM-41 after cobalt loading since all the catalyst samples retained narrow pore-size distributions of approximately 3 nm, the same as the original MCM-41.

The XRD patterns of the MCM-41-supported cobalt catalysts are shown in figure 2. The ordered structure of MCM-41 gave an XRD peak at low 2θ around 2.58° for the unsupported MCM-41. After impregnation of cobalt, the intensity of the XRD peaks for MCM-41 was decreased for all the catalyst samples and the peaks became broader owing to the structure of MCM-41 becoming less ordered by the impregnation of cobalt or because of the secondary scattering of the X rays. The structure of MCM-41 was not destroyed, but the long-range order of MCM-41 may have shrunk [28].

The XRD patterns at higher diffraction angles of the MCM-41-supported cobalt catalysts prepared with

Table 1

Characteristics of Co/MCM-41 catalysts prepared from different cobalt precursors

Catalyst	Co ^a (wt%)	BET S.A. ^b (m ² /g)	dp ^c Co ₃ O ₄ (nm)
MCM-41	—	1234	—
Co/M-Ac	8.3	756	<5
Co/M-AA	7.8	675	<5
Co/M-Cl	7.1	646	15.0
Co/M-NO	8.1	747	6.3

^aElemental analysis using atomic adsorption spectroscopy. Error of measurement = ±2%.

^bUsing N₂ physisorption at 77 K. Error of measurement = ±10%.

^cFrom XRD line broadening. Error of measurement = ±5%.

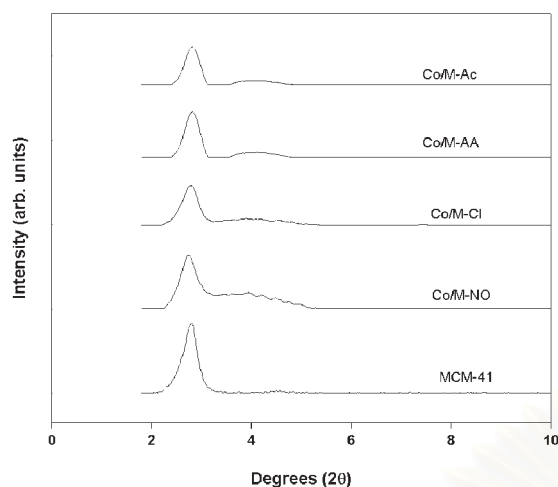


Figure 2. Effect of cobalt precursors on the XRD patterns of Co/MCM-41 catalysts (low 2θ).

different cobalt precursors in the calcined state are shown in figure 3. Co/M-NO and Co/M-Cl exhibited diffraction peaks at 2θ of ca. 31.3° , 36.8° , 45.1° , 59.4° , and 65.4° , indicating the presence of Co_3O_4 spinel in the catalyst particles. Surprisingly, Co/M-Ac and Co/M-AA did not exhibit any distinct XRD patterns. This suggests that the crystallite size of cobalt oxide prepared from cobalt acetate and cobalt acetylacetonate on MCM-41 was below the lower limit for XRD detectability (5 nm) even though cobalt loading was as high as 8 wt%. It is also possible that on Co/M-Ac and Co/M-AA, cobalt did not form Co_3O_4 crystallites but may have formed an amorphous cobalt oxide similar to what has been

suggested for Co/TiO₂ prepared from cobalt EDTA [23]. For Co/M-NO and Co/M-Cl, the average cobalt oxide crystallite sizes calculated using the Scherrer's equation [29] were found to be 6.3 and 15.0 nm, respectively. These cobalt particles were much larger than the average pore diameter of MCM-41 (3 nm), suggesting that using cobalt nitrate and cobalt chloride precursors to prepare MCM-41-supported cobalt catalysts by incipient wetness impregnation resulted in some large cobalt oxide particles deposited on the external surface of MCM-41.

SEM and elemental mapping were carried out for all the catalyst samples. Typical SEM micrographs of catalyst granules are shown in figure 4. The term "granule" here refers to a catalyst particle composed of cobalt and silica. In all the SEM figures, the white or light spots on the catalyst granules represent a high concentration of cobalt and its compounds, while the darker areas of the granules indicate the support with minimal/no cobalt present. The dark background is due to the carbon tape used for holding the catalyst samples. The SEM micrographs for catalyst granules prepared with different cobalt precursors show similar catalyst granule sizes of 30–50 μm . The elemental mappings for cobalt are shown in figure 5. The presence of very large cobalt clusters nonuniformly distributed on the granule exteriors was observed for Co/M-Cl. Dispersion of the cobalt was better for the other catalysts.

SEM-EDX was performed on cross-sectioned catalyst granules in order to determine the cobalt concentration at different locations on the catalyst granules (in the pores versus on the external surface). The SEM

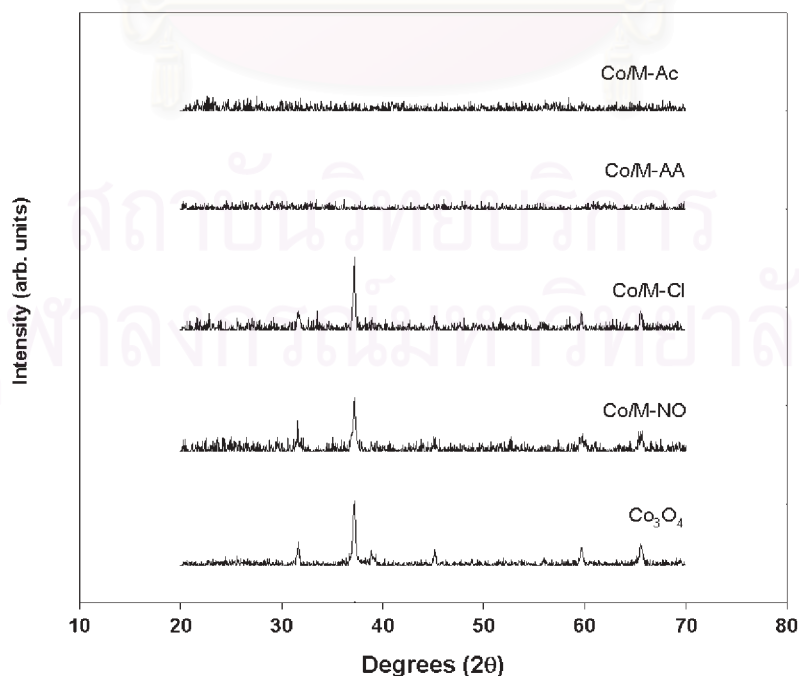


Figure 3. Effect of cobalt precursors on the XRD patterns of Co/MCM-41 catalysts (high 2θ).

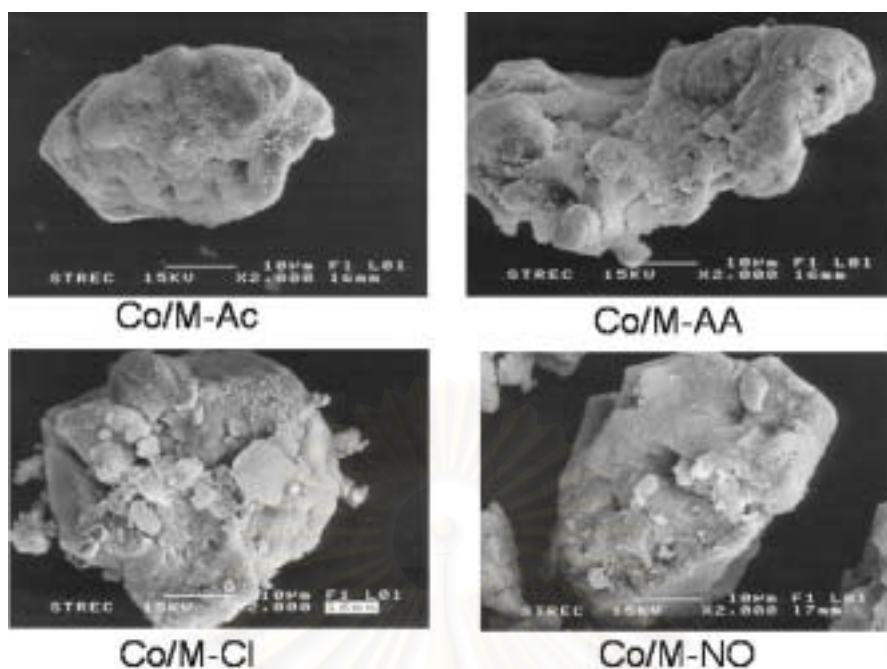


Figure 4. SEM micrographs of Co/MCM-41 catalysts prepared with different cobalt precursors.

micrographs of cross-sectioned catalyst granules with locations of EDX analysis are shown in figure 6. The corresponding elemental distributions are reported in table 2. Again, we observed a very high concentration of

cobalt on the external surface of Co/M-Cl, whereas distribution of cobalt for the other catalysts was not significantly different across the cross-sectioned granules. SEM-EDX results thus confirm that, except for

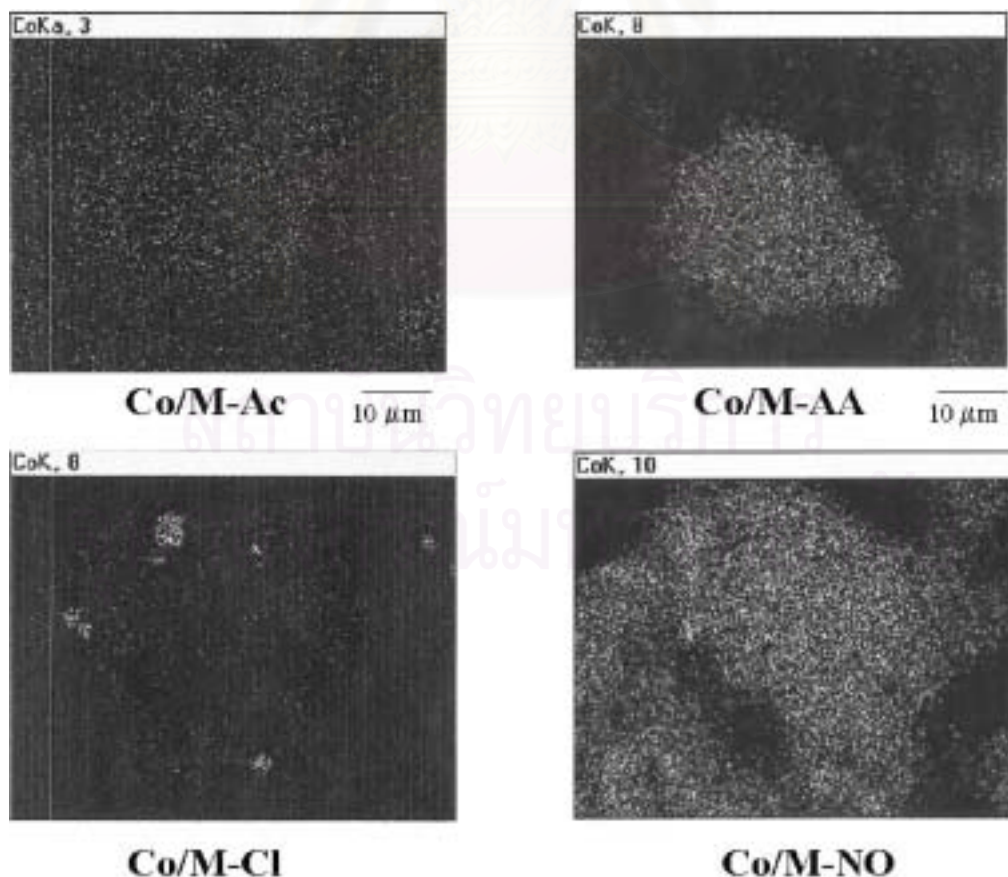


Figure 5. Distribution of cobalt on the exteriors of different Co/MCM-41 catalyst granules from SEM elemental mappings.

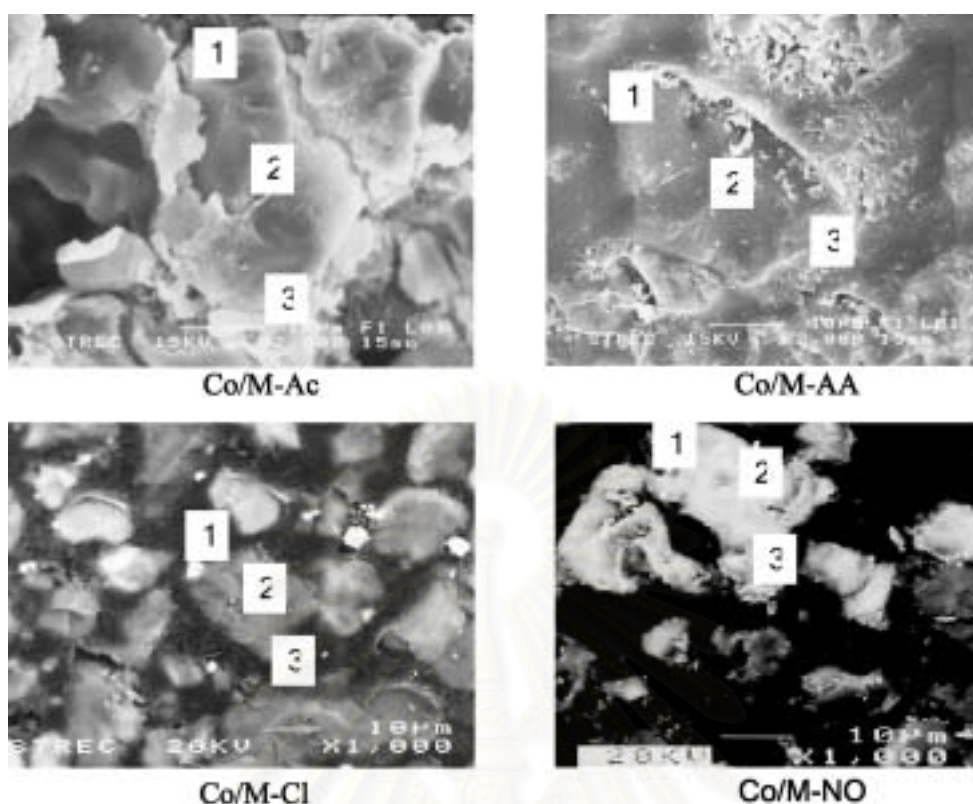


Figure 6. SEM micrograph of the cross-sectioned catalysts with locations of EDX analysis.

Co/M-Cl, the cobalt catalysts had their cobalt primarily located in the pores of MCM-41.

TEM micrographs were taken for all the catalysts in order to physically measure the size of cobalt oxide particles and/or cobalt clusters (figure 7). TEM images were found to be in accordance with the results from XRD and EDX that very large cobalt clusters (1–2 μm) were present on Co/M-Cl, while dispersion of the cobalt was better for the other catalysts. Although TEM measurements were only done for a very small portion of each catalyst, the results are able to provide further evidence about cobalt dispersion.

The degrees of reduction, the relative rankings of cobalt dispersion, and the CO hydrogenation rates of the catalysts are reported in table 3. The degrees

of reduction of the catalysts in the TGA experiments from 30–800 $^{\circ}\text{C}$ were not significantly different, ranging from 53–64%, with Co/M-NO showing the highest degree of reduction. Any cobalt not reducible during the H_2 reduction up to 800 $^{\circ}\text{C}$ is identified as “nonreducible” cobalt silicate [30,31].

The relative ranking of cobalt dispersion was calculated from CO-pulse chemisorption experiments. Since for CO chemisorption on cobalt, bridge bonding may occur, there is no precise ratio of CO molecules to cobalt metal surface atoms that can be used. However, for strictly identical measurement conditions, CO chemisorption can yield a relative ranking of cobalt dispersion. It was found that CO chemisorption was only measurable for Co/M-AA and Co/M-NO, with Co/M-AA exhibiting higher amount of CO chemisorption than Co/M-NO. Co/M-Cl exhibited negligible chemisorption probably due to its low dispersion of cobalt and/or due to residual Cl^- blocking the cobalt sites. Residual Cl^- has been found in other supported metal catalysts when Cl-containing compounds are used as the catalyst precursor [32–34]. Figure 8 shows the XRD pattern of bulk CoCl_2 after calcination at 500 $^{\circ}\text{C}$, where residual Cl^- can be observed. However, residual Cl^- was probably highly dispersed or present in very low amounts so that it could not be detected by XRD in case of the Co/M-Cl catalyst. One should note that residual Cl^- has been shown to be significantly decreased in metal catalysts when water vapor is

Table 2
Elemental analysis using SEM-EDX on different locations of the cross-sectioned catalysts

Catalyst	Co (wt%) ^a		
	Location 1	Location 2	Location 3
Co/M-Ac	7.5	10.6	7.8
Co/M-AA	11.4	12.4	6.5
Co/M-Cl	18.6	4.9	6.9
Co/M-NO	7.9	6.0	7.7

^aError of measurement = $\pm 10\%$.

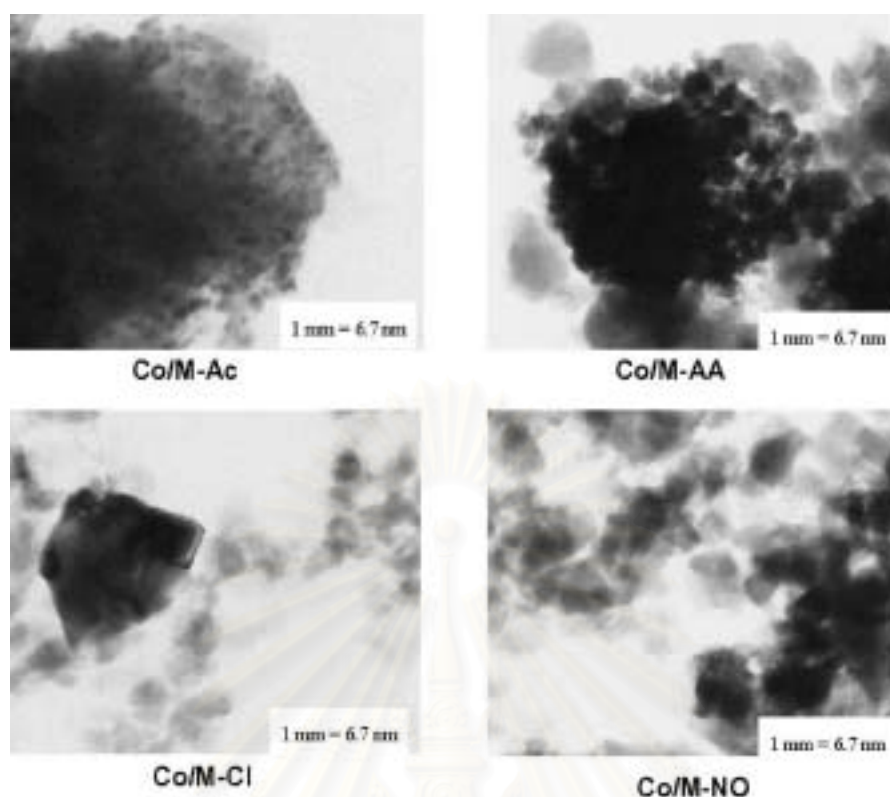


Figure 7. TEM micrographs of Co/MCM-41 catalysts prepared with different cobalt precursors.

present, such as during CO hydrogenation. Co/M-Ac had well-dispersed cobalt as determined by XRD and TEM; therefore, it is surprising that no CO adsorption could be measured at the conditions used.

The test reactions for CO hydrogenation were carried out at 220 °C, 1 atm, and H₂/CO ratio = 10 for all catalyst samples. A relatively high H₂/CO ratio was used in order to minimize deactivation due to carbon deposition during reaction. It was found that at the reaction conditions used, Co/M-NO exhibited a much higher CO hydrogenation rate than all other catalysts in this study. The low activity of Co/M-Ac and Co/M-AA is probably due to the unstable small cobalt particles forming cobalt silicates during reduction in H₂ [31,35] due to the water vapor generated.

The results of this study were found to be in agreement with the well-established trends in the literature on the influence of cobalt precursors on different supported cobalt Fischer–Tropsch catalysts [22–26]. It should be emphasized that our results support the need for a balance between dispersion-enhancing, strong support-precursor interaction and loss of metallic cobalt as a result of metal-support compound formation in order to obtain high-activity-supported cobalt catalysts, in agreement with the recent suggestions of Soled *et al.* [26]. The type of cobalt precursor must be carefully chosen, especially when restricted pore-structure supports such as MCM-41 are used. Cobalt particles small enough to fit into the pores of MCM-41 could be unstable at commercially relevant

Table 3
Results from TGA, CO-pulse chemisorption, and CO hydrogenation reaction

Catalyst	Reducibility ^a (30–800 °C)	CO chemisorption (CO/Co) ^b × 100	Rate ^c × 10 ⁴ (g _{CH₄} /g _{cat.} /h)	
			Initial	Steady state
Co/M-Ac	59	Nil	0.068	0.057
Co/M-AA	53	7.6	0.338	0.071
Co/M-Cl	58	Nil	0.012	0.050
Co/M-NO	64	2.6	1.810	1.150

^aFrom thermogravimetric experiments.

^bThe relative %Co dispersion from pulse CO chemisorption experiments.

^cCO hydrogenation was carried out at 220 °C, 1 atm, H₂/CO = 10 (H₂/CO/Ar = 20/2/8 cc/min).

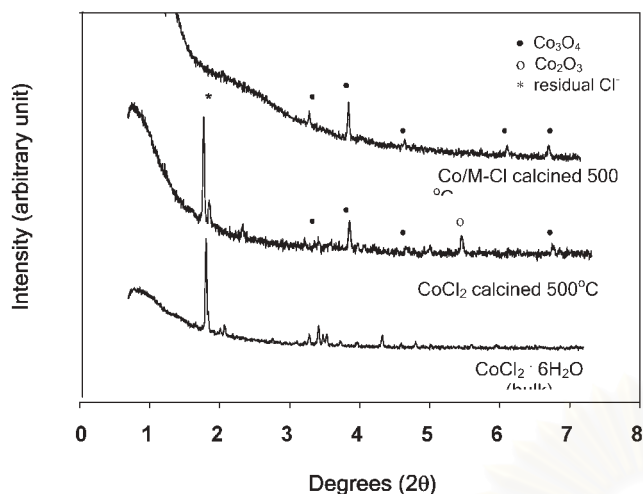


Figure 8. XRD pattern of residual Cl^- after calcination at 500°C for 2 h.

synthesis conditions and thus have limited practical use.

4. Conclusion

Using organic precursors such as cobalt acetate or cobalt acetylacetonate instead of inorganic ones such as cobalt nitrate or cobalt chloride results in very small cobalt particles uniformly distributed throughout the pore structure of MCM-41. Extremely large cobalt particles/clusters are evident on Co/MCM-41 prepared from cobalt chloride. The results suggest, however, that there may be an optimum cobalt particle size and dispersion to maximize the surface cobalt availability since cobalt silicate formation during reduction may occur (especially for highly dispersed cobalt) and result in lower CO hydrogenation activity. Only surface cobalt metal atoms are active for CO hydrogenation. Among the four types of cobalt compounds used in this study, cobalt nitrate seems to be the best (optimum) cobalt precursor to prepare MCM-41-supported cobalt catalysts with significant CO hydrogenation activity at commercially relevant synthesis conditions.

Acknowledgment

Financial support by the Thailand Research Fund (TRF) and TJTTP-JBIC is gratefully acknowledged.

References

- [1] R.B. Anderson, *The Fischer-Tropsch Synthesis* (Academic Press, San Diego, 1984).

- [2] J.G. Goodwin Jr., *Prep. ACS Div. Petr. Chem.* 36 (1991) 156.
 [3] E. Iglesia, *Appl. Catal. A* 161 (1997) 50.
 [4] R.C. Reuel and C.H. Bartholomew, *J. Catal.* 85 (1984) 78.
 [5] L.B. Backman, A. Rautiainen, A.O.I. Krause and M. Lindblad, *Catal. Today* 43 (1998) 11.
 [6] G.J. Haddad and J.G. Goodwin Jr., *J. Catal.* 157 (1995) 25.
 [7] J. van de Loosdrecht, M. van der Haar, A.M. van der Kraan and J.W. Geus, *Appl. Catal. A* 150 (1997) 365.
 [8] A.R. Belambe, R. Oukaci and J.G. Goodwin Jr., *J. Catal.* 166 (1997) 8.
 [9] D. Schanke, A.M. Hilmen, E. Bergene, K. Kinnari, E. Rytten, E. Adnanes and A. Holmen, *Catal. Lett.* 34 (1995) 269.
 [10] J.H.A. Martens, H.F.J. van't Blik and R. Prins, *J. Catal.* 97 (1986) 200.
 [11] J. Li and N.J. Coville, *Appl. Catal. A* 181 (1999) 201.
 [12] J.S. Beck, J.C. Vartuli, W.J. Roth, M.E. Leonowicz, C.T. Kresge, K.D. Schmitt, C.T.-W. Chu, D.H. Olson, E.W. Sheppard, S.B. McCullen, J.B. Higgins and J.L. Schlenker, *J. Am. Chem. Soc.* 114 (1992) 10834.
 [13] C.T. Kresge, M.E. Leonowicz, W.J. Roth, J.C. Vartuli and J.S. Beck, *Nature* 359 (1992) 710.
 [14] E. Zhao, J. Feng, Q. Huo, N. Melosh, G.H. Fredrickson, B.F. Chmelka and G.D. Stucky, *Science* 279 (1998) 548.
 [15] E. Zhao, Q. Huo, J. Feng, B.F. Chmelka and G.D. Stucky, *J. Am. Chem. Soc.* 120 (1998) 6024.
 [16] C. Song and K.M. Reddy, *Appl. Catal. A* 176 (1999) 1.
 [17] F. Schuth, A. Wingen and J. Sauer, *Microporous and Mesoporous Mater.* 44–45 (2001) 465.
 [18] J. Panpranot, J.G. Goodwin Jr. and A. Sayari, *J. Catal.* 211 (2002) 530.
 [19] A. Jentys, N.H. Pham, H. Vinek, M. Englisch and J.A. Lercher, *Microporous Mater.* 6 (1996) 13.
 [20] A. Jentys, N.H. Pham, H. Vinek, M. Englisch and J.A. Lercher, *Catal. Today* 39 (1998) 311.
 [21] S. Suvanto, J. Hukkamaki, T.T. Pakkanen and T.A. Pakkanen, *Langmuir* 16 (2000) 4109.
 [22] J. van der Loosdrecht, M. van der Haar, A.M. van der Kraan, A.J. van Dillen and J.W. Geus, *Appl. Catal. A* 150 (1997) 365.
 [23] M. Kraum and M. Baerns, *Appl. Catal.* 186 (1999) 189.
 [24] M.P. Rosynek and C.A. Polansky, *Appl. Catal.* 73 (1991) 97.
 [25] S. Sun, N. Tsubaki and K. Fujimoto, *Appl. Catal. A* 202 (2000) 121.
 [26] S.L. Soled, E. Iglesia, R.A. Fiato, J.E. Baumgartner, H.B. Vroman and S. Miseo, Paper 293, *18th North American Catalysis Society Meeting*, Cancun, Mexico, 1–6 June 2003.
 [27] M. Kruk, M. Jaroniec and A. Sayari, *Microporous Mesoporous Mater.* 35–36 (2000) 545.
 [28] L. Pasqua, F. Testa, R. Aiello, F. Di Renzo and F. Fajula, *Microporous and Mesoporous Mater.* 44–45 (2001) 111.
 [29] H.P. Klug and L.E. Alexander, *X-ray Diffraction Procedures for Polycrystalline Amorphous Materials*, 2nd ed. (Wiley, New York, 1974).
 [30] L.B. Backman, A. Rautiainen, A.O.I. Krause and M. Lindblad, *Catal. Today* 43 (1998) 11.
 [31] A. Kogelbauer, J.C. Webber and J.G. Goodwin Jr., *Catal. Lett.* 34 (1995) 259.
 [32] N. Mahata and V. Vishwanathan, *J. Catal.* 196 (2000) 262.
 [33] Y. Zhou, M.C. Wood and N. Winograd, *J. Catal.* 146 (1994) 82.
 [34] P. Johnston and R.W. Joyner, *J. Chem. Soc. Faraday Trans.* 89 (1993) 863.
 [35] J.M. Jablonski, M. Wolcyrz and L. Krajczyk, *J. Catal.* 173 (1998) 530.

Influence of Cobalt Precursors on the characteristics and Catalytic Properties of Co/MCM-41 Catalysts

Sujaree Kaewkun*, Joongjai Panpranot, and Piyasan Praserttham

Center of Excellence on Catalysis and Catalytic Reaction Engineering,
Department of Chemical Engineering, Chulalongkorn University, Bangkok, 10330 Thailand
E-mail: Sujaree.K@student.chula.ac.th

Co/MCM-41 catalysts were prepared using the incipient wetness impregnation technique with aqueous solutions of different cobalt compounds such as cobalt nitrate, cobalt chloride, cobalt acetate, and cobalt acetylacetonate. Using organic precursors such as cobalt acetate and cobalt acetylacetonate resulted in very small cobalt oxide particles that could not be detected by XRD even for a Co loading as high as 8 wt%. The cobalt oxides prepared from cobalt acetate were found to be not active for CO-chemisorption due probably to the formation of cobalt silicates during reduction. This was not a problem when cobalt acetylacetonate was used. Inorganic precursors such as cobalt chloride resulted in very large cobalt particles/clusters (1-1.5 μm) and/or residual Cl^- blocking sites, consequently very small active area. Cobalt nitrate resulted in a number of small cobalt particles dispersed throughout MCM-41 and some larger particles located on the external surface of MCM-41.

Keywords: Preparation of Cobalt catalyst, Cobalt precursors, MCM-41, CO hydrogenation, Fischer-Tropsch synthesis

INTRODUCTION

Cobalt-based catalysts are widely used in CO hydrogenation or Fischer-Tropsch synthesis (FTS) especially when high molecular weight paraffins are preferred (Anderson, 1984; Goodwin, 1991; Iglesia, 1997). To increase their activity, cobalt is usually deposited on a high surface area support to obtain a high metal dispersion. The commonly used supports include silica (Reuel and Bartholomew, 1984; Backman *et al.*, 1998; Haddad and Goodwin, 1995), alumina (van de Loosdrecht *et al.*, 1997; Belambe *et al.*, 1997; Schanke *et al.*, 1995), and titania (Martens *et al.*, 1986; Li and Coville, 1999). Recently, attention has focused on the use of ordered mesoporous materials such as MCM-41 as catalyst supports. MCM-41 possesses excellent support properties such as high BET surface area and well-ordered hexagonal pore structures that can be tailor-made in the pore diameter range of 1.5-10 nm (Beck *et al.*, 1992; Kresge *et al.*, 1992). In a previous study (Panpranot *et al.*, 2002), we reported the high F-T activity of Ru-promoted MCM-41-supported cobalt catalysts. However, using incipient wetness impregnation and cobalt nitrate as the precursor, cobalt was found to be

non-uniformly distributed on the MCM-41 support.

It is known that cobalt dispersion depends on the type of cobalt precursors. van de Loosdrecht *et al.* (van de Loosdrecht *et al.*, 1997) showed that alumina-supported cobalt catalysts prepared by incipient wetness impregnation using cobalt EDTA and cobalt citrate precursors resulted in very small cobalt oxide particles compared to the one prepared from cobalt nitrate. The use of cobalt oxalate, cobalt acetate, and cobalt acetylacetonate as cobalt precursors for titania-supported cobalt catalysts, have been found to give higher cobalt dispersion than catalysts prepared from cobalt nitrate (Kraum and Baerns, 1999). Nevertheless, less is known about the influences of cobalt precursors on the dispersion of cobalt when restricted pore structure supports such as MCM-41 are used.

The purpose of this study was to investigate the effect of different organic and inorganic cobalt precursors on the characteristics and the catalytic properties of MCM-41-supported cobalt catalysts in CO hydrogenation reaction.

EXPERIMENTAL

Catalyst preparation

Pure silica MCM-41 was prepared in the same manner as that of Kruk *et al.* (Kruk *et al.*, 2000) using the following gel composition: (1.0 SiO₂): (0.317 TMAOH): (0.45 CTMABr): (66.7 H₂O), where TMAOH denotes tetramethylammonium hydroxide and CTMABr denotes cetyltrimethyl ammonium bromide. The Co/MCM-41 catalysts were prepared by the incipient wetness impregnation of the supports with aqueous solution of different cobalt precursors such as cobalt nitrate (Aldrich), cobalt acetate (APS), cobalt acetylacetonate (Aldrich) and cobalt chloride (Fluka). Cobalt loading was approximately 8% by weight of catalyst. The samples were dried at 110°C for 1 day and then were calcined in air at 500°C for 2 h. These catalysts with different cobalt precursors are respectively designated as Co/M-NO, Co/M-Cl, Co/M-AA and Co/M-Ac in which Co/M refers to cobalt supported on MCM-41 and the last two letters reflect the type of the cobalt precursor used: NO for cobalt nitrate, Cl for cobalt chloride, AA for cobalt acetylacetonate and Ac for cobalt acetate.

Catalyst characterization

Atomic adsorption spectroscopy

The bulk composition of cobalt was determined using a Varian Spectra A800 atomic adsorption spectrometer.

N₂ physisorption

The BET surface area, pore volume, average pore diameter, and pore size distribution of the catalysts were determined by N₂ physisorption using a Micromeritics ASAP 2000 automated system. Each sample was degassed in the Micromeritics ASAP 2000 at 150°C for 4 hours prior to N₂ physisorption.

X-ray diffraction (XRD)

The XRD spectra of the catalysts were measured using a SIEMENS D5000 X-ray diffractometer, using Cu K α radiation with a Ni filter in the 2-8° or 10-80° 2 theta angular region.

Scanning Electron Microscopy (SEM)

Catalyst granule morphology and elemental distribution were obtained using a JEOL JSM-

35CF scanning electron microscope. The SEM was operated at 20 kV. After the SEM micrographs were taken, elemental mappings were performed to determine the elemental concentration distribution on the catalyst granules using Link Isis 300 software.

Transmission Electron Microscopy (TEM)

The cobalt oxide particle size and distribution of cobalt on MCM-41 was observed using a JEOL-TEM 200CX transmission electron microscope operated at 100 kv.

CO-pulse experiment

Cobalt dispersion was determined by pulsing carbon monoxide over the reduced catalyst. Approximately 0.2 g of catalyst was filled in a quartz tube, incorporated in a temperature-controlled oven and connected to a thermal conductivity detector (TCD). Prior to chemisorption, the catalyst was reduced in a flow of hydrogen (50 cc/min) at 400°C for 2 h. Afterward, the sample was purged with helium at 400°C for 1 h and finally cooled down to room temperature. Carbon monoxide was pulse at 25°C over the reduced catalyst until the TCD signal was constant.

RESULTS AND DISCUSSION

The actual amounts of cobalt loading (determined by atomic adsorption spectroscopy), the BET surface areas, the cobalt oxide crystallite sizes (derived from XRD and TEM), and the percentages of cobalt dispersion (calculated from CO-pulse chemisorption) for the catalyst samples are given in Table 1. In this study, cobalt loading on the catalyst samples was approximately 7-8 wt.% in order to make it close to that required for a commercial catalyst. The pure silica MCM-41 support before cobalt impregnation had a BET surface area of 1,223 m²/g and a pore volume of 0.85 cm³/g. The BET surface areas of the cobalt catalysts prepared with different cobalt precursors were found to be in the range of 646-756 m²/g and in the order of Co/M-Ac > Co/M-NO > Co/M-AA > Co/M-Cl. The significant decrease in surface area of the original support material suggests that cobalt was deposited significantly in the pores of MCM-41. The Co precursor did not have a significant impact on the average pore diameter of MCM-41 after cobalt loading since

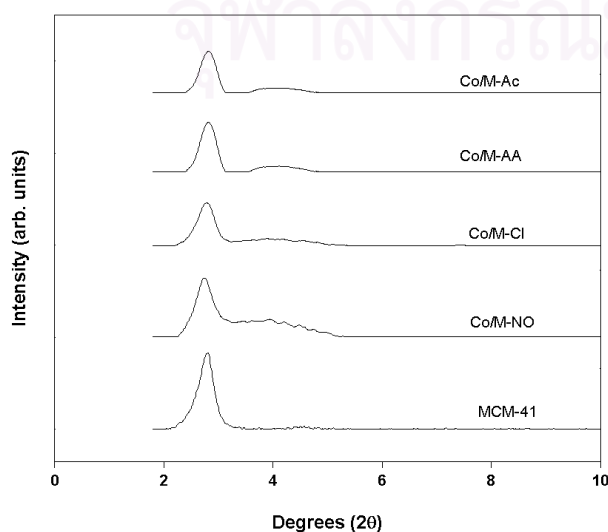
all catalyst samples retained narrow pore size distributions of approximately 3 nm, the same as the original MCM-41.

Table 1
Characteristics of different Co/MCM-41 catalysts

Catalyst	Co ¹ (wt.%)	BETS.A. ² (m ² /g)	d _p ³ Co ₃ O ₄ (nm)	D _{Co} ⁴ (%)
MCM-41	-	1234	-	-
Co/M-Ac	8.3	756	< 5	n/l
Co/M-AA	7.8	675	< 5	7.61
Co/M-Cl	7.1	646	15.0	n/l
Co/M-NO	8.1	747	6.3	2.60

1. Elemental analysis using atomic adsorption spectroscopy.
2. Using N₂ Physisorption at 77 K.
3. From XRD line-broadening.
4. From pulse-CO chemisorption experiments.

The X-ray diffraction patterns of the MCM-41-supported cobalt catalysts are shown in Figure 1. The ordered structure of MCM-41 gave XRD peak at low 2θ angles around 2.58 degrees for the unsupported MCM-41. After impregnation of cobalt the intensity of the XRD peaks for MCM-41 was decreased for all catalysts samples and the peaks became broader due to the structure of MCM-41 becoming less ordered by impregnation of cobalt or due to secondary scattering of the x-rays. The structure of MCM-41 was not destroyed but the long-range order of MCM-41 may have shrunk (Pasqua *et al.*, 2001).



The XRD patterns at higher diffraction angles of the MCM-41-supported cobalt catalysts prepared with different cobalt precursors in the calcined state are shown in Figure 2. Co/M-NO and Co/M-Cl exhibited the diffraction peaks at 2θ of ca. 31.3°, 36.8°, 45.1°, 59.4°, and 65.4°, indicated the presence of Co₃O₄ spinel in the catalyst particles. Surprisingly, Co/M-Ac and Co/M-AA did not exhibit any distinct XRD patterns. This suggests that the crystallite size of cobalt oxide prepared from cobalt acetate and cobalt acetylacetonate on MCM-41 was below the lower limit for XRD detectability (5 nm) even though Co loading was as high as 8 wt.%. It is also possible that on Co/M-Ac and Co/M-AA, Co did not form Co₃O₄ crystallites but may have formed an amorphous cobalt oxide similar to what has been suggested for Co/TiO₂ prepared from cobalt EDTA [16]. For Co/M-NO and Co/M-Cl, the average cobalt oxide crystallite sizes calculated using the Scherrer's equation (Klug and Alexander, 1974) were found to be 6.3 and 15.0 nm, respectively. These cobalt particles were much larger than the average pore diameter of MCM-41 (3 nm), suggesting that using cobalt nitrate and cobalt chloride precursors to prepare MCM-41-supported Co catalysts by incipient wetness impregnation resulted in some large cobalt oxide particles deposited on the external surface of MCM-41.

SEM and elemental mapping were carried out for all the catalyst samples. Typical SEM micrographs of catalyst granules are shown in Figure 3. The term "granule" here refers to a catalyst particle composed of cobalt and silica. In all the SEM figures, the white or light spots on the catalyst granules represent a high concentration of cobalt and its compounds while the darker areas of the granules indicate the support with minimal/no cobalt present. The dark background is due to the carbon tape used for holding the catalyst samples. The SEM micrographs for catalyst granules prepared with different cobalt precursors show similar catalyst granule sizes of 30-50 micron. The elemental mappings for cobalt are shown in Figure 4. The presence of very large cobalt clusters non-uniformly distributed was observed on Co/M-Cl and/or residual Cl⁻ blocking sites, consequently very small active area. The residual Cl⁻ was also found in other supported metal catalysts when prepared from Cl-containing precursors (Mahata and Vishwanathan, 2000; Zhou *et al.*, 1994; Johnston and Joyner, 1993).

Dispersion of the cobalt was better for the other catalysts.

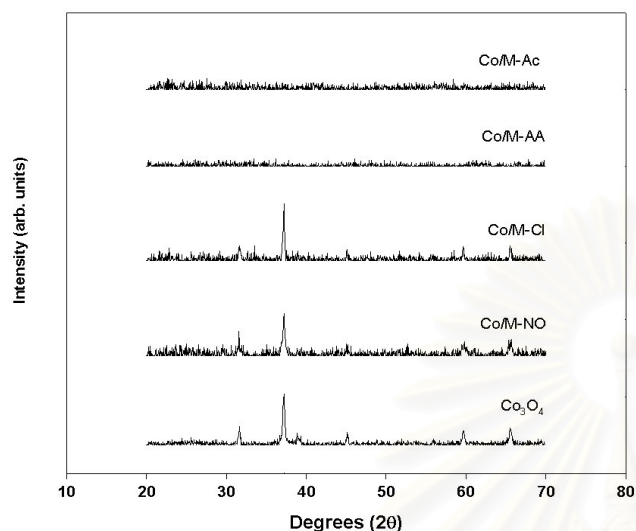


Figure 2. Effect of cobalt precursors on the XRD patterns of Co/MCM-41 catalysts (high degree 2θ)

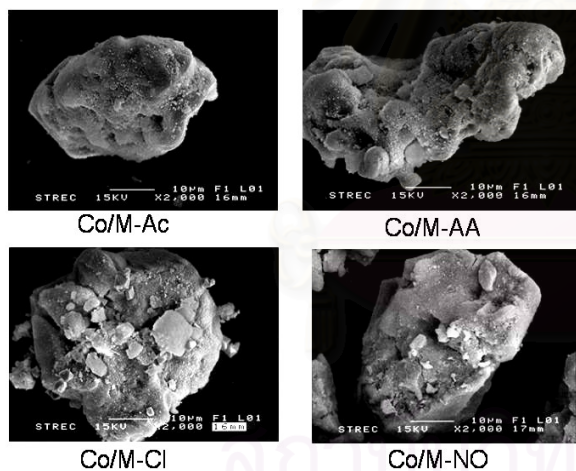


Figure 3. SEM micrographs of Co/MCM-41 catalysts prepared with different cobalt precursors.

TEM micrographs were taken for all the catalysts in order to physically measure the size of cobalt oxide particles and/or cobalt clusters (see Figure 5). The average cobalt oxide particle/cluster sizes for the different catalysts were found to be in accordance with those from XRD and SEM elemental mapping. They were in the order of Co/M-Cl > Co/M-NO > Co/M-AA > Co/M-Ac.

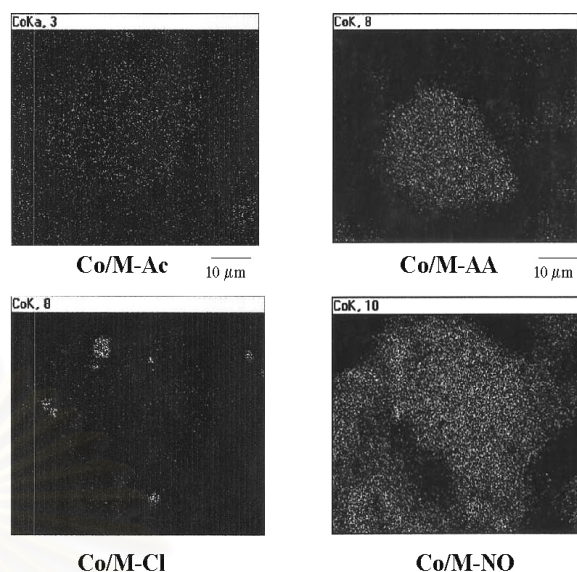


Figure 4. Distribution of cobalt on different Co/MCM-41 catalysts from SEM elemental mappings.

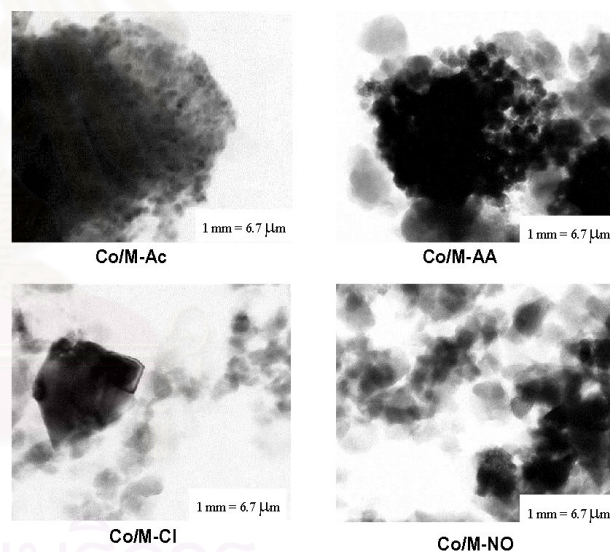


Figure 5. TEM micrographs of Co/MCM-41 catalysts prepared with different cobalt precursors.

CO-pulse chemisorption was applied in order to measure the active cobalt surface available for CO hydrogenation reaction. The technique was based on the assumption that one carbon monoxide molecule adsorbs on one cobalt metal surface site. This appears to be justified only for a relative comparison since bridged bonding was neglected. It was found that CO chemisorption was only measurable for Co/M-AA and Co/M-NO, with Co/M-AA exhibiting almost 3 times higher amount of CO chemisorption than Co/M-NO. It is not surprising that Co/M-Cl exhibiting

negligible chemisorption since its dispersion of cobalt was low due to the Co particles being very large and/or residual Cl⁻ blocking sites, consequently very small active area was measurable. Co/M-Ac, on the other hand, had well dispersed Co as determined by XRD and TEM, so it is surprising that no CO adsorption was able to be measured. This is probably due to the small Co particles in the MCM-41 pores were unstable and form Co-silicates during reduction in H₂ due to the water vapor generated (Kogelbauer *et al.*, 1995).

CONCLUSION

Using organic precursors such as cobalt acetate or cobalt acetylacetonate, instead of inorganic ones such as cobalt nitrate or cobalt chloride results in very small cobalt particles uniformly distributed throughout the pore structure of MCM-41. Extremely large cobalt particles/clusters are evident on Co/MCM-41 prepared from cobalt chloride and/or residual Cl⁻ blocking sites, consequently very small active area. Since only surface Co metal atoms are active for CO hydrogenation, the results suggest that there may be an optimum Co particle size and dispersion to maximize surface Co availability while minimizing Co-silicate formation during reduction.

ACKNOWLEDGEMENT

Financial support by the Thailand Research Fund (TRF) and TJTTP-JBIC is gratefully acknowledged.

REFERENCES

- Anderson, R. B., "The Fischer-Tropsch Synthesis", Academic Press, San Diego, (1984).
- Backman, L.B., Rautiainen, A., Krause, A.O.I., and Lindblad, M., *Catal. Today* 43, 11 (1998).
- Beck, J. S., Vartuli, J. C., Roth, W. J., Leonowicz, M. E., Kresge, C. T., Schmitt, K. D., Chu, C. T., Oslon, D. H., Sheppard, E. W., McCullen, S. B., Higgins, J. B., and Schlemker, J. L., *J. Am. Chem. Soc.* 114, 10834 (1992).

- Belambe, A.R., Oukaci, R., and Goodwin, J.G., Jr., *J. Catal.* 166, 8 (1997).
- Goodwin, J. G., Jr., *Prep. ACS Div., petr. Chem.* 36, 156 (1991).
- Haddad, G.J., and Goodwin, J.G., Jr., *J. Catal.* 157, 25 (1995).
- Iglesia, E., *Appl. Catal. A* 161, 50 (1997).
- Johnston, P., and Joyner, R. W., *J. Chem. Soc., Faraday Trans.* 89, 863 (1993).
- Klug, H. P., and Alexander, L. E., "X-ray diffraction procedures for polycrystalline amorphous materials", 2nd ed., Wiley, New York (1974).
- Kogelbauer, A., Weber, J.C., and Goodwin, J.G., Jr., *Catal Lett.* 34, 259 (1995).
- Kraum, M., and Baerns, M., *Appl. Catal.* 186, 189 (1999).
- Kresge, C. T., Leonowicz, M. E., Roth, W. J., Vartuli, J. C., and Beck, J. S., *Nature* 359, 710 (1992).
- Kruk, M., Jaronice, M., and Sayari, A., *Microporous and Mesoporous Mater.* 35-36, 545 (2000).
- Li., J., and Coville, N.J., *Appl. Catal. A* 181, 201 (1999).
- Mahata, N., and Vishwanathan, V., *J. Catal.* 196, 262 (2000).
- Martens, J. H. A., van't Blik, H.F.J., and Prins, R., *J. Catal.* 97, 200 (1986).
- Panpranot, J., Goodwin, J. G., Jr., and Sayari, A., *J. Catal.* 211, 530 (2002).
- Pasqua, L., Testa, F., Aiello, R., Di Renzo, F., and Fajula, F., *Microporous and Mesoporous Mater.* 44-45, 111 (2001).
- Reuel, R.C., and Bartholomew, C.H., *J. Catal.* 85, 78 (1984).
- Schanke, D., Hilmen, A.M., Bergene, E., Kinnari, K., Rytten, E., Adnanes, E., and Holmen, A., *Catal. Lett.* 34, 269 (1995).

van der Loosdrecht, J., van der Haar, M., van der Kraan, A. M., van Dillen, A. J., and Geus, J. W., *Appl. Catal. A*. 150, 365 (1997).

Zhou, Y., Wood, M. C., and Winograd, N., *J. Catal.* 146, 82 (1994).



สถาบันวิทยบริการ
จุฬาลงกรณ์มหาวิทยาลัย

VITA

Miss Sujaree Kaewgun was born in December 26th, 1981 in Bangkok, Thailand. She finished high school from Samsen Wittayalai School, Bangkok in 1998, and received bachelor's degree in Chemical Engineering from the department of Chemical Engineering, Faculty of Engineering, Kasetsart University, Bangkok, Thailand in 2002.



สถาบันวิทยบริการ
จุฬาลงกรณ์มหาวิทยาลัย